NTNU – Trondheim
Norwegian University of
Science and Technology

Control and Estimation of Wave Energy Converters

Annette Kristin Brask

Marine Technology
Submission date: June 2015
Supervisor: Roger Skjetne, IMT
Co-supervisor: Asgeir Sørensen, IMT

Norwegian University of Science and Technology
Department of Marine Technology

NTNU Trondheim
Norwegian University of Science and Technology
Department of Marine Technology

PROJECT DESCRIPTION SHEET

Name of the candidate: Annette Kristin Brask

Field of study: Marine control engineering

Thesis title (Norwegian): Estimator design for bølgeenergiomformer

Thesis title (English): Estimator design of wave energy converters

Background

There is an increasing energy demand in the world. Currently the main energy resources are fossil fuels, which are non-renewable energy resources that eventually will drain out. In addition the emissions produced from fossil fuels contribute to global warming. In order to maintain a sustainable future, these energy sources should be phased out by more suitable alternatives. The hope is that Wave Energy Converters (WECs) and other renewable energy sources can pay a part as substitutes and contribute to create a more sustainable future. However, WECs are still in the developing phase, facing challenges of efficiency in terms of power output and cost.

The power output and, hence, the earnings from a WEC may be increased by controlling the oscillation in order to approach an optimum interaction between the WEC and the incident wave. Several control strategies have been proposed; however, the control functions of most of the strategies have proved to be non-causal. In order to utilize the control strategies, the measurement quantities have to be predicted some seconds into the future. This makes short time prediction of the oncoming waves an important problem in the field of wave energy. By finding a good solution to this prediction or estimation problem, the benefit could be to achieve an optimal effectiveness and power takeout of the devices.

Work description

1) Perform a literature review to provide background and relevant references on:
   - Wave energy converters (WECs) and other relevant energy producers.
   - Modelling of WECs.
   - Methods for control of WECs.
   - Methods for estimation of WECs and general sea-state estimation.

   Write a list with abbreviations and definitions, and a selection explaining particularly relevant terms and concepts related to WECs and estimation in an alphabetic order.

2) Develop a mathematical model of the behavior of the Ocean Oasis under influence of a control system. Perform a set of simulation test cases to qualitatively verify correct behavior of the numerical model.

3) Decide upon one or more suitable methods for predicting the non-causal parameters of the controller. Derive corresponding mathematical estimator algorithms and discuss analytically their robustness and performance in regards to stability and sensitivity to measurement noise, parameter uncertainty, and unmodeled dynamics.

4) Verify, through simulations, the derived methods for estimation of the fundamental parameters that need to be predicted for control purposes. This should include a comparison of their nominal performance and when subjected to measurement noise and model uncertainties.

5) Explore the possibility of increasing energy production by using prediction as a part of the control scheme.

Guidelines
The scope of work may prove to be larger than initially anticipated. By the approval from the supervisor, described topics may be deleted or reduced in extent without consequences with regard to grading.

The candidate shall present personal contribution to the resolution of problems within the scope of work. Theories and conclusions should be based on mathematical derivations and logic reasoning identifying the various steps in the deduction.

The report shall be organized in a rational manner to give a clear exposition of results, assessments, and conclusions. The text should be brief and to the point, with a clear language. The report shall be written in English (preferably US) and contain the following elements: Abstract, acknowledgements, table of contents, main body, conclusions with recommendations for further work, list of symbols and acronyms, references, and optional appendices. All figures, tables, and equations shall be numerated. The original contribution of the candidate and material taken from other sources shall be clearly identified. Work from other sources shall be properly acknowledged using quotations and a Harvard citation style (e.g. *natbib* Latex package). The work is expected to be conducted in an honest and ethical manner, without any sort of plagiarism and misconduct. Such practice is taken very seriously by the university and will have consequences. NTNU can use the results freely in research and teaching by proper referencing, unless otherwise agreed upon.

The thesis shall be submitted with a printed and electronic copy to 1) the main supervisor and 2) the external examiner, each copy signed by the candidate. The final revised version of this thesis description must be included. The report must appear in a bound volume or a binder according to the NTNU standard template. Computer code, pictures, videos, data series, and a PDF version of the report shall be included electronically.

Start date: 14 January 2015 **Due date:** As specified by the administration.

Supervisor: Prof. Roger Skjetne

Co-advisor: Prof. Asgeir J. Sørensen
PhD Anne Marthine Rustad

Trondheim

_____

Roger Skjetne
Supervisor

Abstract

The increasing scarcity of fresh water threatens the well being of both humans and the environment. Wave power desalination is a method of producing freshwater that has been in the developing stages since 1970. One of the concepts is Ocean Oasis which was studied during the DNV GL summer project, and it is also the subject of this thesis.

The main focus of this thesis has been on real-time control and estimation strategies which aim to increase the extracted power, thus the amount of fresh water produced. For real-time applications of marine structures the system dynamics must be modeled in time domain. This may cause challenges due to the convolution integrals which are a part of the model described by Cummins equation. Furthermore, for most control strategies developed for wave energy converters the measurement quantities must be predicted seconds into the future. This makes short-time prediction an important problem in the field of wave energy.

Earlier work on the topic includes a concept study on the effect of Latching control on the wave energy converter in regular waves. In this thesis the Latching control algorithm was extended for use in irregular waves and in real time. A system model was developed, where a linear time-variant parametric model of the fluid-memory effect was found. A method for calculating the non-causal excitation forces was studied. For prediction of the unknown control parameters an Extended Kalman filter was selected.

The structure dynamics, as well as control and estimation strategies were tested by simulations in MATLAB & Simulink. The uncontrolled model was validated to perform as expected. In addition, the control algorithm gave correct behavior. However, this resulted in neither an increase in efficiency nor a reduction in intermittency. Thus, it was concluded that Latching control is not a suitable control algorithm for the Ocean Oasis. The estimation algorithm gave satisfactory performance for low-medium noise levels (noise power of 0.01 - 0.1 m), with standard deviations in the range $\sigma = 0.01 - 0.03$ m for a sea state defined by $H_s = 2.5$ and $T_p = 9.1$. However, if the measurement noise was expected to contain higher levels of noise, the filter should be reconsidered or further developed.

Sammendrag

Den økende vannmangelen truer utviklingen til både mennesker og miljøet. Avsalting av saltvann ved bruk av bølgekraft er en metode for ferskvannsproduksjon som har vært under utvikling siden 1970. Et av prosjektene er Ocean Oasis som ble studert i DNV GLs sommer prosjekt 2014, og dette prosjektet er også temaet for denne avhandlingen.

Hovedfokuset i denne avhandlingen har vært på sann tid kontroll og estimerings strategier med målsetning om å øke den utvinnende kraften, og derfor mengden av ferskvann produsert. For sann tid annvending av marine strukturer må systemets dynamikk være modellert i tids domene. Dette kan forårsake utfordringer på grunn av konvulsjonsintegraler som er en del av modellen beskrevet av Cummings ligning. Videre, for flesteparten av kontroll strategier som er utviklet for bølgekraftkonvertere må målekvantitetene predikeres sekunder i fortid. Dette gjør korttids predikering til en viktig utfordring i fagområdet bølgekraft.

Tidlige arbeider på området inkluderer et konsept rundt effekten av fastholdingskontroll av bølgekraftverket i regulære bølger. I denne avhandlingen ble fastholdingskontrollalgoritmen utvidet til bruk på irregulære bølger og i sann tid. En systemmodell ble utviklet hvor en lineær parametrisk tidsvariant modell av fluid-memory effekten ble funnet. En modell for kalkulasjon av de ikke kausale eksitasjonskreftene ble undersøkt. For å predikere de ukjente kontroll parameterne ble et Kalman filter valgt.

Struktur dynamikken, i tillegg til kontroll og estimeringsstrategier, ble testet med simulering i MATLAB& Simulink. Den ukontrollerte modellen ble validert til å fungere som forventet. I tillegg ga kontroll algoritmen korrekt adferd. Imidlertid førte dette ikke til en økning eller en reduksjon i effektivitet. Derfor ble det konkludert med at fastholdingskontrollalgoritmen ikke er en brukbar kontrollalgoritme for Ocean Oasis prosjektet. Estimasjonsalgoritmen ga tilfredsstillende ytelse for bølger med lav og medium støynivå (støynivå på 0.01-01m), med en varians i måleområdet, $\sigma = 0.01 - 0.03$ m for en sjø status som er definert av $H_s = 2.5$ and $T_p = 9.1$. Hvis den forventede målestøyen er høyere må filteret bli revurdert eller videre utviklet.

Acknowledgement

This master thesis is written during the spring 2015 as a final part of the master program at the department of Marine Technology at the Norwegian University of Science and Technology (NTNU) in Trondheim.

The thesis stands as a contribution to the studies of the Ocean Oasis wave energy converter studied during the DNV GL summer project 2014. The main contribution of this thesis has been to develop a concept for control and estimation of the wave energy converter. The control algoithm used in this project was developed for regular waves by Eirik Schultz during his project thesis fall 2014 and extended to irregular waves in this thesis.

First of all I wish to thank my supervisor Professor Roger Skjetne from the Department of Marine Technology for all his advise and guidance throughout this project. Thanks to co-supervisor Professor Asgeir Sørensen for inspiration and guidance, and co-supervisor Associate professor Anne Marthine Rustad for advice on report writing and proofreading. Last, I would like to thank the enthusiastic wave power pioneer, Johannes Falnes, for answering all my questions.

June 27, 2015, Trondheim

Annette Kristin Brask

Nomenclature

Abbreviations

DSWP	Deterministic Sea Wave Prediction
EKF	Extended Kalman Filter
ES	Earth System
OWC	Oscillating Sater Columns
PB	Planet Boundary
PSD	Power Spectral Density
PTO	Power Take-Off
STD	Standard Deviation
WEC	Wave Energy Converter

Greek Symbols

ρ	Density of seawater
σ	Standard deviation
λ	State adjoint matrix
μ	Fluid-memory effect
ω_w	Angular frequency of wave
ϕ	Velocity potential
ϕ_ζ	Random phase of wave
ϕ_F	Phase of angle of excitation force transfer function

ε	Random phase of wave
ζ	Wave elevation
ζ_A	Wave elevation amplitude
ζ_{est}	Estimated wave elevation

Roman Symbols

$\angle h_{\zeta F}$	Phase angle of excitation force transfer function
ΔT	Time step of numerical calculations of Kalman filter
A_{33}	Added mass in heave
B_33	Damping
B_p	Damping of power take-off system
C_{33}	Hydrostatic stiffness
E	Wave energy
F_e	Excitation Force
F_{em}	Estimated excitation force
F_L	Latching control force
G	Control matrix
g	Gravitatonal acceleration
g	Retardation function
H	Hamiltonian matrix
H_s	Significant wave height
$h_{\zeta F}$	Amplitude of transfer function
J	Wave power level
K	Retardation function
k	Wave number
K_k	Kalman gain
m_{11}	Mass of plate

m_{22}	Mass of disc
P_0	Initial value of estimation error covariance
P_a	Upper bound for power
P_k	Estimation error covariance
P_w	Wave power
Q_k	Process covariance matrix
R_i	Intrinsic impedance
R_k	Measurement covariance matrix
S	Wave spectrum
T_p	Peak period
u	control vector
V	Volume of wave energy converter
v_k	Measurement noise
w_k	Process noise
z	WEC displacement
$\mathbf{M}$	Mass matrix

Contents

List of Figures

List of Tables

Chapter 1

Introduction

The Ocean Oasis Wave Energy Converter (WEC) stands as a contribution to the debate on how to create a more sustainable future. Two global challenges are adequate supplies of both useful energy and fresh water. At the same time, the amount of greenhouse gases caused by emission from energy production should be decreased. The device studied in this thesis utilizes energy in the ocean waves directly for desalination of seawater, hence produces fresh water in an environmentally friendly manner. The quote below enlightens the importance of finding ways to produce clean drinking water.

Universal access to safe drinking water and water resources is an imperative that cuts all internationally agreed development objectives, including Miullennium Development Goals. Improving access to water improves health and education outcomes. It increases agricultural productivity. It is a force for gender equality and women's empowerment.

- Ban Ki-moon, Secretary of the United Nations (2012)[1]

1.1 Motivation

It is desirable to maximize the amount of power extracted from the waves, while at the same time producing fresh water. This may be done by developing a structure design for optimum power extraction. However, the design can only be optimized for one sea state. For several WEC types a controller may be installed with the goal of influencing the oscillatory motion to achieve optimal or sub-optimal power outtake from the waves for all sea states. This is done by controlling the WEC into resonance with the wave.

[1] *The United Nations World Water Development Report 4: Managing Water under Uncertainty and Risk.* (2012)

Many of the control algorithms developed for WECs require future information of the incoming wave. In order to control the WEC into resonance, appropriate control action must be applied for the whole wavelength of each wave. Thus future wave patterns may be estimated quite accurately. It is not enough to have information about present and previous values. For regular waves the incoming wave is known, thus finding the oscillatory motion which optimizes extracted power is trivial. However, in the case of irregular waves, the incoming waves are unknown and random. This results is a prediction requirement. Hence, short time prediction of the oncoming waves an important problem in the field of wave energy.

1.2 Previous Work

The Ocean Oasis is a modified version of the DynOcean wave energy conversion concept which was originally an idea by Thomas B. Johannessen. DynOcean is a combined wave energy converter (WEC) and desalination device. It was meant for operation in West-Africa, where there are areas with water scarcity. The DynOcean buoy is a two-body WEC, which consists of an inner disc inside of the moonpool of an outer buoy. Energy is extracted from the relative motion in heave, pitch and roll between the two bodies, caused by the incoming waves. The energy is extracted by piston pumps and fresh water is produced directly, without conversion to electric energy. Fresh water is produced from seawater by a reverse osmosis process. The concept is described in Johannessen, Brandsvoll & Palmstrøm (2011), where the authors analyses the vertical relative motion between the two bodies and concludes that the WEC can deliver desalinated water at a relatively low cost.

Hydrodynamic model tests were completed during the Master's Thesis work of Andreas Palmstrøm and Rolf Anders Brandsvoll (Palmstrøm & Brandsvoll 2011). The performance and feasibility of the DynOcean buoy was investigated, in addition a numerical model of the device that reproduced the results from the model test in the time domain was produced. The model test results indicated that the DynOcean buoy concept was viable, with an estimated power output of 180 kW for the best buoy configuration.

Inspired by the DynOcean, the Ocean Oasis wave energy converter was developed during the DNV GL summer project 2014. The shape of the hull was changed so that it would make a better wave maker. The modifications were inspired by Berkely Wedge Madhi, Sinclair & Yeung (2014). The lower part of the hull was designed slimmer than the hull of the DynOcean. Different alternatives were tested and it was concluded that the shape shown in Figure 3.2 was the best wave absorber.

In addition, a storm handling system was developed for the Ocean Oasis. The WEC was not dimensioned to operate in extreme conditions. In extreme conditions the WEC should go into survival mode. In survival mode the ballast water would be shifted down to an extra set of tanks in the bottom of the structure. In addition winches would be installed so that the disc could be elevated and pulled against a rudder covered steel rail. An air cussion would

be sealed in the moon pool, that would contribute to the damping and decrease motions.

Some other analyses done during the DNV GL summer project were risk analysis, an assessment of environmental impact, financial analysis and market analysis. It was concluded that the project would give a return on investment and net present value, both of which were highly promising.. The Ocean Oasis was able to produce water at a cost of USD 0.5 per m^3 of freshwater. In addition, the Ocean Oasis was able to produce fresh water at a cost lower than for a typical desalination plant and lower than the DynOcean.

The work on Ocean Oasis was continued by Eirik Schultz, participant in the DNV GL summer project, in his project thesis (Schultz 2014). The main focus of this project was to analyse the possibility of increasing power output by enhancing the control system. The control method proposed was latching, which is a common method for optimal control of WECs. A simulation model was developed so that the potential benefits from latching control of the Ocean Oasis in regular monochromatic waves could be assessed. The results of the simulation indicated that the total energy increase from applied latching control across a range of frequencies was neglectable. However the latching control did result in increased relative motion between the buoy and disc. It was unknown what the limiting factors were on power output effect of latching. This would be an interesting topic for further studies.

1.3 Main Contributions

The contributions of this thesis are focused upon real-time control and estimation development for the Ocean Oasis. The development of the estimator algorithm is emphasized. A concept study of a Latching control algorithm was studied previously and extended to real-time applications in irregular waves in this thesis. An estimation setup was developed and an estimation method was suggested. Simulations were conducted to validate correct performance of the mathematical model, and then the mathematical model followed by simulations that focused on testing the performance of controller, estimator and full system.

- Conducting a review of previous scientific work on the topic
- Extending the mathematical model for the WEC to time-domain and irregular waves
- Calculating the forces working on the WEC in time-domain and irregular waves
- Extending the developed control algorithm to include the effects of irregular ocean waves
- Developing an estimation setup for the WEC
- Developing an estimator algorithm
- Validating the performance of the uncontrolled model and the controlled model through simulations

- Testing the performance of the Latching controller, Extended Kalman filter and full system performance

Due to lack of simulation data for the Ocean Oasis, the DynOcean wave energy converter data was utilized for the simulations, which is a similar concept.

1.4 Outline of the Thesis

This Master's thesis is built up around the modeling and simulation tests of control and estimation algorithms of the Ocean Oasis in real-time.

Chapter 2: A summary is given of the information retrieved during the literature review. The focus of this chapter is to establish an overview of the work done in the field of wave energy extraction from sea waves. A general review is conducted, but the focus has been on control and estimation of wave energy converters.

Chapter 3: The wave energy converter concept of interest is presented and relevant concept and cite inforamtion is stated.

Chapter 4: The relevant theory of ocean waves and wave energy extraction is presented and utilized in following chapters.

Chapter 5: Mathematical modeling of the wave energy converter and the forces working on the body is carried out.

Chapter 6: The chapter focuses on control system design. Optimum control condition is explained and the Latching control algorithm is given.

Chapter 7: An estimation setup is suggested and an Extended Kalman filter estimation algorithm is developed.

Chapter 8: This chapter presents the simulation and model tests setup and results. Simulations and model test are performed for both regular and irregular waves.

Chapter 9: The final chapter presents the main conclusions of the work and provides suggestions for further work.

Chapter 2

Wave Energy Converter Background

This chapter gives a short summary of general information about wave energy converters retrieved as a part of the litterature review. The focus has been on attaining a general overview of the work done in the field of wave energy conversion and future potential. Information about ocean waves, control and estimation is given in separate chapters. Fresh water production is out of the scope of this thesis. However a short section about environmental concerns is included.

2.1 A Brief Historical Account

For more than two centuries, inventors have proposed many different devices for utilizing wave power for human purposes (Falnes 2007). The first patent on a wave power device was filed in 1799 (Ross 1995). However, after the First World War petroleum became the most important modern source of energy and the interest for wave energy utilization faded.

In the late 1940s, however, Yoshio Masuda, a Japanese wave-power pioneer redeveloped interest in the topic and started testing and developing wave-energy devices. The oil crisis in 1973 was an important milestone for the wave energy development, amplifying the interest in alternative energy sources (Cruz 2008). Many researchers at different institutions took up the subject. Pioneers like Stephen Salter in Edinburgh and Kjell Budal and Johannes Falnes in Norway initiated wave power research. In the US Michael E. McCormick also did wave power research. Large government funded programs were started in the date 1970s in the UK, Sweden and Norway, latterly also in other countries (Falnes 2007). In this period a lot of research was done and basic understanding of wave energy was developed.

Two landmark papers were published in the journal Nature. One paper by Stephen Salter from the University of Edinburgh, who proposed a design which has since been famously known as the Salter Duck (Salter 1974). His narrow-tank tests revealed two-dimensional efficiencies in excess of 80 percent effectively conveying the message that it is possible to extract a large fraction of energy from the waves that are incident of the device. The other paper was by Budal and Falnes from the Norwegian Institute of Technology (NTH, now

NTNU), who introduced the term 'point absorber' to classify devices with horizontal dimensions much smaller than the wavelength. They also introduced the parameter 'absorption length' (now better known as 'capture width'), defined as "the width of a wavefront across which passes an average amount of power equal to that converted by the point absorber," and went on to show the remarkable result that it is possible for a point absorber to have an absorption length greater than its dimension.

Much of the fundamental theory of wave energy absorption was laid out in the period which spanned roughly from the mid 1970s to the mid 1980s. In the early 1980s the price of petrolium declined, and the government funding reduced immensely in many countries (Ross 1995). As a consequence the development and innovation in the field of wave energy decreased. However, some first generation prototypes were tested in the sea.

With growing awareness of the negative impacts of fossil fuels on global warming, interest in wave energy was renewed. In 1991 the European Commission agreed to include wave energy in their Research and Development Program of Renewable Energy. Since then, multiple wave power projects have been initiated and a manifold of different ideas for utilizing wave energy have been proposed. Many of these are at the R&D (research and development) stage, with only a small range of devices having been tested at large scale, deployed in the oceans. However, these devices are heavily dependent on government subsidies to continue operations until prototypes are ready for major installations. There is a lack of convergence on the best method for extracting energy from waves. Generally innovation has focused on the concept and design of the primary interface, in additions how to best optimize the power train is an important question.

Europe still regards the WEC technology to be in the R&D stage. However, at least two designs have been incorporated by European utilities for prototype purposes. In the U.S. several installations are planned along the coasts. China, India and Japan are also involved in wave energy; however their involvement is mostly institutional (Muetze & Vining 2006).

2.2 Environmental Concerns

In 1987 the UN report "Our Common Future" was issued by the UN World Commission on Environment and Development (also called the Brundtland Comission). At this time there was a high degree of realization and international consensus that forced changes should be made towards a more sustainable path of development in order to avoid collapse of several natural resources (Hals 2010). In the report the concept of sustainability was introduced. The use of recourses are sustainable if they are consumed at a lower rate than they are formed on earth, and their use does not lead to harmful emissions.

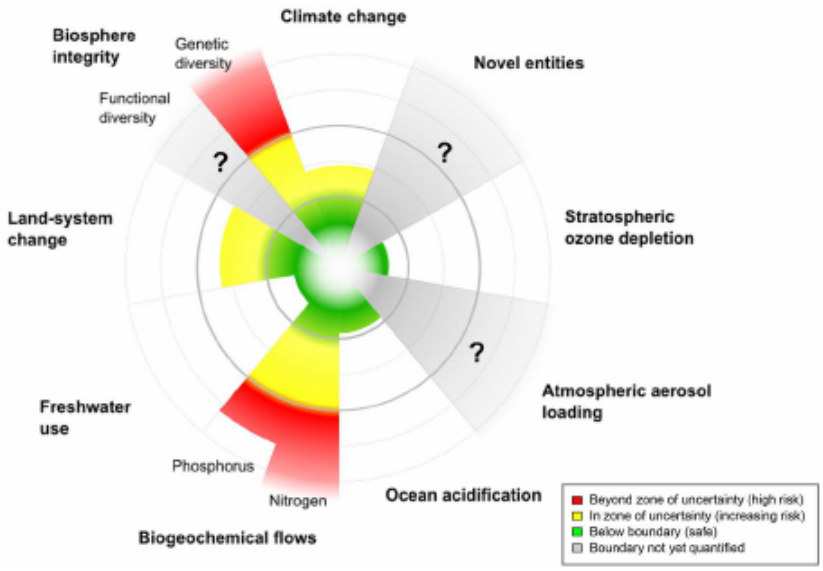

Figure 2.1: The current status of the control variables for seven of the nine planetary boundaries (Steffen et al. 2015).

Still there is a growing focus on the environment in many countries of the world. It has been apparent to people through scientific research that human activity affects the processes of the earth, the Earth System (ES). Some argue that the ES's resilience is threatened by the way humans act and that our influence may cause changes which are destructive for life on earth as we know it. Not knowing the actual effect of human activity it is natural to question the necessity of making changes, of what should be done and to what extent. Many scientists have explored this question and there seems to be a growing consensus that humans are having a negative effect on the earth, and that some changes should be done to reduce this effect.

Many contributions can been mentioned on this topic. One recent supplication to the debate is given by a group of scientists in Steffen, Richardson, Rockström, Cornell, Fetzer, Bennett & Biggs (2015). They develop the planetary boundary (PB) framework, which aims to define a safe operating space for human society based on our evolving understanding of the functioning and resilience of the ES. Nature is in constant change. Typically the processes tend to stabilize in equilibrium positions in between periods of change, where both the equilibrium and changing phases are of varying length. The precautionary principle suggests that human societies would be unwise to drive the Earth System substantially away from a Holocene-like condition. The Holocene is the current geological epoch of the earth. In recent time humans have improved their ability to observe, but also predict these processes scientifically. These skills have lead scientists to explore the opportunity to influence the change, and possibly prevent the Earth System from leaving the current equilibrium state of the Holocene-like condition.

Figure 2.1 illustrates the theory of the research group. The earth is through to have nine

planetary boundaries, and seven of them are shown in the figure. The green zone is the safe operating space, the yellow represents the zone of uncertainty, and the red is the high risk zone. According to Steffen et al. (2015) the climate change is in a zone of uncertainty and increasing risk. The climate change refers to the increasing average temperature caused by an increasing CO_2 level in the atmosphere, which is again partially caused by large human emission. It is suggested that this challenge should be met in order to keep livable conditions for humans on earth. One suggestion for meeting this requirement is to develop more environmental friendly energy source alternatives. Some suggestions for such energy sources are renewable energy sources, for example solar, wind and wave energy.

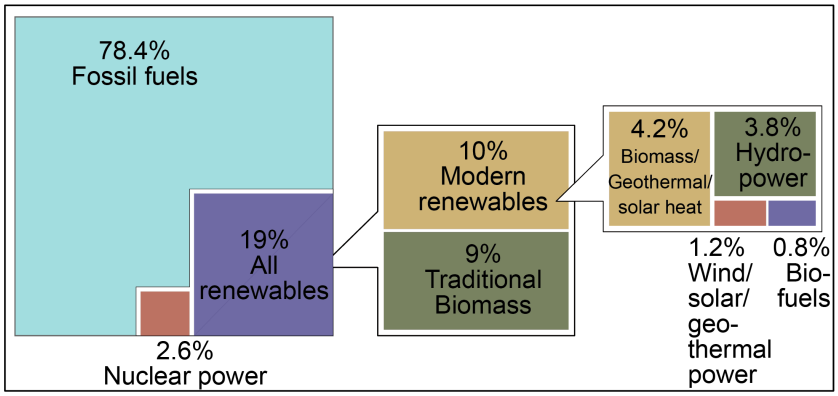

Figure 2.2: Estimated renewable energy share of global final energy consumption, 2012. Remake from Ren21 (2014).

Today, the world's main energy sources are fossil fuels (Ren21 2014). From Figure 2.2 it can be seen that fossil fuels contribute with about 78,4 percent of the global energy consumption, while renewable energy sources only 19 percent. Oil and gas work great as energy sources. However, they are non-renewable, which means that they will run out eventually. As mentioned above, the emissions contribute to climate change. It is therefore important that fossil fuels are substituted with more sustainable alternatives.

2.3 Characterization of WECs

There are no set rules for modeling WECs, as the structures vary much in shape, size and function. However, the methods of wave energy conversion has been systematised by several researchers. Common ways of characterizing the WECs are given in WEC review papers like Drew, Plummer & Sahinkaya (2009), Falnes (2007) and Thorpe (1999). The WECs are characterized in manner of type, mode of operation and power take off method. A summary of the grouping is given below.

2.3.1 Type

The characterization of different types are based on the form and function of the WEC. A description of the three main types are given below. Figure 2.3 gives an illustration of the concepts.

Attenuator Attenuators 'ride' the waves while lying parallel to the predominant wave direction.

Point absorber The point absorber is small of dimension relative to the wavelength of the incident wave. Due to the small dimensions the wave direction is not of importance. There is developed two types of point absorbers. One that float on the sea surface and a submerged concepts relies on pressure differential.

Terminator The terminator device physically intercepts the waves, while having their principal axis perpendicular to the predominant wave direction, thus parallel to the wave front.

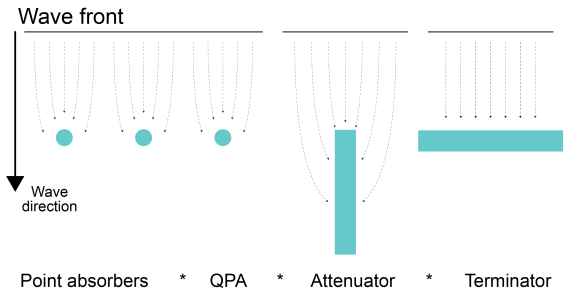

Figure 2.3: Illustrations of different types. Remake fromFalnes (2015).

2.3.2 Modes of Operation

There are also different ways of converting the wave energy into useful energy. Four common modes of operation are described below. The modes of operation give information about the manner of the wave energy conversion. Some of the modes appearing often are explained below.

Submerged pressure differential For a submerged point absorber one way of generating power is using the pressure difference above the device between wave crests and though. This mechanism is named submerged pressure differential. The device consists of two parts, a movable upper cylinder and a lower cylindrical chamber which is filled with air and fixed to the sea floor. As a crest passes over the device, the upper cylinder is pressed down, which causes compression of the air within the cylinder. Accordingly, the upper cylinder is rised when a trough passes, as the pressure above the device is reduced. This type of device will not be subject to the threatening slamming forces induced on the floating devices.

Oscillating wave surge converter An oscillating wave surge converter is generally comprised of a hinged deflector, positioned perpendicular to the wave direction (a terminator), that moves back and forth exploiting the horizontal particle velocity of the wave.

Oscillating water column An oscillation water column (OWC) consists of a chamber, applying pressure on the air within the chamber. This air escapes to atmosphere through a turbine. As the water retreats, air is then drawn in through a turbine. A low-pressure wells turbine is often used in this application as it rotates in the same direction irrespective of the flow direction, removing the need to rectify the airflow. It has been suggested that one of the advantages of the OWC concept is its simplicity and robustness.

Overtopping device An overtopping device captures sea water of incident waves in a reservoir above sea level, then releases the water back to sea through turbines.

2.3.3 Power Take-off

The PTO system is the internal machinery of the WEC that converts mechanical motion into some desired output. The output depends on application and could be electricity, pressure, and so on. Various PTO systems have been researched and implemented in the past, ranging from directly driven turbines, pneumatic turbines to hydraulic circuits connected to induction generators. Figure 2.4 shows an example of a PTO system for a one degree of freedom floating system.

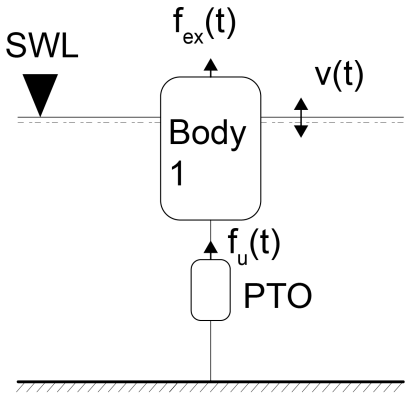

Figure 2.4: A one-degree-of-freedom floating system for wave-energy conversion. The lower side of the power take-off is anchored to the sea bed, which creates a relative motion that is the cause of power generation. Remake from Ringwood et al. (2014).

Electrical linear generation The possibility of using electrical linear generators has been investigated. It has been concluded that these typed of machines are too heavy, expensive and inefficient. However, new technology has been developed utilizing magnetic materials and

reducing costs of frequency converting. This makes electrical linear generation an alternative technology or the PTO system.

Hydraulics Hydraulic systems are well suited to absorbing energy from ocean waves because the waves apply large forces at slow speeds (Henderson 2006). If size and weight are an issue it is advantageous to use hydraulics. With a pressure of for instance 400 bar this will create forces that are larger than for electrical machines.

Rotary generator types On-line synchronous generators are used by traditional power stations. The variable energy input must be converted into smooth electrical power operated at the frequency of the grid connection. However, the generators used may also be of variable speed, depending on the conversion system (Drew et al. 2009).

Turbine transfer The PTO system of devices where the flow of either sea water or air drives a turbine is named 'turbine transfer'. The turbine is directly connected to a generator. The types of devices using direct transfer include OWCs and overtopping devices.

2.4 Wave Energy Concepts

Design concepts for extracting power from ocean waves are many. EMEC (2015) shows an overview of today's wave energy converters and there are listed 176 concepts. There are many patents as well. However the industry at a whole is quite immature (Hals 2010), seeing as most of the concepts are in a development stage and have not been full scale tested.

Salter's Duck The Salter's Duck is developed and tested by Stephen Salter (Salter 1974). It is an example of a terminator type WEC. When the waves impact the duck, rotations of gyroscopes inside it provide electrical energy through an electrical generator. The Salter's Duck is one of the most efficient devices and is able to absorb 100 percent of the energy contained in a wave (Baker & Mueller 2001). Configurations to use the Salter's Duck for desalination is also considered and developed.

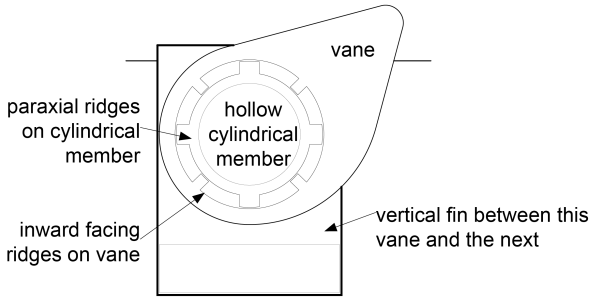

Figure 2.5: Scetch of Salter's Duck. Remake from Salter (1974).

Budal's buoys During the 1970s Budal and his research team at NTH, Trondheim, tested a number of point absorbers. One example of such a buoy is given in Figure 2.6 (right). There were several suggestions of different concepts and their performance was tested. Figure 2.6 (left) shows a model test of one of the concepts. These studies contributed greatly to research and development in the field of wave power. For instance the idea of latching control was developed in this period (see Section 6.3 for information about latching control).

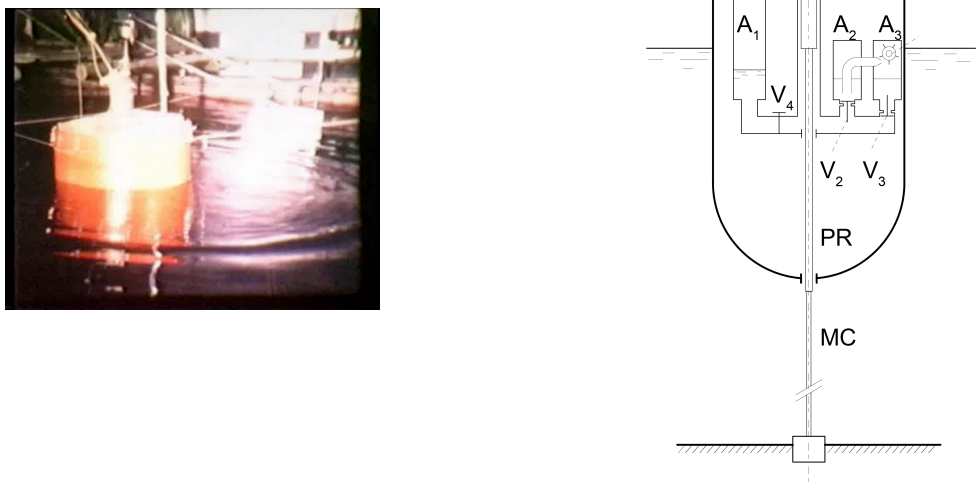

Figure 2.6: Left-hand-side shows a picture of model test of Budal's concept E. Right-hand-side shows concept sketch of Budal's concept E. Remake from Falnes (2015).

Pelamis The Pelamis is a commercial wave power system operating in Northern Portugal. The technology is developed by Pelamis Wave (formerly OPD) in Scotland. The pelamisis is an example of an attenuator. It looks like a snake in the sea. The device is made up of four floating cylindrical segments joined together by hinges. The motion of the waves induced movement in the joints between each segment. The movement is resisted by hydraulic rams which pump oil through hydraulic motors driving electrical generators to produce electricity (Fernandes n.d.) . The Pelamis was first tested full scale in 2004. Later a second prototype was developed and it was the first wave power machine to be purchased by a utility company. It generated 750 kW (EMEC n.d.).

Figure 2.7: Pelamis wave energy converter (NNMREC 2015).

Other LIMPET (Land Installed Marine Power Energy Transmitter) is an example of an overtopping device OWC. It was installed at the shoreline at Islay, Scotland in 2000. It is the world's first commercial wave power device to be connected to the UK National Grid. The capacity of LIMPET was 500 kW, later downgraded to 250kW. The device was developed by Wavegen in cooperation with Queen's University Belfast. Other established concepts are Archimedes Wave Swing (Drew et al. 2009), which is a submerged pressure differential, the Wave Bob which is an point absorber floating in the surface, the Aquamarine Power-Oyster and the Wave Dragon. The last three of which are described at Fernandes (n.d.).

2.5 The Challenges of Wave Energy Converters

Utilizing WEC technology as an energy source is problematic. One challenge is due to the high degree of variation in the waves. The waves are slow (~ 0.1 Hz), random, and high-force oscillatory motion(Drew, Plummer & Sahinkaya 2009). This causes challenges of the conversion into useful motion to drive a generator with output quality acceptable to the utility network. The power levels vary according to the variations in height and period. Thus this variable input must be converted into smooth electrical power output. This necessitates an energy storage system, or other means of compensation. In addition the direction of the waves changes. The mooring must then be installed such that the WECs align themselves accordingly on compliant, or they should be symmetric. In the near shore area, the directions of waves are highly determined by the natural phenomenon of refraction and reflection. This problem is not found in the case of wind power since the wind only blows in one direction at one time.

Moreover, these variations cause challenges of design. The device and corresponding systems have to be rated for the most common wave power levels in order to operate efficiently. The WEC should be designed for good wave absorption. This type of design is dependent on

the incoming waves. Everything from the hull to the machinery should be properly designed for the operational states. However, with variable incoming waves, the design will only be optimal in some sea states. This problem can be addressed by considering sophisticated control systems.

In addition, to being highly variable, the waves cause an extensive environmental impact on the WEC. Thus the WEC must be structurally robust and strict environmental requirements must be met. A common problem for full scale testing is that the test model has been ruined due to the environmental impact. Another environmental challenge is the correctional environment, which causes the need for the WEC to be anti-corrosion robust. Hence, in order to be able to commercialize a concept, a robust structure must be made and at the same time the requirements of material use and structure for absorption must be upheld. The WEC should be designed for extended component lifetime.

All these requirements bring us to the challenge of cost. The design should be made so that the costs of investment, operation and maintenance (in terms of money, resources and energy) can be justified by the availability and potential earnings (Hals 2010). The WEC must be robust and contain a comprehensive machinery, at the same time it can not be too expensive. In addition, there is a need for smart solutions for installation, operation and maintenance. Bringing the electricity onshore is extremely expensive. Also the electrical system is subject to due currents, tides and other factors. On the whole one great challenge is reducing the cost-benefit ratio the WEC low cost-benefit ratio.

2.6 Potential of Wave Energy

The ultimate source of wave energy is the sun. Uneven distribution of pressure regions in the Earth's atmosphere are created which causes movement of the air (Karimirad 2014). When the air blows over the seas and oceans boundary layers are created over the water surface and water particles start to move, creating waves. The energy in the waves is of higher density than that of the wind which they are created from. It is estimated that there is 15-20 times more available energy per square meter for waves than for wind or solar.

Figure 2.8 shows the relative total amount of all the renewable energy resources of the world. As can be seen from the figure there is most solar energy. There is 100 times more wind energy than wave and tidal. The utilization factor for wave power – the ratio of yearly energy production to the installed power of the equipment is typically 2 times higher than that of wind power. However, a wind power plant only delivers energy corresponding to full power 25 percent of the time. A wave power plant is expected to deliver full potential 50 percent of the time.

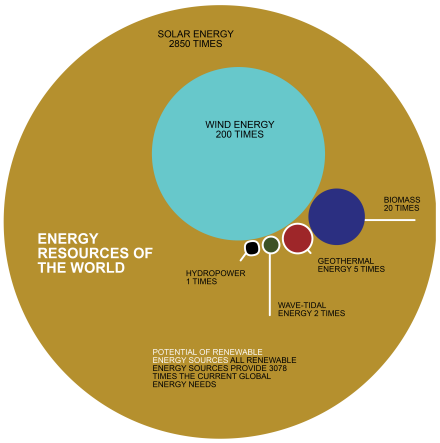

Figure 2.8: Renevable energy recources of the world. Remake from Hals (2010).

Some feasability studies have been done on the topic of wave energy conversion. It is estimated that there is approximately 2 TW wave energy in the entire ocean, which is is of the same order of magnitude as world electricity consumption (Barstow, Mørk, Mollison & Cruz 2008, Thorpe 1999). Estimates conclude that marine and tidal currents combined contain about 5 TW of energy. However the exploitable limit of wave power is probably at most about 10-25 percent of the recourse. This makes the energy resource a potential contributor to the human energy demands, but it can not be the only supply.

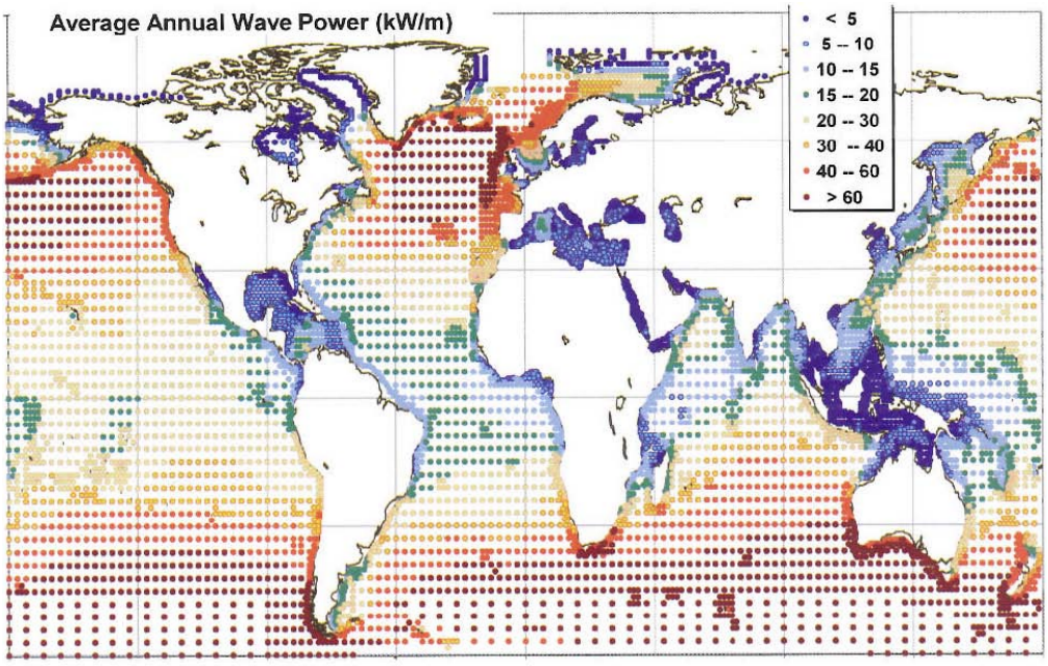

Figure 2.9: Average Annual Wave Power (Cruz 2008).

Figure 2.9 shows the wave power at different locations of the world. The potential of WEC

farms at different locations can be predicted from the figure. Similar to the oil resource, the wave energy amount is unevenly distributed. This wave energy can travel thousands of miles with little energy loss, so small inputs over a large ocean can accumulate and be harvested at or near the ocean's edge (Muetze & Vining 2006). Hence, the wave energy that reaches the shore in some country has traveled from far offshore. If the energy is subtracted by a WEC farm offshore, the wave energy will not reach shore. This fact arises the question stated by Falnes Falnes (2015), which will be an important early step in global WEC development.

Who owns the waves?

However, there has not been a huge interest for claiming wave energy. This might be due to the fact that wave energy, at its present stage is not beneficial. Figure 2.10 from the World Energy Council report from 2013 shows the cost of wave energy relative to other common energy sources (Counsil 2013). From the figure it can be seen that wave energy is quite expensive compared to energy sources like oil and gas, and even wind. This creates a challenge for further development of WEC technology. Every project is highly dependent on governmental subsidies. However, the hight price might be due to the fact that this industry is immature compared to the other energy types. There are different opinions on whether wave energy has potential as a future energy resource or not. The technology faces immense challenges, as discussed in Section 2.5. However the energy source is 'clean' and the global society is in search of new energy alternatives as discussed in Section 2.2 . At this point WEC technology is not competitive compared to solar and wind technology, however it might be beneficial with a combination of all the renewable energy sources in order to meet the global energy demand in an environmentally friendly manner.

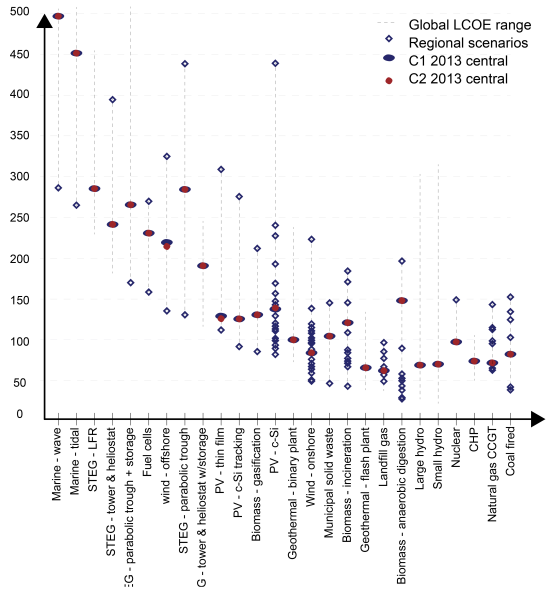

Figure 2.10: Global levelised cost of energy in 2013 [USD/MWh]. Remake from Counsil (2013). Q1 = first quarter, Q2 = second quarter, LCOE = levelized cost of electricity.

2.7 Common Control Methods

There are several approaches to controlling wave energy converters. The strategies vary a lot for different types of structures and modes. In this section some of the most common control methods for point absorbers and heaving buys will be mentioned. The goal is to control the motion of the WEC such power outtake is maximised. In general, it can be said that the goal it to 'push' the WEC into resonance with the wave. For further elaborations and mathematical formulations of optimal control see Chapter 6.

Reactive Control There are two methods of controlling to achieve optimum condition of the WEC motion, as described in Section 6.1. One method is called 'Reactive Control' or 'Complex Conjugate Control'. In this case one controls to achieve the optimum condition (6.10). This type of control requires reactive machinery forces. Machinery forces are reactive if the associated power flow is both in and out of the system. By requiring that the machinery force matches the intrinsic reactance of the body, the device can be forced to oscillate with optimal phase (see (Falnes 2002) for further explanation). Large forces and power flow are required and for this reason reactive control is difficult from an engineering point of view. In addition, the control strategy requires bidirectional flow which makes it necessary for the generator to operate as a motor in periods (Tedeschi & Molinas 2010). Stability margins should be considered, as the system can become unstable (Hals 2010). An alternative is approximate complex-conjugate control. In this control method causal approximation to the optimal force are found. For instance constant hydrodynamic parameters corresponding to the values obtained for an angular frequency ω_k that can be optimized for each sea state.

Phase Control The second method of controlling to achieve optimum condition is phase control, where the desired machinery force depends on the oscillation phase. In this case one is controlling to achieve the optimum condition (6.11). This condition means that the oscillation velocity needs to be in phase with the excitation force, and secondly, the velocity amplitude $|\dot{z}| = |F_e|/2R_i$.

Latching and Clutching Control If the optimal conditions $\alpha(\omega) \geq 0$ can not be achieved, and $E_{u,P} > 0$ see equation 6.9, the result is suboptimal control. One example of such suboptimal control is Latching control. Latching belong to the class of discrete control algorithms, that is, algorithms that implement an on/off PTO force, usually through a braking mechanism. In this control method the buoy is blocked from moving in parts of the period to obtain optimal phase. In that way optimal phase condition can be obtained without reactive power flow in the machinery. The challenge with Latching control is prediction the instances for latching and delatching of the body in irregular sea states. Latching control is discussed further in Chapter 6. Clutching is a type of phase control where the control decouples and couples the machinery so that the body may move freely in periods.

Passive Loading 'Passive Loading' or 'Resistive Loading' is the term characterizing a control system where the loading is pure resistive and time-invariant. The machinery force is restricted not provide reactive power, which results in a better phase relation between the excitation and the velocity. This type of converter has been used for testing prototypes and as a reference in performance studies (Hals 2010).

Model Predictive Control (MPC) By using a discrete-time model of WEC combined with a prediction of the excitation force, the performance can be optimized over a short period T_h at the time. For instance, the optimization can be carried out by solving a quadratic programming optimization with respect to power output (Bjørnstad 2011). MPC has the ability to consider constraints on the system forces and limitations in system velocity and position in the context of current future desired velocity or position (Hals 2010).

Tracking of approximate velocity Another way of utilizing phase control is tracking the optimal velocity in to achieve an approximation of the intrinsic mechanical resistance $R_i(\omega)$. If it is replaced with a constant value the optimal condition becomes $\dot{z} = \frac{F_e}{2R_i(\omega_k)}$. Then the tracking can be realized by implementing a P or PI controller(Hals 2010).

2.8 Sea State Estimaiton

Several methods for exists for measuring the sea state. Moored directional buoys have been the main method employed for sea state estimation since the 1970s Bjerregård (2014). This method is mostly used in coastal areas of reasonably shallow water depts, where the mooring installations is no problem. However, these buoys are subject to damage and loss and require an extensive network to cover the area of interest. An alternative method being investigated in the literature is the wave buoy analogy where the vessel is considered as a wave buoy.

Sensors are installed on board the vessel. Similarly to the directional buoys, the thethod utilizes inertial measurements for the sea state estimation. Ship responses are used as a basis to estimate wave spectra and associated sea state parameters see Nielsen (2008) and Hua & Palmquist (1994). However, large vessel with complicated response transfer functions compared with a buoy, the inverse problem of calculating the wave spectrum from the motion spectrum is no longer trivial. Figure 2.11 illustrates the two methods.

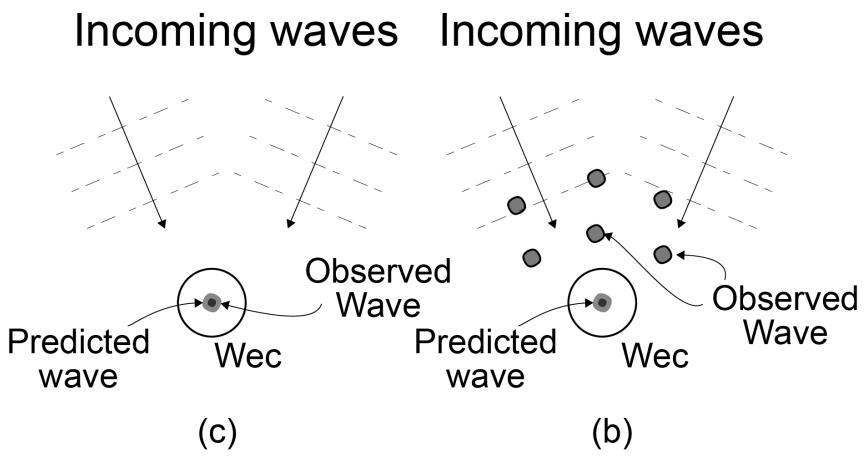

Figure 2.11: Two main approaches to wave forecasting. (a) Prediction based only on local single-point measurements. (b) Prediction based on up-wave measurements. Up-wave prediction requires the addition of extra sensors, while the time series approach in (a) simply forecasts future excitation force based on the measured device motion. Remake from Ringwood et al. (2014).

Other measurement methods are developed in more recent time. One commercial product is X-band radar, which measures three dimensional wave spectrums used for e.g. navigation. See Wavex® by the company Miros. This technology is quite expensive. Another method is Ocean Surface Topography measured form satellites as suggested by Giron-Sierra & Jimenez (2010). This has been tested by three satellites previously and the Jason-3 is scheduled for launch 2015 NASA/JPL (n.d.) extensive network of such satellites could potentially provide global sea state information live to vessels.

With knowledge of the wave response transfer function fro the vessel, the inverse can be used to solve for the wave spectrum from the measured motion spectrum. Conceptually, two methods are considered: (1) Parametric Modeling which assumes the wave spectrum to be composed of parameterized wave spectra, so that the underlying wave parameters are sought from an optimization, or (2) Bayesian Modeling (non-parametric) where the directional wave spectrum is found directly as the values in a completely discretized frequency-directional domain by minimizing posterior expected loss function Nielsen (2005). In general the methods are based on linear spectral analysis which assumes a linear relationship between the wave excitations and the ship responses.

The forecasting necessity related to wave energy converters is the computation of an optimal reference signal in order to achieve maximum energy extraction. The most common methods utilize up-stream measurements and are described in Fusco (2009). The first approach found in literature was the Kalman Filter, provided by Budal et al. (1979). Another common method is Deterministic Sea Wave Prediction (DSWP), which is described in Belmont et al. (2006). The method of makes use of deterministic linear filters for the wave prediction based on wave observations collected at several locations. A third forecasting method utilized for WECs are digital filters for determination of the future incident wave on a device from distant pressure measurements. In Voronovich et al. (2005) spatial wave forecasting through a linear harmonic model fitted to distant wave elevation observations is utilized. Also it has been tested to predict the wave excitation force, treated as as univariate time series problem, that only part observations at the prediction site are utilized.

Chapter 3

Concept and Modeling Information

The first step of my master thesis was gathering important information about the concept of interest. In this chapter the concept is described, and relevant information is given.

3.1 DynOcean

The DynOcean consists of two parts, an axisymmetrical buoy enclosing a large moonpool which is open to the sea below and a disc floating in the moonpool. The disc covers the surface of the moonpool and is connected to the buoy with vertical pistons. The pistons are part of a piston pump which pressurizes the seawater which goes directly through a Reverse Osmosis desalination plant, which is located in the top section of the buoy. Figure 3.1a and 3.1b show the DynOcean concept.

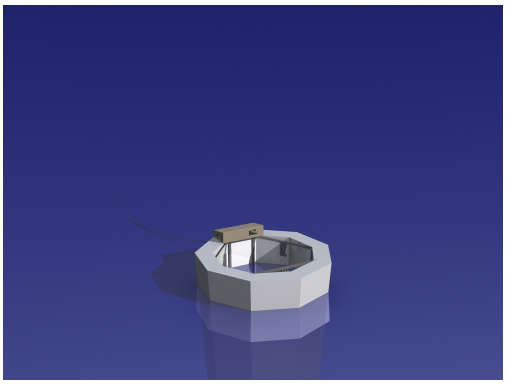

(a) DynOcean wave energy conversion concept.

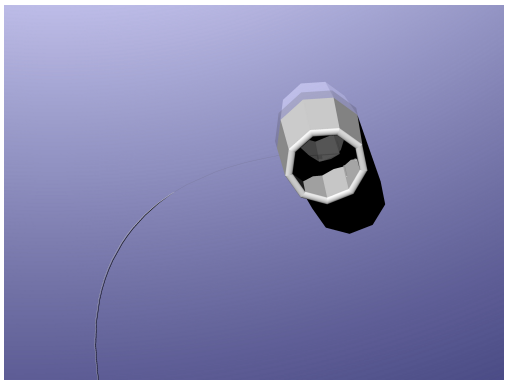

(b) Below water view of the plant.

The buoy and the disc have different natural periods in heave. If we have excitation at periods between the natural periods of the two systems, this gives large relative motions. Rotation in roll and pitch will also give contributions to the relative motion. Energy is captured through these relative motions by the pistons connected to both the buoy and the disc in the moon pool. In this way the energy runs the desalination process without being converted to electricity.

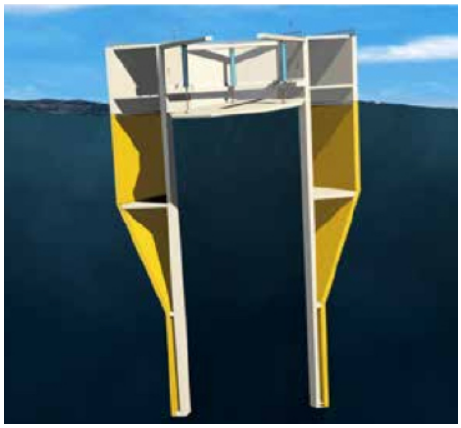

Figure 3.2: Ocean Oasis wave energy converter (DNV GL 2014).

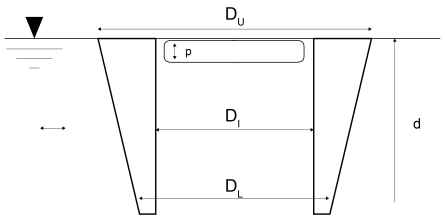

Figure 3.3: DynOcean dimensions. Remake from Johannessen et al. (2011)

name	*foo*
$D_U[m]$	24.0
$D_I[m]$	14.0
$D_L[m]$	17.0
$d[m]$	22.5
Displacement [Mt]	4060
Linear coefficient for power take-off , $C_1[kN(m/s)^-1]$	614
Values needed in verification analysis only(about SWL)	
VCG [m]	-9.0
Metacentric height [m]	3.8
Radius of gyration about vertical axis [m]	8.0
Radius of gyration about horizontal axis [m]	12.0

Table 3.1: DynOcean information(Johannessen et al. 2011).

3.2 Operational Site

The operational site for this wave energy converter is Cape Point, South Africa. Figure 3.4a shows an overview picture of the location of Cape Point and the specific location of the site

is indicated with a red circle in Figure 3.4b.

(a) Location of Cape Point (modified illustration form DNV GL (2014)).

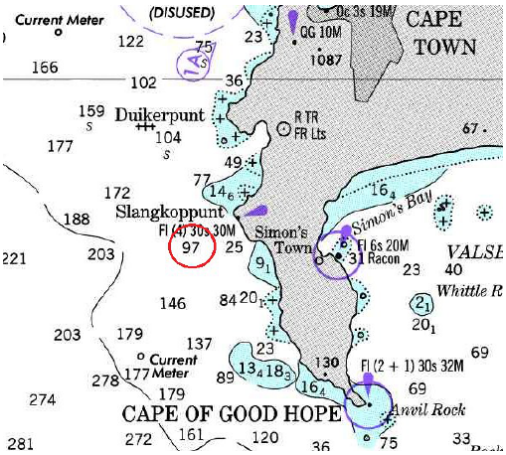

(b) Specific location of WEC (DNV GL 2014).

The JONSWAP was assumed to be an appropriate description of the sea state at the location of the Ocean Oasis. The spectrum was used on the form given in the equations 4.13 til 4.14. A scatter diagram of the long term distribution of wave periods and wave heights from the operational cite at Cape Point is given in DNV GL (2014). The scatter diagram is also given in table 4.1.

Hs[m]/Tp[m]	4-5	5-6	6-7	7-8	8-9	9-10	10-11	11-12	12-13	13-14	14-15	>15
11-12	-	-	-	-	-	-	-	-	-	-	-	-
10-11	-	-	-	-	-	-	-	-	-	-	-	-
9-10	-	-	-	-	-	-	-	-	-	-	-	-
8-9	-	-	-	-	-	-	-	-	-	0,001	0,001	-
7-8	-	-	-	-	-	-	-	-	0,001	0,001	0,001	0,001
6-7	-	-	-	-	-	-	-	0,001	0,002	0,002	0,003	0,002
5-6	-	-	-	-	-	-	0,001	0,003	0,008	0,008	0,009	0,006
4-5	-	-	-	-	0,001	0,002	0,007	0,016	0,022	0,024	0,013	0,008
3-4	-	-	0,001	0,002	0,002	0,008	0,023	0,054	0,067	0,046	0,024	0,014
2-3	-	0,002	0,008	0,004	0,008	0,030	0,079	0,125	0,092	0,046	0,021	0,016
1-2	-	0,002	0,003	0,003	0,008	0,027	0,049	0,046	0,020	0,012	0,006	0,007
0-1	-	-	-	-	-	-	-	-	-	-	-	-

Table 3.2: Scatter diagram for cite location (DNV GL 2014).

By using these values, an average weighted wave spectrum can be found according to equation 3.1 (DNV GL 2014). The individual spectrums are calculated according to the JONSWAP spectrum.

$$S_{Mean}(\omega) = \sum_{i=1}^{N} S_i(\omega) P_i \tag{3.1}$$

The sea state with the most frequent occurrence is the one with the characteristic values: $H_s = 2 - 3$ and $T_p = 11 - 12$. Therefore the sea state used in the calculations in this Thesis was chosen to be $H_s = 2.5$ and $T_p = 11.5$. The parameters of the spectrum were set to be:

$$\gamma = 3.3 \tag{3.2}$$

$$\sigma = \begin{cases} 0.07 & w \leq w_P \\ 0.09 & w > w_P \end{cases} \tag{3.3}$$

$$\alpha = \left[1 - 0.287 \ln(\gamma)\right] \frac{5}{16 g^2} H_S^2 \omega_p^4 = 0.33 \tag{3.4}$$

$$\tag{3.5}$$

These values were chosen in accordance with the DNV standard *Recommended Practice DNV-Rp-C205 - Environmental Conditions and Environmental Loads* (2010).

In my project the excitation forces on the boy for incoming frequencies were pre-calculated using the computer program WADAM by Thomas Johannessen (Johannessen et al. 2011). The values are given in Appendix A.

Chapter 4

Ocean Waves

The wave energy converter is meant to be oscillating in ocean waves. In this thesis the waves are described according to theory of hydrodynamics, with reference to texts like Faltinsen (1998) and Newman (1977) for further elaborations. Important results will be given and extensive derivations will not be conducted. Knowledge of advanced calculus is assumed.

4.1 Wave Model

Regular waves may be described as given in (4.1). A model for irregular, long crested waves can be found by modeling. To get irregular waves one uses the superposition principle and think that the wave elevation consists of n regular waves with different amplitude, frequency and phase. Then the wave elevation ζ_n for each wave component is given by the (4.2). The phases ε are modeled as stochastic variables, that are statistically independent and identical, rectangularly distributed between 0 and 2π. All the waves are summed up to a resulting wave given in (4.3). for deep water the equivalent equation is given by (4.4).

$$\zeta = \zeta_A \sin(\omega t - kx) \tag{4.1}$$

$$\zeta_n = \zeta_{An} \sin\left(w_n t - k_n x + \varepsilon_n\right) \tag{4.2}$$

$$\zeta(x,t) = \sum_{n=1}^{N} \zeta_{An} \sin\left(w_n t - k_n x + \varepsilon_n\right) \tag{4.3}$$

$$w_n^2 = g k_n \tag{4.4}$$

Variable	Description
ζ	wave elevation
ζ_A	wave amplitude
ω	angular frequency
k	wavenumber
x	is a position along the wave's direction of travel
t	time at which wave is described
ε	phase

4.2 Linear Wave Theory

A short summary of the assumptions, simplification ans results of linear theory is given in this section. The waves are described according to potential theory (Newman 1977). When applying potential theory, some the following assumptions are made

- Ideal or inviscid
- Incompressible
- Irrotational
- Small amplitude

Viscous stresses are significant only within a thin layer close to surfaces such as the ship's hull, if the Reynolds numbers are large. The viscous stresses are a consequence of large gradients in the fluid velocity, and these large gradients are only in the boundary layer, hence the fluid can be said to be inviscid outside of the boundary layer. Moreover, if the body's radii of curvature are large compared to the thickness of the boundary layer, the flow is relatively insensitive to the from of the boundary (Newman 1977). When the fluid is incompressible the motion takes place without loss of mechanical energy. The reason that the amplitude should be small is that the equations of the potential theory are linearized in order to find a solution. For big amplitudes, the equations given in the following might be inaccurate. For the studies in this thesis an additional assumption is as following

- Deep water

The water is deep when $h/\lambda > 1/2$. In this case the given in equation holds, which further simplifies the equation.

$$\frac{\cosh k(h+z)}{\cosh kh} \approx 0 \tag{4.5}$$

If these conditions are satisfied, the velocity potential can be derived (4.6) (Pettersen 2007). From this the particle velocity can be found from (4.7) and the pressure under the wave can be found from (4.8).

$$\phi = \frac{\zeta_A g}{w} \exp^{kz} \cos(kx - wt) \tag{4.6}$$

$$\vec{U} = (\vec{u}, \vec{v}, \vec{w}) = (\frac{\vec{\partial\phi}}{\partial x}, \frac{\vec{\partial\phi}}{\partial y}, \frac{\vec{\partial\phi}}{\partial z}) \tag{4.7}$$

$$p = -\rho\frac{\partial\phi}{\partial t} - \rho g z - \frac{1}{2}\rho|\nabla\phi|^2 \tag{4.8}$$

4.3 Statistical Description

The sea state is typically described in terms of the wave spectrim $S(\omega)$, which is a statistical representation. A wave spectrum gives information about the wave energy in waves for different frequencies. The theory of this section is written according to Myrhaug (2007). The spectrum can be plotted is divided into N components as illustrated in Figure 4.1. Then the energy in eah compinent, n, can be found according to (4.9).

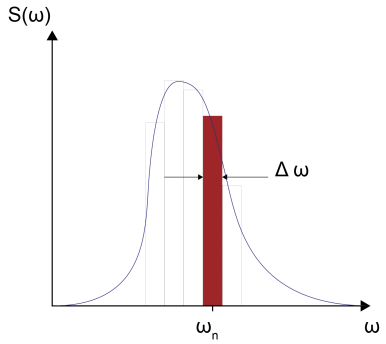

Figure 4.1: Wave spectrum, S(ω), divided into n components. Remake from Myrhaug (2007).

$$S(w_n)\Delta w = \frac{E_n}{\rho g} = \frac{1}{2}\zeta_{An}^2 \tag{4.9}$$

From the equation 4.9 and 4.10 the amplitude of the wave elevation of a regular wave of frequency ω_n is found if the spectrum is know. Furthermore, the wave elevation for each w_n can be found acordin to (4.11).

$$\zeta_{An} = \sqrt{2S(w_n)\Delta w} \tag{4.10}$$

$$\zeta_n = \sqrt{2S(w_n)\Delta w}\cos\left(w_n t - k_n x + \varepsilon_n\right) \tag{4.11}$$

Finally, the resulting wave elevation for a irregular wave can be found by summing up all the wave components of the sea state as in (4.12).

$$\zeta(x,t) = \sum_{n=1}^{N} \sqrt{2S(w_n)\Delta w}\cos\left(w_n t - k_n x + \varepsilon_n\right) \tag{4.12}$$

.

Often a standardized wave spectrums to model the sea states. One example of such a standardized spectrum is the JONSWAP spectrum, which is developed to describe sea states in the North Sea. The JONSWAP spectrum can be written in the from given in equations 4.13 and 4.14.

$$S(\omega) = \alpha\frac{g^2}{\omega^5}e^{-\frac{5}{4}(\frac{\omega_p}{\omega})^4}\gamma^{e^{-\frac{1}{2}\left(\frac{\omega-\omega_p}{\sigma\omega_p}\right)^2}} \tag{4.13}$$

where

$\gamma =$ peak parameter

$$\sigma = \begin{cases} \sigma_a & \text{for } \omega \leq \omega_p \\ \sigma_b & \text{for } \omega > \omega_p \end{cases} \tag{4.14}$$

$\alpha =$ parameter that decides the form of the spectrum in the high frequency part.

The peak period T_p corresponds to the peak frequency, which is the frequency that gives the peak of the wave spectrum graph. The connection between the two is given in (4.15).

$$w_p = \frac{2\pi}{T_p} \tag{4.15}$$

4.4 Energy in Each Wave

By assuming that linear wave theory holds, the energy in one regular wave the kinetic wave energy and the potential wave energy are of the same magnitude given by (4.16). λ is the wave length ρ is the density of sea water and g is the gravitational constant.

$$E_k = E_p = \frac{1}{4}\rho g|\zeta_A|^2\lambda \tag{4.16}$$

This gives the total stored wave energy according to (4.17).

$$E = E_k + E_p = \frac{1}{2}\rho g|\zeta_A|^2\lambda \tag{4.17}$$

The equations gives the energy for one wavelength per unit length in y-direction. The wave energy level (transported energy unit crest length) is given by the formula (4.18) for deep water.

$$J_r = \frac{1}{2}\rho g\zeta^2 \cdot \frac{c_W}{2} = \frac{1}{32\pi}\rho g^2 H^2 T \tag{4.18}$$

This is the theoretical maximum power in the sea state. Therefore the power carried by a monochromatic wave of period T = 11.5 s and wave height H = 2.5 m is about 70 kW/m.

The wave energy level tells us how much energy is transported. For the case of a progressive plane harmonic wave the energy transport velocity is equal to (4.19).

$$J_r = v_g E \tag{4.19}$$

Accordingly, the wave energy level for in irregular wave is given by equation 4.20

$$J_i = \frac{1}{64\pi}\rho g^2 H_s^2 T_e \tag{4.20}$$

where

$$T_e = 2\pi\frac{m_{-1}}{m_0} \qquad\qquad m_n = \int_0^\infty f^n S(f) df \tag{4.21}$$

See Falnes (2002) for further details.

4.5 Absorption of Wave Energy

According to the physical law of conservation of energy the interaction between the waves and the WEC must happen in such a manner that the amount of energy in the sea is reduced (energy must be removed from the waves). This may be considered as a phenomenon of interference.

To absorb a wave means to generate a wave. (Falnes 2015)

In order to absorb the wave energy, the device must generate a wave, which interferes destructively with the sea wave. Thus the devise should be a good wave generator. Moreover, to destroy a wave is to create a wave (Falnes 2015). Figure 4.2 illustrates the principles of interference. In the left-hand-side figure the incoming wave and the reflected wave interfere and the resulting wave is increased. This in the natural consequence without destructive interference. The right-hand-side figure shows the case where the wave and the wall interfere destructively. The wall moves with a wave motion and absorbs all the energy from the incoming wave. Hence the reflected wave is canceled by the generated wave.

Another illustration of the phenomenon is given in Figure 4.3, simplified to the case of two dimensional motion. The figure shows how the device motion can cause complete absorption of the wave energy in the incident wave. Figure a represents an undisturbed incident wave. Curve b illustrates symmetric wave generation (on otherwise calm water) by means of a body oscillating in heave. Curve c illustrates antisymmetric wave generation. The bottom curve represents the superposition of the three waves. From the curve it can be seen that there is no motion downstream of the buoy. This is due to the destructive interference with the incoming wave. Hence, complete destruction leads to complete absorption of the wave energy. In order for a WEC to absorb wave energy it is necessary to displace water in an oscillatory manner and with correct phase (timing) and amplitude.

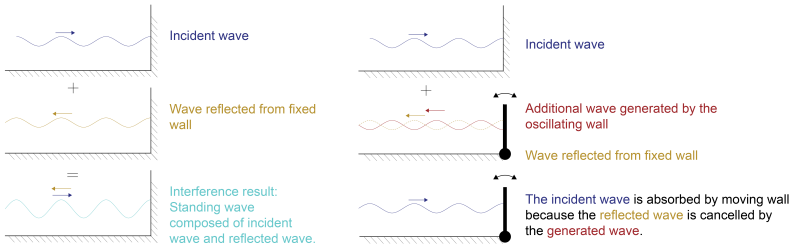

Figure 4.2: Illustration of interference. The left-hand-side figure shows the case where there is no interference. The right-hand-side shows how the wall and the wave interfere destructively. Remake from Falnes (2015).

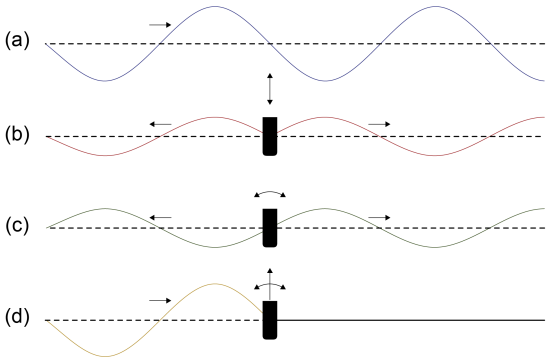

Figure 4.3: Destructive interference. Remake from Falnes (2002).

If the wave-power level is $J = v_g E = \frac{1}{32\pi}\rho g^2 H^2 T$ (see Section 4.4) and the wave length is $\lambda = (g/2\pi)T^2$ the maximum amount of power that can possibly be extracted from the wave per unit length is the total amound of power in the wave which is given in (4.22).

$$P_w = \frac{\rho g^2 H^2 T^3}{64\pi^2} \tag{4.22}$$

However, in reality a lower amount can is absorbed by the WEC. This was theoretically described by Budal and Falnes (**??**). They argued that the total volume V of the body sets limits for both the maximum excursion, velocity and excitation force in heave. They found a theoretical upper bound for the power P_a which is given in (4.23). This is illustrated in Budal's diagram in Figure 4.4.

$$P_a = \frac{\pi \rho g H V}{4T} \tag{4.23}$$

From the formula it becomes apparent that the power outtake is dependent on the volume. Larger volume will shift the curve to the right. The goal is to design a WEC where the volume is as small as possible and at the same time absorbs as much as possible energy. This is done by making the cross point for the most frequent wave periods.

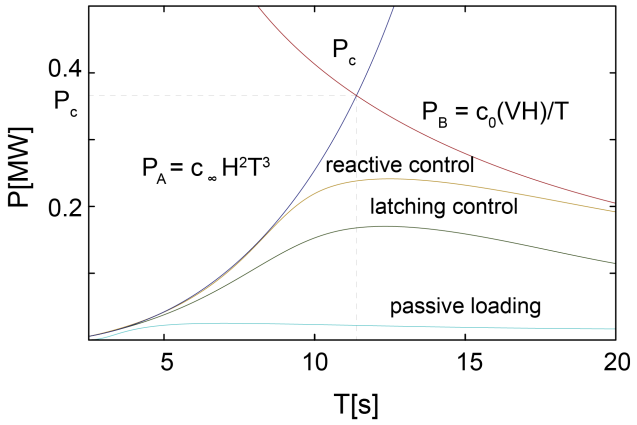

Figure 4.4: Budals diagram. Remake from Falnes (2015).

"It should be considered as an advantage that practically all the volume, of e.g a heaving-float system could be "used to displace fluid and thus to generate outgoing waves". Several proposed wave-energy converters have, however, relatively large proportions of "dead" volume not participating in such wave generation".
(Falnes 2007)

The capture width of a WEC is defined as the width of a wavefront an average amount of power, equal to that converted by the point absorber P_u, passes across. The equation is given in (4.24).

$$W = \frac{P_u}{P_w} \tag{4.24}$$

The 'absorption picture' is a bit different for the case of three dimensional motion. For a point absorber or heaving buoy the interference can be illustrated as in Figure 4.5. In the illustration the incident waves are long crested, however the body radiates a circular wave pattern. The wave energy transported by the incident wave front of width equal to the wavelength divided by 2π, is the maximum energy which may be extracted by a heaving axisymmetrical body (Falnes 2002). This width is the 'capture width'.

Figure 4.4 also illustrates the effect of a Latching controller. In this thesis a Latching controller will be studied. There has been done studies on possible benefit of using controllers, and a typical result is given in Figure4.4. The picture shows that there is improvement on the power outtake when using controllers. There is a possibility for huge benefit.

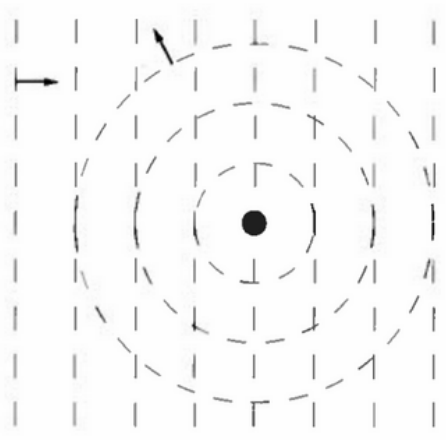

Figure 4.5: Wave pattern of two interference waves seen from above. When a point absorbs energy from an incident wave, it generates a circular wave radiating away from the absorber's immersed surface (Falnes 2002).

Chapter 5

Wave Energy Converter Dynamics

The WEC studied in this thesis will be modeled according to the theory developed for multiple body heaving buoy wave energy converters (WECs). This theory is similar to that of point absorbers. The Ocean Oasis and the DynOcean are two-body WEC extracting energy from the relative motions in heave, roll and pitch. The scope of this project is limited to the study of power extraction due to heave motion in irregular waves. Seeing as the focus of the thesis is real time control of the WEC the equations of motion must be developed in time domain. In this chapter the mathematical model for the motion of the WEC, the controller and the estimator will be derived in following sections.

5.1 Loads on the Body

The wave-body interactions may be divided into two parts: radiation and the exciation. The waves generated if the body is forced into oscillation by external means on otherwise still water are radiated waves. If the body is immobolized and there is an incident wave the body experiences foces. These forces are called excitation forces. Both these types of interactions may occur when the body is free to move in water. The forces working on the WEC are modeled according to the theory of hydrodynamics with reference to Newman (1977) and Faltinsen (1998). The amplitudes of the oscillations and waves are assumed to be small, thus the interactions are approximately linear.

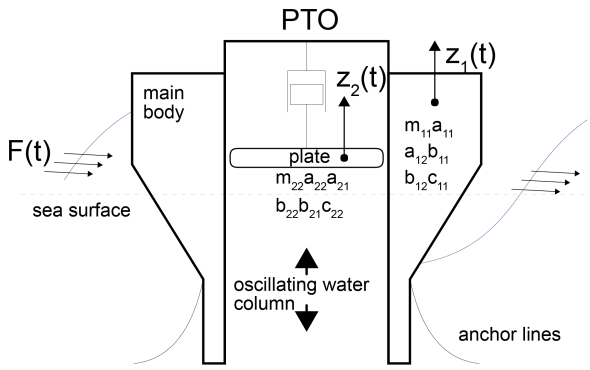

Figure 5.1: Modeling of Ocean Oasis. Remake from Schultz (2014).

A figure of the model studied in this thesis is given in Figure 5.1. The force parameters and the heave motion vectors are given. The indices indicate the body of interest.

$$i = 1 - main\ body/buoy \tag{5.1}$$
$$i = 2 - plate/disc \tag{5.2}$$

The heave motion is denoted by z, and the heave motion of the disc and buoy are then given as z_1 and z_2 respectively. m_{11} and m_{22} denote the mass of the buoy and the disc respectively. a_{11}, a_{22}, b_{11} and b_{22} are the hydrostatic coefficients and a_{12}, a_{21}, b_{12} and b_{21} denote the coupled added mass and damping coefficients of the two bodies. The hydrostatic coefficients are denoted c_{11}, c_{22}. According to Newton's second law, the dynamic equation for the oscillating body may be written as following.

$$\boldsymbol{F}_I + \boldsymbol{F}_r + \boldsymbol{F}_s = \boldsymbol{F}_e + \boldsymbol{F}_v + \boldsymbol{F}_m + \boldsymbol{F}_u + \boldsymbol{F}_o \tag{5.3}$$

F_e are the hydrodynamic excitation forces, F_r are the hydrodynamic radiation forces, F_s are the hydrostatic stiffness forces, F_v are the viscous forces, F_m are the mooring forces, F_u are the forces applied intentionally for control and power take-off, F_o are the other environmental forces. As a first step viscous forces, the influence of mooring forces or other environmental forces will not be considered and will therefore not be included in the calculations. However, to find accurate solutions these forces should not be neglected and should be included at a later stage of the research. In addition only the heave forces will be considered and therefore only the forces due to heave motion are given in the following. The simplified version, written for heave motion, may then be written as following.

$$F_{I3} + F_{r3} + F_{s3} = F_{e3} + F_{u3} \tag{5.4}$$

Inertia forces The inertia forces is the resistance of the WEC to change in its state of motion. It represents stored kinetic energy and power needed to change momentum. The

inertia forces can be calculated from the equation:" $m_i\ddot{z}_i(t)$", where m_i is the mass of object i and $\ddot{z}_i$ is the acceleration of object i.

Stiffness The stiffness forces are hydrostatic forces that restore the motion of the WEC. The forces are proportional to the movement and can be written $C_{33}z_i$.

Power take-off As stated in earlier work on the topic (Schultz 2014), the PTO system can be described as a damping term as given in equation 6.12. This is a simplification. A real power take off system is much more complex, however the power take off system is out of the scope for this project.

$$F_u = B_p(t)\dot{z}_{rel}(t) + F_L \tag{5.5}$$

Where $\dot{z}_{rel}$ is the velocity of the WEC and $B_p(t)$ is the time varying damping. F_L is the latching control force (see Chapter 6.

5.2 Excitation Force

The oscillating forces acting on the WEC when it is held still are the excitation forces. They are found by integrating the dynamic pressure over time. It is often assumed a linear relation between the excitation force and the incident wave. This relation is correct for infinity small movements, however the approximation is also shown to be sufficient for motions that cause laminar movements of the water, and does not shed vortexes. Then the excitation force can be written according to (5.6), in frequency- and time domain respectively.

$$F_{e3}(\omega) = H_{F_{e3}\zeta}(\omega)\zeta(\omega) \qquad F_{e3}(t) = \int_{\infty}^{\infty} h_{F_{e3}\zeta}(\tau)\zeta(\tau - t)d\tau \tag{5.6}$$

5.2.1 Pre-Calculated Time Series

The excitation force can be pre-calcuated directly, based on the hydrodynamic parameters. If the wave spectrum of the sea state is known a good approximation of the excitation forces can be calculated from pre-calculated time series, as described in Hals (2010). For frequency component k corresponding to angular frequency $\omega_k = k\Delta\omega$, the wave elevation spectrum is $S_{\zeta,k} = S_\zeta(k\Delta\omega)$. The excitation force coefficient is given by (5.7).

$$\hat{H}_{F\zeta,k} = \hat{H}_{F\zeta}(\omega_k) = |\hat{H}_{F\zeta}(\omega)|e^{j\angle\hat{H}_{F\zeta}(\omega_k)} \tag{5.7}$$

The excitation force spectrum, $S_{F,k}$ and phase, $\phi_{F,k}$ can then be calculated from (5.8).

$$S_{F,k} = |\hat{H}_{F,\zeta,k}|^2 S_{\zeta,k} \qquad \phi_{F,k} = \angle\hat{H}_{F\zeta} \tag{5.8}$$

Furthermore, the complex excitation force amplitude for component k is given by (5.9). $\phi_{\zeta,k}$ is the phase of the wave.

$$\hat{F}_{e,k} = \sqrt{2S_{F,k}\Delta\omega}e^{j(\phi_{\zeta,k}+\phi_{F,k})} \tag{5.9}$$

The excitation force is now calculated as (5.10) for the N components.

$$F_e(t) = \sum_{k=1}^{N} \Re\big[\hat{F}_{e,k}e^{j\omega_k t}\big] \tag{5.10}$$

5.2.2 Calculating Excitation Force From Measurement

For simulation purposes, statistical information of the wave is assumed to be unknown. Hence, another method for calculating the excitation force is needed. There are two approached for calculating the excitation force given the excitation force coefficient and phase, and an estimation of the wave elevation. The first approach is to inverse Fourier transform the excitation force coefficient, and calculate the excitation force by solving the non-causal convolution integral in time domain. The second approach is to Fourier transform the wave elevation and use the method for pre-calucated time series to calculate the excitation force. An approach to the first method is given in Falnes (2002) and approaches to both methods are given in Hals (2010). The latter method was chosen for this thesis.

The following was derived according to the theory for complex expression for response variables in Faltinsen (2005). The wave elevation of the k'th wave component can be written as (5.12), $\hat{\zeta}_k$ where is the complex amplitude of the wave elevation given by (5.13).

$$\zeta_k = \zeta_{A,k}\cos(\omega_k t + \varepsilon_k) \tag{5.11}$$

In the complex plane, the wave elevation can be written as

$$\zeta_k = \hat{\zeta}_k e^{j\omega_k t} \tag{5.12}$$

The complex amplitude of the wave elevation is given as following

$$\hat{\zeta}_{A,k} = \zeta_{R,k} + i\zeta_{I,j} \tag{5.13}$$
$$\zeta_{R,k} = |\zeta_k|\sin\varepsilon_k \tag{5.14}$$
$$\zeta_{I,k} = -|\zeta_k|\cos\varepsilon_k \tag{5.15}$$

where

$$\varepsilon_k = \tan^{-1}\left(\frac{\zeta_{R,k}}{-\zeta_{I,k}}\right) \tag{5.16}$$

Euler's equation can be written as following

$$e^{i\omega t} = \cos\omega t + i\sin\omega t \tag{5.17}$$

The real part of the wave elevation can be derived and is found to be (5.18).

$$\Re\big[(\zeta_{R,j} + i\zeta_{I,j})e^{j\omega_k t}\big] = \zeta_{R,j}\cos\omega t - \zeta_{I,j}\sin\omega t \tag{5.18}$$

The complex amplitude of the wave elevation is given according to (5.19) where $\phi_{m,k}$ is the phase found from Fourier analysis of the measures signal.

$$\mathcal{F}(\zeta_{m,k}) = \hat{\zeta}_{m,k}(j\omega) = |\hat{\zeta}_{m,k}|e^{\phi_{m,k}} \tag{5.19}$$

The excitation force given by the measured signal, for the k'th component can then be written according to(5.20) and the total excitation can be found by adding all the components as given in (5.21).

$$\hat{F}_{em,k} = \hat{H}_{F\zeta,k}\hat{\zeta}_{m,k} \tag{5.20}$$

$$F_{em}(t) = \sum_{k=1}^{N} \Re\big[\hat{F}_{em,k}e^{j\omega_k t}\big] \tag{5.21}$$

5.3 Motion Responce

The equations in the following are derived according to Schultz (2014). The dynamic equation of a body in a monochromatic wave can according to (5.22). It can be seen from the equation that the hydrodynamic coefficients vary with frequency. This makes it convenient to express the equations of motion in frequency domain. (5.4)

$$[m + a(\omega)]\ddot{z} + b(\omega)\dot{z} + cz = f_{ex} \tag{5.22}$$

Frequency-Domain

In frequency domain the dynamic equations can be written as given in (5.23) and (5.24). See Section 5.1 and Figure 5.1 for explanations of the equation parameters and variables.

$$\begin{aligned}[m_{11} + a_{11}(\omega)]\ddot{z}_1(j\omega) + a_{12}(\omega)\ddot{z}_2(j\omega) + b_{11}(j\omega)\dot{z}_1(j\omega) + b_{12}(j\omega)\dot{z}_2(j\omega) \\ - B_p[\dot{z}_1(j\omega) - \dot{z}_2(j\omega)] + c_{11}z(j\omega) = f_{1,ex}(j\omega)\end{aligned} \tag{5.23}$$

$$\begin{aligned}[m_{22} + a_{22}(\omega)]\ddot{z}_2(j\omega) + a_{21}(\omega)\ddot{z}_1(j\omega) + b_{22}(j\omega)\dot{z}_2(j\omega) + b_{21}(j\omega)\dot{z}_1(j\omega) \\ - B_p[\dot{z}_1(j\omega) - \dot{z}_2(j\omega)] + c_{22}z(j\omega) = f_{2,ex}(j\omega)\end{aligned} \tag{5.24}$$

These equations can be combined to a matrix formulation. Equation (5.25) gives the heave motion state vector.

$$\boldsymbol{z(j\omega)} = \begin{bmatrix} z_1(j\omega) \\ z_2(j\omega) \end{bmatrix} \tag{5.25}$$

The dynamic equaiton matrix formulation can then be given as in (5.26), where the matrices

are given in (5.28).

$$[\boldsymbol{M} + \boldsymbol{A_{33}}(\omega)]\ddot{\boldsymbol{z}}(j\omega) + [\boldsymbol{B_{33}}(\omega) + \boldsymbol{B_p}]\dot{\boldsymbol{z}}(j\omega) + \boldsymbol{C_{33}}\boldsymbol{z}(j\omega) = \boldsymbol{F}(j\omega) \tag{5.26}$$

$$\boldsymbol{M} = \begin{bmatrix} m_{11} & m_{12} \\ m_{21} & m_{22} \end{bmatrix} \quad \boldsymbol{A_{33}(\omega)} = \begin{bmatrix} a_{11}(\omega) & a_{12}(\omega) \\ a_{21}(\omega) & a_{22}(\omega) \end{bmatrix} \quad \boldsymbol{B_{33}(\omega)} = \begin{bmatrix} b_{11}(\omega) & b_{12}(\omega) \\ b_{21}(\omega) & b_{22}(\omega) \end{bmatrix} \tag{5.27}$$

$$\boldsymbol{B_p} = \begin{bmatrix} b_p & -b_p \\ -b_p & b_p \end{bmatrix} \quad \boldsymbol{C_{33}} = \begin{bmatrix} c_{11} & 0 \\ 0 & c_{22} \end{bmatrix} \quad \boldsymbol{F(j\omega)} = \begin{bmatrix} f_{1,e}(j\omega) \\ f_{2,e}(j\omega) \end{bmatrix} \tag{5.28}$$

Time-Domain

The reason for modeling in time-domain, not frequency which is more convenient, is that it is necessary to know the time dependence when controlling in real-time.

By inverse Fourier transformation the time-domain one dimentional dynamics can be described by *Cummings Equation* (Taghipour et al. 2008). For the two parts of the DynOcean the equations are given according to (5.29) and (5.30).

$$\begin{aligned}[m_{11} + a_{11}(\infty)]\ddot{z}_1(t) + a_{12}(\infty)\ddot{z}_2(t) + \int_0^t k_{11}(t-\tau)\dot{z}_1(\tau)d\tau + \int_0^t k_{12}(t-\tau)\dot{z}_2(\tau)d\tau \\ - B_p[\dot{z}_1(t) - \dot{z}_2(t)] + c_{11}z_1(t) = f_{1,ex}(t)\end{aligned} \tag{5.29}$$

$$\begin{aligned}[m_{22} + a_{22}(\infty)]\ddot{z}_2(t) + a_{21}(\infty)\ddot{z}_1(t) + \int_0^t k_{22}(t-\tau)\dot{z}_2(\tau)d\tau + \int_0^t k_{21}(t-\tau)\dot{z}_1(\tau)d\tau \\ + B_p[\dot{z}_1(t) - \dot{z}_2(t)] + c_{22}z_2(t) = f_{2,ex}(t)\end{aligned} \tag{5.30}$$

$a_{ii}(\omega)$ is the constant infinite-frequency added mass matrix. The convergence value of the added mass as the frequency approaches infinity. k_{ii} are the retardation functions. These equations can be combined in matrix formulation which is given in (5.31)-(5.34).

$$\boldsymbol{z(t)} = \begin{bmatrix} z_1(t) \\ z_2(t) \end{bmatrix} \tag{5.31}$$

$$[\boldsymbol{M} + \boldsymbol{A_{33}}(\infty)]\ddot{\boldsymbol{z}}(t) + \int_0^t \boldsymbol{K_{33}}(t-\tau)\dot{\boldsymbol{z}}(\tau)d\tau + \boldsymbol{C_{33}}\boldsymbol{z}(t) = \boldsymbol{F_e}(t) \tag{5.32}$$

$$\boldsymbol{A_{33}(\infty)} = \begin{bmatrix} a_{11}(\infty) & a_{12}(\infty) \\ a_{21}(\infty) & a_{22}(\infty) \end{bmatrix} \qquad \boldsymbol{K_{33}(t-\tau)} = \begin{bmatrix} k_{11}(t-\tau) & k_{12}(t-\tau) \\ k_{21}(t-\tau) & k_{22}(t-\tau) \end{bmatrix} \tag{5.33}$$

$$\boldsymbol{F(j\omega)} = \begin{bmatrix} f_{1,e}(j\omega) \\ f_{2,e}(j\omega) \end{bmatrix} \tag{5.34}$$

5.4 Radiation Forces

The radiation forces are oscillating forces of the waves generated by a moving body. There are two contributions, the added mass and damping. In frequency domain the added mass force is proportional to the acceleration and damping force to the velocity. The forces are written $A(\omega)\ddot{z}_i(\omega)$ and $B(\omega)\dot{z}_i(\omega)$, where A is the added mass coefficient and B is the damping coefficient. For modeling and control design purposes these coefficients shold be identified. Computed hydrodynamic data can be used for such system identification and to obtain a parametric approximation of the Cummins equation. The data provided by hydrodynamic codes is in the frequency domain, therefore it is natural with a frequency domain approach to the system identification.

Time-domain models are useful for simulation and control system design. In time-domain the radiation forces are given by the fluid memory effect and infinite added mass

$$\int_0^t \boldsymbol{K}(t-\tau)\dot{\boldsymbol{z}} \qquad\qquad \mathbf{A_{33}}(\infty) \tag{5.35}$$

The convolution term captures the effect of the changes in momentum of the fluid at a particular time affects the motion at the subsequent times - this is known as fluid memory effect. The infinite added mass is the convergence term of the added mass when the frequency approaches infinity. The relation between the parameters of the time-domain representation and frequency-domain representation is given in Ogilvie (1964).

$$\mathbf{A}(\omega) = A - \frac{1}{\omega}\int_0^\infty \mathbf{K}(t)\sin(\omega\tau)d\tau \tag{5.36}$$

$$\mathbf{B}(\omega) = \int_0^\infty \mathbf{K}(t)\cos(\omega\tau)d\tau \tag{5.37}$$

from which it follows that

$$\mathbf{K}(t) = \frac{2}{\pi}\int_0^\infty \mathbf{B}(\omega)\cos(\omega t)d\omega \tag{5.38}$$

and

$$\mathbf{A} = \lim_{\omega\to\infty}\mathbf{A}(\omega) = \mathbf{A}(\infty) \tag{5.39}$$

Transforming the data from frequency domain to time domain may cause errors due to finite amount of data. One approach is given in (Perez & Fossen 2009).
Solving a differential equation including a convolution integral may be problematic. This may be solved by developing linear time-domain models to approximate the fluid-memory models in the Cummins equation. One such approach is given in (Perez & Fossen 2009), which develops a Matlab toolbox for parametric identification of radiations force models of ships and offshore structures. A linear time-invariant parametric model is developed by using a least squares fitting (see (Perez & Fossen 2009) for further explanations). An appropriate order should be selected for the fitting, and this is done by trial and error until a satisfactory result is obtained. The result of the procedure is a transfer function which approximates the retardation function of the fluid memory effect in frequency domain

$$\boldsymbol{K}(j\omega) \approx \hat{\boldsymbol{K}}(j\omega) = \hat{\boldsymbol{C}}(j\omega \boldsymbol{I} - \hat{\boldsymbol{A}})^{-1}\hat{\boldsymbol{B}} \tag{5.40}$$

$$\hat{K}_{is}(s) = \frac{P_{ik}(s)}{Q_{ik}(s)} = \frac{p_r s^r + p_{r-1}s^{s-1} + ... + p_0}{s^n + q_{n-1}s^{n-1} + ... + q_0} \tag{5.41}$$

n is the order of the system, which is selected by trial and error. In time domain the transfer be reformulated as a linear state space equation as given in (5.54) - (5.56). An approximate solution to the fluid memory can then be found by solving this state space equation.

$$\boldsymbol{\mu} = \int_0^t \boldsymbol{K}(t-\tau)\dot{\boldsymbol{z}}(\tau)d\tau \approx \tag{5.42}$$

$$\dot{\boldsymbol{x_r}} = \hat{\boldsymbol{A}}_{\boldsymbol{r}}\boldsymbol{x_r} + \hat{\boldsymbol{B}}_{\boldsymbol{r}}\dot{\boldsymbol{z}} \tag{5.43}$$

$$\hat{\boldsymbol{\mu}} = \hat{\boldsymbol{C}}_{\boldsymbol{r}}\boldsymbol{x_r} \tag{5.44}$$

The vector $\boldsymbol{x}$ corresponds to the order of the approximating system and the matrices $\hat{\boldsymbol{A}}, \hat{\boldsymbol{B}}$ and $\hat{\boldsymbol{C}}$ are constant matrices.

In addition, the infinite-frequency added mass matrix A_∞ can be found by using the toolbox. See Perez & Fossen (2009) for further details.

5.4.1 Canonical Form

When the approximation $\boldsymbol{\mu}$ is found, in the form of a transfer function in frequency domain, a state space model can be found by a canonical observable transformation as described in Hespanha (2009). The state space representation of the transfer function can be given according to the following matrices.

$$\hat{\boldsymbol{A}} = \begin{bmatrix} -q_{n-1} & 1 & 0 & ... & 0 \\ -q_{n-2} & 0 & 1 & ... & 0 \\ -q_{n-3} & 0 & 0 & ... & 0 \\ \vdots & \vdots & \vdots & \ddots & \vdots \\ -q_0 & 0 & 0 & ... & 0 \end{bmatrix}_{n\times n} \qquad \hat{\boldsymbol{B}} = \begin{bmatrix} p_r \\ p_{r-1} \\ p_{r-2} \\ \vdots \\ p_0 \end{bmatrix}_{n\times 1} \tag{5.45}$$

$$\hat{\boldsymbol{C}} = \begin{bmatrix} 1 & 0 & ... & 0 & 0 \end{bmatrix}_{1\times n} \tag{5.46}$$

5.4.2 Stability, Passivity and Validation

The resulting system may not be stable. Stability can be tested by evaluating the eigenvalues of the system matrix, $\hat{A}$. If they are of magnitude strictly smaller than 1 the system is stable Hespanha (2009). If the system is not stable Perez & Fossen (2009) gives a method for obtaining a stable model, based on reflecting the unstable poles around about the imaginary axis and re-computing the denominator polynomial.

The mapping $\dot{\mathbf{z}}$ into a force introduced by the fluid-memory convolution is passive (Perez & Fossen 2008a). The least-squares fitting problem does not enforce passivity, however passivity is required . The approximation is passive if

$$Re\{\frac{P_{ik}(j\omega_l,\theta)}{Q_{ik}(j\omega_l,\theta)}\} > 0 \tag{5.47}$$

When checking for passivity the transfer function should be evaluated at frequencies below and above the frequencies used for parameter estimation.

In addition, the added-mass and damping based on the identified parametric approximation should be estimated via

$$\hat{A}_{ik}(\omega) = Im\{\omega^{-1}\hat{K}_{ik}(j\omega)\} + A_{\infty,ik} \tag{5.48}$$

$$\hat{B}_{ik}(\omega) = Re\{\hat{K}_{ik}(j\omega)\} \tag{5.49}$$

and compared to the A_{ik} and B_{ik} given by the hydrodynamic code. The order of the approximation can be increased if the fitting is not satisfactory.

The radiation forces in the frequency-domain given in Cummins equation can be expressed as (5.50). This function can also be used for comparing the results of the identified model with the values given by the hydrodynamic code.

$$A_{ik}(j\omega) \triangleq \frac{B_{ik}}{j\omega} + A_{ik}(\omega) \tag{5.50}$$

5.5 State Space Equation

The total equation can now be written

$$(\boldsymbol{M} + \boldsymbol{A_{33}}(\infty))\ddot{\boldsymbol{z}}(t) + \boldsymbol{\mu} + \boldsymbol{B_p}\dot{\boldsymbol{z}}(t) + \boldsymbol{C}\boldsymbol{z}(t) = \boldsymbol{F_e}(t) \tag{5.51}$$

By defining the states as following as in (5.54) the state space formulation can be written as in (5.53)-(5.55).

$$\boldsymbol{x(t)} = \begin{bmatrix} \boldsymbol{z}(t) \\ \dot{\boldsymbol{z}}(t) \end{bmatrix} = \begin{bmatrix} z_1(t) \\ z_2(t) \\ \dot{z_1}(t) \\ \dot{z_2}(t) \end{bmatrix} \tag{5.52}$$

$$\dot{\boldsymbol{x}} = \boldsymbol{f}(x, u, w) \tag{5.53}$$

$$\dot{\boldsymbol{x}} = \boldsymbol{A}\boldsymbol{x}(t) - \boldsymbol{E}\boldsymbol{\mu} + \boldsymbol{E}\boldsymbol{F_e} \tag{5.54}$$

$$A = \begin{bmatrix} \boldsymbol{0}_{2x2} & \boldsymbol{I}_{2x2} \\ -\frac{C_{33}}{(\boldsymbol{M}+\boldsymbol{A_{33}}(\infty))} & -\frac{B_p}{(\boldsymbol{M}+\boldsymbol{A}_{33}(\infty))} \end{bmatrix} \qquad E = \begin{bmatrix} \boldsymbol{0}_{2x1} \\ \frac{1}{(\boldsymbol{M}+\boldsymbol{A}_{33}(\infty))} \end{bmatrix} \qquad \boldsymbol{x}(0) = \begin{bmatrix} \boldsymbol{0}_{2x1} \\ \boldsymbol{0}_{2x1} \end{bmatrix} \tag{5.55}$$

The fluid memory effects, μ, can be written as

$$\begin{aligned} \boldsymbol{\mu} &= \begin{bmatrix} \mu_{11} + \mu_{12} \\ \mu_{21} + \mu_{22} \end{bmatrix} \approx \\ \dot{\boldsymbol{x_r}} &= \hat{\boldsymbol{A}}_{\boldsymbol{r}}\boldsymbol{x_r} + \hat{\boldsymbol{B}}_{\boldsymbol{r}}\dot{\boldsymbol{z}} \\ \hat{\boldsymbol{\mu}} &= \hat{\boldsymbol{C}}_{\boldsymbol{r}}\boldsymbol{x_r} \end{aligned} \tag{5.56}$$

$$\hat{\mathbf{A}}_{\mathbf{r}} = \begin{bmatrix} \hat{\mathbf{a}}_{\mathbf{11,r}} & \mathbf{0} & \mathbf{0} & \mathbf{0} \\ \mathbf{0} & \hat{\mathbf{a}}_{\mathbf{12,r}} & \mathbf{0} & \mathbf{0} \\ \mathbf{0} & \mathbf{0} & \hat{\mathbf{a}}_{\mathbf{21,r}} & \mathbf{0} \\ \mathbf{0} & \mathbf{0} & \mathbf{0} & \hat{\mathbf{a}}_{\mathbf{22,r}} \end{bmatrix} \qquad \hat{\mathbf{B}}_{\mathbf{r}} = \begin{bmatrix} \hat{\mathbf{b}}_{\mathbf{11,r}} & \mathbf{0} \\ \mathbf{0} & \hat{\mathbf{b}}_{\mathbf{12,r}} \\ \hat{\mathbf{b}}_{\mathbf{21,r}} & \mathbf{0} \\ \mathbf{0} & \hat{\mathbf{b}}_{\mathbf{22,r}} \end{bmatrix} \tag{5.57}$$

$$\hat{\mathbf{C}}_{\mathbf{r}} = \begin{bmatrix} \hat{\mathbf{c}}_{\mathbf{11,r}} & \hat{\mathbf{c}}_{\mathbf{12,r}} & \mathbf{0} & \mathbf{0} \\ \mathbf{0} & \mathbf{0} & \hat{\mathbf{c}}_{\mathbf{21,r}} & \hat{\mathbf{c}}_{\mathbf{22,r}} \end{bmatrix} \tag{5.58}$$

5.6 Power Output

The absorbed power from the WEC is caused by the relative motion between the buoy and plate. It given as the PTO force multiplied by the relative velocity.

$$P_u = F_u\dot{z}_{rel} = B_p\dot{z}_{rel}^2 \tag{5.59}$$

Chapter 6

Control

This chapter gives a short overview of the theory of control of Wave Energy Converters (WECs) and describes some common control strategies. The focus will lye on Latching, the method utilized in this thesis.

6.1 Optimum Control for Maximising Converted Energy

In Chapter 4 the theory of ocean waves and maximum energy absorpton was given. However, by using a control system, the possible energy output is increased. The power output from a WEC may be increased by controlling the oscillation in order to approach an optimum interaction between the WEC and the incident wave. In other words controlling the WEC in to resonance with the incoming wave. In the following the theory of optimum control is given. The average useful power is given by (6.1). This gives the converted useful energy which is given in both time domain and frequency domain in (6.2).

$$P_u = -\overline{F_u(t)\dot{z}_(t)} \tag{6.1}$$

$$E_u = -\int_{-\infty}^{\infty} F_u(t)\dot{z}(t)dt = \frac{1}{2\pi}\int_{-\infty}^{\infty} -\{F_u(\omega)\dot{z}^*(\omega) - F_u^*(\omega)\dot{z}(\omega)\}d\omega \tag{6.2}$$

This equation can be rewritten on the from given in 6.3 (shown in Falnes (2002), p. 205).

$$E_u = \frac{1}{2\pi}\int_0^{\infty}\left\{\frac{|F_e(\omega)|^2}{2R_i(\omega)} - \frac{\alpha(\omega)}{2R_i(\omega)}\right\} \tag{6.3}$$

where

$$\alpha(\omega) = F_e(\omega)F_e^*(\omega) + 2R_i(\omega)[F_u(\omega)\dot{z}^*(\omega) + F_u^*(\omega)\dot{z}(\omega)] \tag{6.4}$$

$$R_i(\omega) = \frac{Z_i(\omega) + Z_i^*(\omega)}{2} \tag{6.5}$$

$$Z_i(\omega)u(\omega) = F_e(\omega) + F_u(\omega) = F_{ext}(\omega) \tag{6.6}$$

$R_i(\omega)$ is the real part of the intrinsic mechanical resistance. The mechanical impedance is the ratio between the complex force amplitude and the complex velocity amplitude. The adjective 'intrinsic' in because of all the terms relate to the terms of the oscillating systems. It includes the radiation impedance, but not effects of the control and power take off. For further elaborations, see Falnes (2002), chapter 5. It can be proven that $\alpha(\omega) \geq 0$ and that $\alpha \equiv 0$ gives optimum condition. This implies that the maximum condition is given as in (6.7).

$$E_{u,MAX} = \frac{1}{2\pi} \int_0^\infty \frac{|F_e(\omega)|^2}{2R_i(\omega)}\, d\omega \tag{6.7}$$

$$E_u = E_{u,MAX} - E_{u,P} \tag{6.8}$$

$$E_{u,P} = \frac{1}{2\pi} \int_0^\infty \frac{\alpha(\omega)}{2R_i(\omega)} d\omega \tag{6.9}$$

$E_{u,P}$ is lost-energy penalty for not operating at optimum. In order to show that $\alpha \geq 0$ (6.6) can be used to eliminate either $F_e(\omega)$ or $F_u(\omega)$ from (6.5). From this it can also be shown that the optimum condition is as given in (6.10), and that an alternative way of writing the optimum condition is given in (6.11).

$$F_u(\omega) = -Z_i^*(\omega) u(\omega) \tag{6.10}$$

$$F_e(\omega) = 2R_i(\omega)\dot{z}(\omega) \text{ or } \dot{z}(\omega) = \frac{F_e(\omega)}{2R_i(\omega)} \tag{6.11}$$

6.2 Force Actuation Control Objective

The force actuation control objective can be formulated as following

Maximize the energy output of the power take-off

The selected control strategy for this thesis was Latching, which is a phase controller. Thus the criterium to be achieved is (6.11). However, for the system dynamics described in Chapter 5 this requirement can be reformulated as (6.12). Hence, the maximum energy output can be found by maximizing (6.12).

$$E_u(t) = \int_0^\infty F_u \dot{z}_2(t) dt = \int_0^\infty b_p(t) {\dot{z}_2}^2(t) dt \tag{6.12}$$

6.3 Latching Control

As discussed in Section 2.7, Latching is a suboptimal type of phase control. The principle is to latch and unlatch the relative velocity at appropriate time instances in order to achieve optimum phase and optimum power output. The optimum power output is achieved if the motion is unlatched in an time instance such that the oscillatoriy motion is at its maximum at the same time as the excitation force is at its maximum. In this way it is possible to force the WEC into resonance with the the incoming wave. Then the movement is maximized and hence the power output.The latching is done when the relative velocity is zero. If the wave is a sinusoidial, as shown in Figure 6.1 the time of maximum excitation force is known. However, for the case of irregular waves, one does not know when the optimum time instance is and the finding the optimum unlatching instance is no longer trivial. A control algorithm must be developed, and the excitation force must be predicted some time into the future.

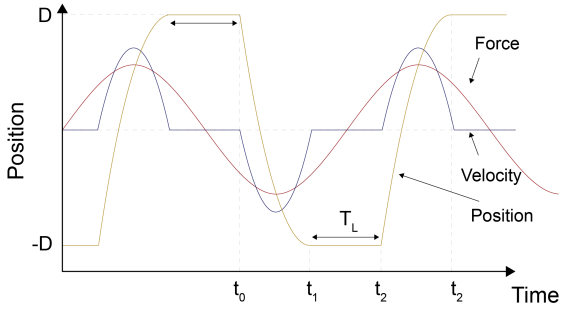

Figure 6.1: The evolution of system variables under latching control. Remake from Ringwood et al. (2014).

Figure 6.1 shows how the system variables evolves under a latching strategy. At time t1 latching is applied and at t2 the device is releaced. The latched duration is T_L. The positive displacements and potential energy iseffectively increased during each half cycle. The overall energycapture is increased even thiough the velocity is zero for parts of the cycle. This is because the velocity is in phase with the excitation force.

6.4 Latching Control Force

According to Schultz (2014) a weak modeling technique can be used to implement latching control on the WEC. The PTO-coefficient is controlled by a hydraulic damper with open/close valves. The motion can be locked/latched by controlling a binary input sequence (6.13). Thus the force of the latching controller can be written according to (6.14). $L = \infty$ is the idealconstant to simulate latching. However, the force will be included in numerical computations and the size will affect computing time. Hence, this constant will be approxi-

mated by a lower value. An appropriate value will be given by (6.15). By choosing $k = 1000$ it is ensured that the other forces are overrided by the control force.

$$u(t) =\in \{0, 1\} \tag{6.13}$$

$$\boldsymbol{F_L} = u(t)\boldsymbol{L}\boldsymbol{z}(t) \qquad \boldsymbol{L} = \begin{bmatrix} l & -l \\ -l & l \end{bmatrix} \tag{6.14}$$

$$\boldsymbol{L} = (k(\|\boldsymbol{M}\|_\infty + \|\boldsymbol{A_{33}}\|_\infty) \tag{6.15}$$

The following matrix will be added to the state space formulation.

$$G = \begin{bmatrix} \mathbf{0}_{2x2} & \mathbf{0}_{2x2} \\ \mathbf{0}_{2x2} & \frac{\boldsymbol{L}}{(\boldsymbol{M}+\boldsymbol{A}(\infty))} \end{bmatrix} \tag{6.16}$$

6.5 Optimal Control

The captured energy over time horizon T can be written according to (6.17).

$$\mathbf{E}(x) = \int_0^T b_p(\dot{z}_1 - \dot{z}_2)^2 dt = \int_0^T \dot{\mathbf{z}}^{\mathbf{T}}\mathbf{B_p}\dot{\mathbf{z}} = \int_0^T \mathbf{x}^T\mathbf{Q}\mathbf{x}dt = \int_0^T \mathbf{R}(\mathbf{x})dt \quad \mathbf{Q} = \begin{bmatrix} \mathbf{0} & \mathbf{0} \\ \mathbf{0} & \mathbf{B_p} \end{bmatrix} \tag{6.17}$$

The optimal binary sequence can be found by solving (6.18). $\mathbf{Lx}(t)$ is an expression for absorbed power by the WEC at every instant in time. The expression is maximized by utilizing optimal control. In this case the performance index is u, and the Hamiltonian (6.19) and (6.20) can be defined according to optimal control theory. For the WEC studied in this thesis the equation can be given according to (6.21).

$$\max_u \quad E(\mathbf{x}) = \int_0^T \mathbf{R}(\mathbf{x})dt \tag{6.18}$$

$$\mathbf{H}(\mathbf{x}, \mathbf{u}, \mathbf{F_e}, \lambda) = \mathbf{L}(\mathbf{x}) + \lambda^T \mathbf{f}(\mathbf{x}, \mathbf{u}, \mathbf{F_e}) \tag{6.19}$$

$$\lambda = \begin{bmatrix} \lambda_1(t) \\ \lambda_2(t) \end{bmatrix} \tag{6.20}$$

$$\mathbf{H}(\mathbf{x}, \mathbf{u}, \mathbf{F_e}, \lambda) = \mathbf{x}^T\mathbf{Q}\mathbf{x} + \lambda^T\left[\mathbf{A}\mathbf{x}(t) + u\mathbf{G}\mathbf{x} + \mathbf{E}\mu + \mathbf{E}\mathbf{F_e}\right] \tag{6.21}$$

λ is the adjoint state vector, and can be derived form equation (6.22), which can be combined in a vector according to (6.25), which is subject to the final time constraint (6.26).

$$\dot{\lambda}_i = \frac{\partial \mathbf{H}}{\partial x_i}(\mathbf{x}, \mathbf{u}, \mathbf{F_e}, \lambda) \tag{6.22}$$

$$\dot{\lambda} = \mathbf{g}(\mathbf{x}, \mathbf{u}, \mathbf{F_e}, \lambda) \tag{6.23}$$
$$= -2\mathbf{x}^T\mathbf{Q} + \lambda^T(\mathbf{A} + \mathbf{uG})^T \tag{6.24}$$
$$= -\mathbf{A^T}\lambda - \mathbf{uG}\lambda - \mathbf{2Qx} \tag{6.25}$$

$$\lambda(T) = \begin{bmatrix} 0 & 0 & 0 & 0 \end{bmatrix}^T \tag{6.26}$$

The optimal condition sequence that maximises (6.18) is the same u that maximises the Hamiltonian equation. The derviative of (6.19) with respect to u can be given as in (6.27). The optimal condition can be found as the values on u that makes the derivative equal to zero. Hence, the optimal control sequence can be formulated as (6.28).

$$\frac{\partial \mathbf{H}}{\partial u} = \lambda^T \mathbf{Gx} \tag{6.27}$$

$$u(t) = \begin{cases} 1 & \lambda^T\mathbf{Gx} > 0 \\ 0 & \lambda^T\mathbf{Gx} \leq 0 \end{cases} \tag{6.28}$$

6.6 Iterative Algoritm for Finding u

A method for simulating the optimal control algorithm was developed in Babarit & Clément (2006). The iterative algorithm for solving the numerical model is summarised below.

1. Integrate the state dynamics (5.54) forward in time with zero control and disturbance $F_e(t) \forall t \in [0, T]$.

2. The adjoint dynamics (6.25) should be integrated backward in time from t = T to 0 with the same control input and disturbance as in 1. (6.26) should be applied for time T.

3. The Hamilton equation can be maximised for each u at each time step now that the states and adjoint states are known for the given input and disturbance. A new and better time sequence for u can be calculated by following (6.28) a new and better time sequence.

4. Repeat step 1 and 2 with the control input sequence generated by step 3.

5. The steps 1-4 should be repeated M times until the captured energy given by (6.17) has converged. Then the optimal control sequence will be given by the converged value.

6.7 Discretisation

The algorithm will be solved numerically by the computerprogram MATLAB. Thus, the nonlinear state dynamics , Hamiltation term (6.19) and adjont state should be discretized.

The state dynamics could be discretised by using a second order Taylor's Method applied to nonlinear systems according to Kazantzis & Kravaris (1999). If the time step is denoted h, the forward difference is defined according to (6.29). Solving for x_k gives the forward stepping formula (6.30). The time derviative of (5.54) can be found according to (6.31), when $\dot{u} = 0$. As a final step the results can be combined to (6.32).

$$\mathbf{x_{k-1}} - \mathbf{x_k} = \mathbf{f}(\mathbf{x_k}, \mathbf{u_k}, \mathbf{F_e k}) + \frac{\mathbf{h^2}}{\mathbf{2}} \frac{\partial \mathbf{f}}{\partial \mathbf{t}} (\mathbf{x_k}, \mathbf{u_k}, \mathbf{F_e k}) \tag{6.29}$$

$$\mathbf{x_{k-1}} = \mathbf{x_k} + \mathbf{f}(\mathbf{x_k}, \mathbf{u_k}, \mathbf{F_e k}) + \frac{\mathbf{h^2}}{\mathbf{2}} \frac{\partial \mathbf{f}}{\partial \mathbf{t}} (\mathbf{x_k}, \mathbf{u_k}, \mathbf{F_e k}) \tag{6.30}$$

$$\frac{\partial \mathbf{f}}{\partial \mathbf{t}} = \frac{\partial \mathbf{f}}{\partial \mathbf{x}} \dot{\mathbf{x}} + \frac{\partial \mathbf{f}}{\partial \mathbf{u}} \dot{\mathbf{u}} + \frac{\partial \mathbf{f}}{\partial \mathbf{F_e}} \dot{\mathbf{F}}_\mathbf{e} = (\mathbf{A} + \mathbf{uG})\mathbf{x} + \dot{\mathbf{u}}\mathbf{G}\mathbf{x} + \mathbf{E}\dot{\mathbf{F}}_\mathbf{e} \tag{6.31}$$

$$\mathbf{x_{k-1}} = \mathbf{x_k} + \mathbf{h}(\mathbf{A}\mathbf{x_k} + \mathbf{u_k}\mathbf{G}\mathbf{x_k} + \mathbf{E}\mathbf{F_{ek}}) + \frac{\mathbf{h^2}}{\mathbf{2}} \left[(\mathbf{A} + \mathbf{uG})(\mathbf{A}\mathbf{x_k} + \mathbf{u_k}\mathbf{G}\mathbf{x_k} + \mathbf{E}\mathbf{F_{ek}}) + \mathbf{E}\dot{\mathbf{F}}_\mathbf{ek} \right] \tag{6.32}$$

The adjont dynamics is integrated backwards in time. Thus, it is desirable to keep the discretisation explicit to avoid computational complexity. Backward difference and Taylor's method can be used for solving the adjoint dynamics. The equation can be given according to (6.33) and the backward stepping dynamics (6.34) is found by rearranging the formula. By derivating (6.25) in time (6.35) is found. The resulting numerical equation of the adjoint dynamics is found to be (6.36).

$$\lambda_{\mathbf{k+1}} - \lambda_\mathbf{k} = \mathbf{g}(\mathbf{x_{k+1}}, \mathbf{u_{k+1}}, \lambda_{\mathbf{k+1}}) - \frac{\mathbf{h^2}}{\mathbf{2}} \frac{\partial \mathbf{g}}{\partial \mathbf{t}} (\mathbf{x_{k+1}}, \mathbf{u_{k+1}}, \lambda_{\mathbf{k+1}}) \tag{6.33}$$

$$\lambda_\mathbf{k} = \lambda_{\mathbf{k+1}} - \mathbf{g}(\mathbf{x_{k+1}}, \mathbf{u_{k+1}}, \lambda_{\mathbf{k+1}}) + \frac{\mathbf{h^2}}{\mathbf{2}} \frac{\partial \mathbf{g}}{\partial \mathbf{t}} (\mathbf{x_{k+1}}, \mathbf{u_{k+1}}, \lambda_{\mathbf{k+1}}) \tag{6.34}$$

$$\frac{\partial \mathbf{g}}{\partial \mathbf{t}} = \frac{\partial \mathbf{g}}{\partial \lambda} \dot{\lambda} + \frac{\partial \mathbf{g}}{\partial \mathbf{u}} \dot{\mathbf{u}} + \frac{\partial \mathbf{f}}{\partial \mathbf{x}} \dot{\mathbf{x}} = -(\mathbf{A^T} + \mathbf{uG})\lambda + \dot{\mathbf{u}}\mathbf{G}\lambda - \mathbf{2Q}\mathbf{x} \tag{6.35}$$

$$\begin{aligned} \lambda_\mathbf{k} = \lambda_{\mathbf{k+1}} + \mathbf{h}(\mathbf{A^T}\lambda_{\mathbf{k+1}} + \mathbf{u_{k+1}}\mathbf{G}\lambda_{\mathbf{k+1}} + \mathbf{2Q}\mathbf{x_{k+1}}) \\ + \frac{\mathbf{h^2}}{\mathbf{2}} \big[(\mathbf{A^T} + \mathbf{u_{k+1}}\mathbf{G})(\mathbf{A^T}\lambda_{\mathbf{k+1}} + \mathbf{u_{k+1}}\mathbf{G}\lambda_{\mathbf{k+1}} + \mathbf{2Q}\mathbf{x_{k+1}}) \\ -\mathbf{2Q}(\mathbf{A}\mathbf{x_{k+1}} + \mathbf{u_{k+1}}\mathbf{G}\mathbf{x_{k+1}} + \mathbf{E}\mathbf{F_{ek+1}}) \big] \end{aligned} \tag{6.36}$$

Chapter 7

Estimation

In order to do the correct control action the forces must be predicted some time in the future. This can be done by measuring the wave elevation and estimating the excitation forces based on these measurements. In this chapter an estimation setup and algorithm is developed.

7.1 Instrumentation Setup

The first step in the estimator development was to decide upon an instrumentation setup and choosing measurements methods. As mentioned in Section 2.8, the most common measurement method for WECs is up-wave measurements, as opposed to installing the measurements devices on the WEC. By utilizing measurements on the WEC itself it is challenging to predict the quantities some seconds into the future. However, up-wave measurements methods also include challenges due to the harsh weather environment which may cause damage to the WECs and the changing wave directions which makes it necessary to install an extinctive amount of WECs in order to cover all the environmental conditions. However, in the case of WEC technology these challenges may be solved naturally.

"A reasonably sized wave-power plant should consist of an array of many (hundreds, or even thousands) power buoy units".

The quote is from Falnes & Hals (2012) where it is argued that the final step of the development of WEC technology is producing a reasonable amount of devices in order to produce a useful amount of electricity, or in this case, fresh water. It was suggested that the devices should be installed in a grid as illustrated in Figure 7.1. For a setup of this kind, measurement devices could be installed on all the WECs and the measurement quantities could be estimated from measurements of the surrounding WECs. In this way the method is a combination of up-wave and on WEC measurements.

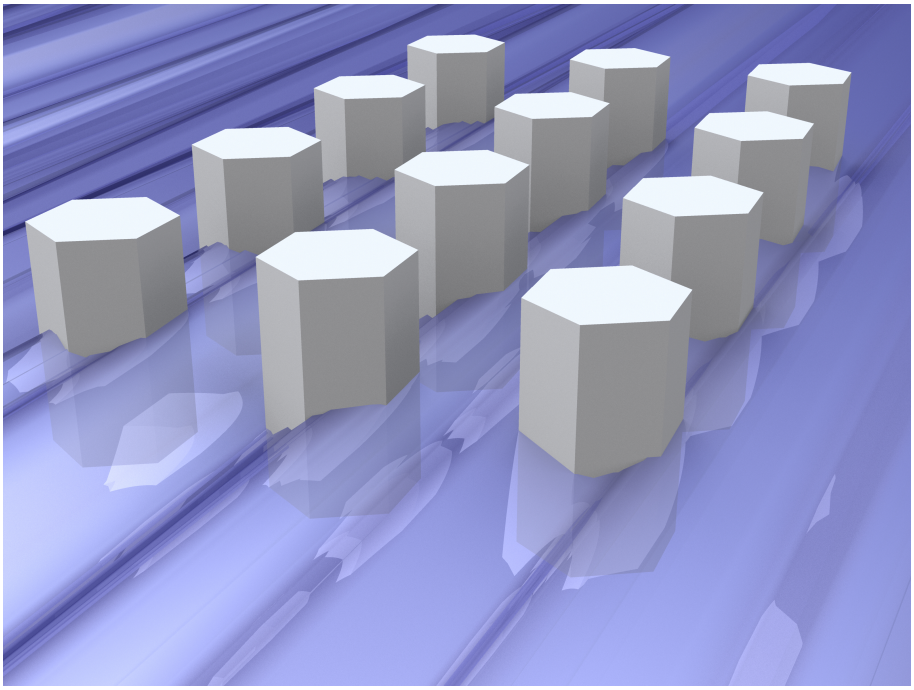

Figure 7.1: Grid of WECs.

In the field of sea state estimation it is common to estimate the wave elevation in order to find information about incoming wave and the sea state in general. If wave elevation is known, the excitation force can be estimated by utilizing Fourier analysis. Also in the recent research of WEC this method in widely spread. Therefore it was proposed that the measured quantity for the WEC of interest should be the wave elevation.

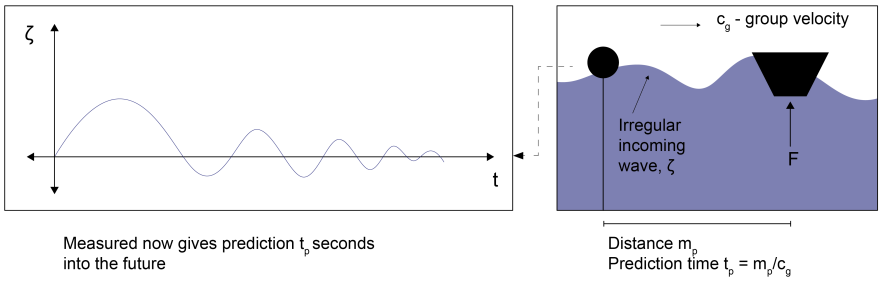

Figure 7.2: Instrumentation setup.

An illustration of a measured time series is shown in Figure 7.2 (left). As a start a simplified model is studied, containing one WEC and one measurement device in irregular sea, see Figure 7.2 (right). In a real life case the measurement device would be replaced with another WEC. For this setup it is assumed that the measurement device is placed directly up-wave of the WEC. If the group velocity of the waves is c_g and the distance between the

two devices is m_p, the wave elevation measured by the buoy will give an estimate of the wave elevation after $t_p = m_p/c_g$ seconds. t_p is the time it takes from the wave group passes the measurement device until it reaches the WEC. This is illustrated in Figure 7.2 (right).

7.2 Estimation Objective

The excitation force must be predicted t_p seconds into the future. This will be done by measuring the wave elevation m_p meters upstream of the wave and generating a time series of t_p seconds of the wave elevation. Wave elevation at the WEC can then be estimated based on the measurements. That is the purpose of the estimator/observer. The excitation force can then be calculated from the estimated wave elevation. The estimation objective can be formulated by the following quote.

Predict the wave elevation t_p seconds into the future based on measurements m_p meters down stream.

7.3 Prediction Length

The challenge of controlling the WECs is knowing when to delatch the two parts of the WEC. A requirement for calculating the optimal control sequence (6.13) according to the theory represented in Chapter 6 the excitation force must be predicted some time into the future. This duration is the prediction time and for the setup described above it equals the time it takes for the wave to travel between the two devices, t_p. m_p is the same distance that should separate all the WECs in the grid in order to assure a sufficiently long prediction span for the excitation force.

$$t_p = \frac{m_p}{c_g} \tag{7.1}$$

If an estimate of an average high value of c_p is known or assumed, the factors involved in deciding t_p and m_p are as following.

- Timespan of prediction needed for the controller.
- Capture width.
- Length of time series necessary to ensure accuracy of reconstructed spectrum and phase angles.

The capture width is defined in Section 4.5. The amount of energy that the WEC absorbs is equal to the amount of energy in a wave front of width equal to the capture width. Thus, the distance between the WECs should be larger than the capture width. However, energy

will not be captured uniformly restricted to this area. The absorption picture is unknown to the author, it is assumed that a distance of two times the capture width is sufficient to ensure maximum power outtake for each WEC. For the a sea state defined by $H_s = 2.5$ and $T_p = 9.1$ the capture width for the DynOcean was calculated to be as given in (7.2). The low value of the capture width indicates that this value will not be determinative.

$$W = 0.0013m \tag{7.2}$$

The controller algorithm optimizes the power output by finding the optimal time instances to latch and delatch. From Figure 8.7 it can be seen that there are two latch-delatch instances per wavelength. Hence, there is one per half of wavelength. It can be concluded the wave elevation should be predicted at least one half of a wavelength into the future for satisfactory performance of the controller. Since irregular waves consist of a range of regular waves, the prediction length should be dimensioned for the longest wave period. From the JONSWAP spectrum 8.1a the smallest frequency is found to be

$$\omega_{min} = 0.4\frac{rad}{s} \qquad T_{max} = \frac{2\pi}{\omega_{min}} = 15.7s \tag{7.3}$$

The calculation of the excitation force was done by reconstruction the spectrum and phase angles form the measured time series. It is necessary with a significant length of the time series so that the correct spectrum is reconstructed. This should be evaluated by simulations.

7.4 Extended Kalman Filter

The Kalman filter is a stochastic estimator, which means that the signal has some element of chance and is not predictable in a deterministic sense. The system models are therefore modeled stochastically. The optimization criterion is linear time-domain minimization of the mean-square estimation error of the random state variables x. This same linear estimate also corresponds to the mean of x conditioned on the entire past measurement stream. The Kalman filter is a recursive algorithm. It produces estimates of x using a series of measurements observed over time, containing noise and other inaccuracies. These estimates tend to be more precise than those based on a single measurement.

This section presents the discrete-time Extended Kalman filter (EKF). The EKF is an extension of the Kalman filter which also considers nonlinear terms which can not be neglected. The system is linearized around a predetermined nominal state trajectory in the linear Kalman filter, the EKF uses the current state estimate as the linearizion trajectory and the linearizion is evaluated at each sampling time instant.There is an extensive amount of publications concerning these estimators, see for instance Simon (2006) and Brown & Hwang (2012). Both the KF and the EKF is broadly used in science and industry and has

proven to be strong observer algorithms.

The system can be written as a discrete nonlinear time-variant state space model where $\hat{x}$ is the state estimate and u_k is the control input.

$$\mathbf{x}_{k+1} = \mathbf{f}_k(\mathbf{x}_k, \mathbf{u}_k) + \mathbf{w}_k \tag{7.4}$$
$$\mathbf{y}_k = \mathbf{h}_k(\mathbf{x}_k) + \mathbf{v}_k \tag{7.5}$$

The process noise $\mathbf{w}_k$ and the sensor noise $\mathbf{v}_k$ are discrete Gaussian white noise processes with known covariance matrices Q and R.

$$\mathbf{w}_k \sim \mathcal{N}(0, R) \tag{7.6}$$
$$\mathbf{v}_k \sim \mathcal{N}(0, Q) \tag{7.7}$$

The covariance matrices of w_k and v_k are given as following, where $E\{\cdot\}$ is the mean value function.

$$E\big[\mathbf{w}_k \mathbf{w}_i^T\big] = \begin{cases} \mathbf{Q}_k & i = k \\ 0 & i \neq k \end{cases} \tag{7.8}$$
$$E\big[\mathbf{v}_k \mathbf{v}_i^T\big] = \begin{cases} \mathbf{R}_k & i = k \\ 0 & i \neq k \end{cases} \tag{7.9}$$
$$E\big[\mathbf{w}_k \mathbf{v}_i^T\big] = \mathbf{0} \quad \text{for all } k \text{ and } i \tag{7.10}$$

RECURSIVE ALGORITHM
The filter is initiated with an initial estimate and estimation error covariance as

$$\hat{\mathbf{x}}_0 = E(\mathbf{x}_0) \tag{7.11}$$
$$\mathbf{P}_0 = E\big[(\mathbf{x}_0 - \hat{\mathbf{x}}_0)^T\big] \tag{7.12}$$

↓ Update
The linearisations of the nonlinear dynamics $\mathbf{f_k}$ and measurement $\mathbf{h}_k$ are made about the current state estimate according to

$$\mathbf{\Phi}_k = \left.\frac{\partial \mathbf{f}_k(\mathbf{x}_k, \mathbf{u}_k)}{\partial \mathbf{x}_k}\right|_{x_k = \hat{x}_k} = \begin{bmatrix} \frac{\partial f_1}{\partial x_1}\big|_{x_k=\hat{x}_k} & \frac{\partial f_1}{\partial x_2}\big|_{x_k=\hat{x}_k} & \cdots & \frac{\partial f_1}{\partial x_n}\big|_{x_k=\hat{x}_k} \\ \frac{\partial f_2}{\partial x_1}\big|_{x_k=\hat{x}_k} & \frac{\partial f_2}{\partial x_2}\big|_{x_k=\hat{x}_k} & \cdots & \frac{\partial f_2}{\partial x_n}\big|_{x_k=\hat{x}_k} \\ \vdots & \vdots & \ddots & \vdots \\ \frac{\partial f_n}{\partial x_1}\big|_{x_k=\hat{x}_k} & \frac{\partial f_n}{\partial x_2}\big|_{x_k=\hat{x}_k} & \cdots & \frac{\partial f_n}{\partial x_n}\big|_{x_k=\hat{x}_k} \end{bmatrix} \tag{7.13}$$

$$\mathbf{H}_k = \left.\frac{\partial \mathbf{h}_k(\mathbf{x}_k)}{\partial \mathbf{x}_k}\right|_{x_k = \hat{\mathbf{x}}_k} = \begin{bmatrix} \frac{\partial h_1}{\partial x_1}\big|_{x_k=\hat{x}_k} & \frac{\partial h_1}{\partial x_2}\big|_{x_k=\hat{x}_k} & \cdots & \frac{\partial h_1}{\partial x_n}\big|_{x_k=\hat{x}_k} \\ \frac{\partial h_2}{\partial x_1}\big|_{x_k=\hat{x}_k} & \frac{\partial h_2}{\partial x_2}\big|_{x_k=\hat{x}_k} & \cdots & \frac{\partial h_2}{\partial x_n}\big|_{x_k=\hat{x}_k} \\ \vdots & \vdots & \ddots & \vdots \\ \frac{\partial h_m}{\partial x_1}\big|_{x_k=\hat{x}_k} & \frac{\partial h_m}{\partial x_2}\big|_{x_k=\hat{x}_k} & \cdots & \frac{\partial h_m}{\partial x_n}\big|_{x_k=\hat{x}_k} \end{bmatrix} \tag{7.14}$$

Compute Kalman gain

$$\mathbf{K}_k = \mathbf{P}_{k-1|k-1}\mathbf{H}_k^T(\mathbf{H}_k\mathbf{P}_{k-1|k-1}\mathbf{H}_k^T + \mathbf{R}_k)^{-1} \tag{7.15}$$

The corrector or a posteriori estimate is given by

$$\hat{\mathbf{x}}_{k|k-1} = \hat{\mathbf{x}}_{k-1|k-1} + \mathbf{K}_k(\mathbf{y}_k - \mathbf{H}_k\hat{\mathbf{x}}_{k-1|k-1}) \tag{7.16}$$

Compute error covariance for updated estimate

$$\mathbf{P}_k = (\mathbf{I} - \mathbf{K}_k\mathbf{H}_k)\mathbf{P}_{k-1|k-1} \tag{7.17}$$

Prediction of State Ahead
Predictor or a priori estimate is given by

$$\hat{\mathbf{x}}_{k+1|k} = \mathbf{\Phi}_{k|k}\hat{\mathbf{x}}_{k|k} \tag{7.18}$$

$$\mathbf{P}_{k+1|k} = \mathbf{\Phi}_k\mathbf{P}_k\mathbf{\Phi}_k^T + \mathbf{Q}_k \tag{7.19}$$

Next Step ↑

The EKF is in general not optimal like the Kalman filter and might diverge if the initial estimate is wrong since the linearizion will not be around the operating point. Furthermore, a poor estimate might lead to a wrong linearizion, in turn leading to an even worse estimate in the next sample. A stability proof is difficult because of the feedback from the measurement into the process model (Brown & Hwang 2012). In spite of these concerns the EKF is the most widely applied nonlinear state estimation technique (Simon 2006) and have been used for a variety of applications.

7.4.1 Estimation Algorithm for DynOcean

Derive corresponding mathematical estimator algorithms and discuss analytically their robustness and performance in regards to stability and sensitivity to measurement noise, parameter uncertainty, and unmodeled dynamics.

Mathematical Model

An approach to the Kalman filter is given in Budal, Falnes & Onshus (1979). The ideas of the development of the following filter are inspired by this. As given in Section 7.4 mathematical formulations of the quantities of interest ingo as a part of the algorithm. It is a challenge to model an irregular wave mathematical. The statistical description given in Section 4.3 is useful to describe average trends in the long run, however will not serve as a tool for describing the wave in real-time. By visual inspection of the propagating water wave there may be some resemblance between a sine wave and a smooth wave. Thus, an approximation to a dynamic model for the wave may, be chosen as a harmonic oscillator with angular frequency ω_k and damping term d (7.20).

$$\ddot{\zeta} + d\dot{\zeta} + \omega_k^2\zeta = 0 \tag{7.20}$$

The damping term in the is included to avoid purely imaginary eigenvalues and numerical problems. Since the force acting upon the model is unknown, it is set to zero. This model is only an approximation to a irregular wave and cannot describe all the waves one can observe. Two major objections are to following.

- ω_k is not a constant, but time varying. All the frequencies of the band width of the spectrum are found in the wave.
- This model can not fit an irregular wave exactly, even if the frequency is adjusted.

The model can, however describe the n'th harmonic in the irregular wave (see Section 4.3). If the spectrum is studied, it can be observed that it has a typical peak, and that much of the energy is centered abound this frequency. From the width of the spectrum one can see the range of frequency variation. But the rate of change of the frequency is still unknown, hence it is convenient to estimate the instantaneous frequency of the wave in order to fit the model as well as possible.

The measured wave can be expressed as (7.21). The measurement equipment may cause a time varying mean which is added as μ in the formula.

$$y = \zeta + \mu \tag{7.21}$$

By defining $x_1 = x$ and $x_2 = \dot{x_1} = \dot{x}$ the system can be written according to (7.22)-(7.24).

$$\dot{x_1} = x_2 \tag{7.22}$$
$$\dot{x_2} = -dx_2 - \omega_k^2 x_1 \tag{7.23}$$
$$y = x_1 + \mu \tag{7.24}$$

In addition to the two state variables given in (7.22) and (7.23), the wave model has two unknown parameters. These can be assumed to be constant and written as following.

$$\begin{aligned} \dot{\omega} &= 0 \\ \dot{\mu} &= 0 \end{aligned} \tag{7.25}$$

By defining $x_3 = \omega$ and $x_4 = \mu$. The physical model can then be defined as (7.26).

$$\begin{aligned} \dot{x}_{1,k} &= x_2 \\ \dot{x_2} &= -dx_2 - \omega^2 x_1 \\ \dot{x_3} &= 0 \\ \dot{x_4} &= 0 \\ y &= x_1 + x_4 \end{aligned} \tag{7.26}$$

Discretization

The model should be discretized because it is supposed to run on a digital computer. The definition of the derivative can be given according to (7.27).

$$\frac{dx}{dt} = \dot{x} \triangleq \lim_{\Delta t \to 0} \frac{x(t) + \Delta T) - x(t)}{\Delta T} \approx \frac{x(t) + \Delta T) - x(t)}{\Delta T} \tag{7.27}$$

By defining $x_k = x(t)$ as the k'th point in time and $x_{k+1} = x(t + \Delta T)$ as the next point the system equation (7.22)-(7.24) can be expressed in discrete form according to (7.28)-(7.32).

$$x_{1,k+1} = x_{1,k} + \Delta T x_{2,k} \tag{7.28}$$
$$x_{2,k+1} = (1 - \Delta T d)x_{2,k} - \Delta T \omega_k^2 x_{1,k} \tag{7.29}$$
$$x_{3,k+1} = x_{k,3} \tag{7.30}$$
$$x_{4,k+1} = x_{k,4} \tag{7.31}$$
$$y_k = x_{1,k} + x_{4,k} \tag{7.32}$$

Extended Kalman Filter

The measurements of the wave elevation will include inaccuracies and can therefore not be utilized directly in the control algorithm. In addition, the mathematical model is simple an will not give sufficient results. However, by combing the two in a Kalman Filter this may give a more accurate result than the two independently. The EKF has two purposes, which are given as following.

- Produce a filtered measurement with less accuracy than the real one.
- Give an estimate of unmeasurable quantities, for instance vertical velocity, angular frequency and time varying mean value of wave measurement.

The state vector is then given as $\mathbf{x} = \begin{bmatrix}\zeta, \dot{\zeta}, \omega, \mu\end{bmatrix}^T$. The system equations can be written according to (7.33) -(7.36). w is the process noise, which includes unknown and unmodeled effects. It will be modeled as Gaussian white noise. The measurement vector is influenced by a Gaussian noise v. The system matrix, Φ, will be updated each iteration.

$$\dot{\mathbf{x}}_k = \mathbf{f}(\mathbf{x}_k, v, t) = \Phi_k x_k + w_k \tag{7.33}$$
$$y_k = g(\mathbf{x}_k, w, t) = \mathbf{H}_k \mathbf{x}_k + v_k \tag{7.34}$$

$$\Phi_k = \left.\frac{\partial \mathbf{f}_k(\mathbf{x}_k, \mathbf{u}_k)}{\partial \mathbf{x}_k}\right|_{x_k = \hat{x}_k} = \begin{bmatrix} 1 & \Delta T & 0 & 0 \\ -\Delta T \omega_k^2 & (1 - \Delta T d) & -2\Delta T \omega_k x_{1,k} & 0 \\ 0 & 0 & 1 & 0 \\ 0 & 0 & 0 & 1 \end{bmatrix} \tag{7.35}$$

$$\mathbf{H}_k = \begin{bmatrix}1 & 0 & 0 & 1\end{bmatrix}^T \tag{7.36}$$

Weighing of Kalman Filter

The two noise components w and v have covariance matrices Q and R respectively, which are defined according to (7.8) and (7.9) and can be given as (7.37).

$$Q = \begin{bmatrix} q_1 & 0 & 0 & 0 \\ 0 & q_2 & 0 & 0 \\ 0 & 0 & q_3 & 0 \\ 0 & 0 & 0 & q_4 \end{bmatrix} \qquad R = r_1 \tag{7.37}$$

The covariance values are usually not known, and should be estimated. One way of estimating the values is evaluating how much the mathematical model of the process and measurement can be 'trusted' relative to each other. The weighing can be explained in the following points.

- "A large Q corresponds to little measurement noise and leads to state estimators that respond fast to change in the measured output" (Hespanha 2009, p. 229).
- "A large R corresponds to small disturbances and leads to state estimates that respond cautiously (slowly) to unexpected changes in the measured output" (Hespanha 2009, p. 229).

Sampling and Reconstruction

When studying discrete signals one should take notice to the sampling frequency. The measurement will be sampled with a frequency of f_s and sampling period of ΔT.

$$f_s = \frac{1}{\Delta T} \tag{7.38}$$

According to Nyquist-Shannon theorem the sampling frequency of a signal should be at least twice the size of the highest system frequency w_{max} (Chabaud et al. 2013). This is a requirement to avoid aliasing and allows the discrete signal to be reconstructed without error. The sampling time ΔT must satisfy the criterion given in (7.39). However it is common to sample at a frequency at least ten times the highest system frequency to assure that aliasing is avoided.

$$\Delta T \leq \frac{\pi}{\omega_{max}} = \frac{\pi}{4} = 0.79s \tag{7.39}$$

In the case of wave elevation measurements the dominating frequency of the sea state is the peak frequency ω_p. The band-width of wave frequencies can be found from the spectrum, see Figure 4.1 in Section 4.3.

Chapter 8

Simulation Results

This chapter describes the simulations to verify mathematical models, as well as the performance of the control and estimation algorithms. The main focus is on the estimator and the effect the estimator has on the complete system. However, to ensure proper behavior of each system component, it was necessary to evaluate all the parts separately. One important part of the simulations has been validating the mathematical models and their implementations in the computer program. MATLAB & Simulink (2014a) were used for computations and simulations.

8.1 Simulation Setup

The simulations and tests conducted for this project can be summarized in the following points.

1. Verify the results of the calculations of the ocean waves (Section 8.2)
2. Verify the results of the excitation forces (Section 8.3)
3. Evaluate the identified radiation force parameters (Section 8.4)
4. Verify correct behavior of the modeled WEC (Section 8.5)
5. Verify correct behavior numerical model of the controller in both regular and irregular waves (Section 8.6)
6. Evaluate the performance of the EKF for rediction of the wave elevation (Section 8.7)
7. Test full system performance, which includes effects of prediction errors (Section 8.8)

For points 1 and 4 the performance was compared to the results given Johannessen et al. (2011). In the paper the response and power output of the DynOcean wave buoy was estimated by utilizing SIMO, a computer program developed by MARINTEK and marketed through DNV GL. In this paper the results are given for $H_s = 2.5$ and $T_p = 9.1$, thus the model performance was validated by studying the sea state defined by this parameter. For this project the waves were modeled according to the JONSWAP spectrum as mentioned in

Section 4.3. However, the comparison paper used a PM-spectrum, hence the value of γ will be set to one for these tests.

For the simulations in point 5 tests were run for the sea state mentioned above. In addition, the sea state with highest probability of occurring, one high energy and one low energy sea state was included, which also had relatively high probability of occurring (see Table 4.1). It was assured that these three cases were sufficient to make provisional conclusions for the system. However, in the case of realization of the concept more thorough analysis should be conducted. Table 8.1 gives the sea state simulation values.

H_s	T_p
2.5	6.5
2.5	11.5
5.5	14.5

Table 8.1: Sea state simulation values.

For most of the simulation cases regular waves were studied as a starting point. In these cases the values related to the two frequencies of (8.1) were used, as given in the tables A.1-A.3.

$$\omega_{w,1} = 0.4 \ \frac{rad}{s} \qquad \omega_{w,2} = 0.85 \ \frac{rad}{s} \tag{8.1}$$

The performance of the estimator (point 7) was tested under influence of white noise. The noise was added by using the 'Band-Limited White Noise' block in Simulink. The noise has correlation of 0, a float power spectral density (PSD), and a total energy of infinity. The block inputs sample time and noise power, p_n. The noise power approximates the covariance of the white noise but is actually the height of the PSD (MathWorks 2015). Three values were used in the simulation: $p_n = \{0.001, 0.01, 0.1\}$.

8.2 Ocean Waves

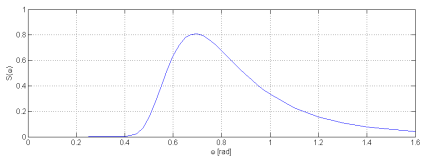

(a) JONSWAP spectrum for $H_s = 2.5$ and $T_p = 9.1$.

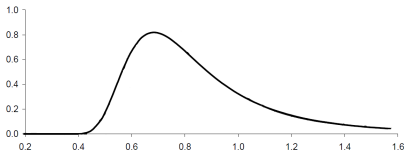

(b) Comparison JONSWAP spectrum for $H_s = 2.5$ and $T_p = 9.1$ remake from Johannessen et al. (2011).

Figure 8.1a shows a plot of the wave spectrum generated for this project and Figure 8.1b shows the spectrum from the comparison paper (Johannessen et al. 2011). The two figures are equal, which is an indicator that the spectrum generated for this thesis simulates the correct JONSWAP spectrum. It can then be concluded that the wave spectrum, and the wave elevation generated by the wave spectrum should be correct. A plot of the resulting wave elevation is shown in Figure 8.2.

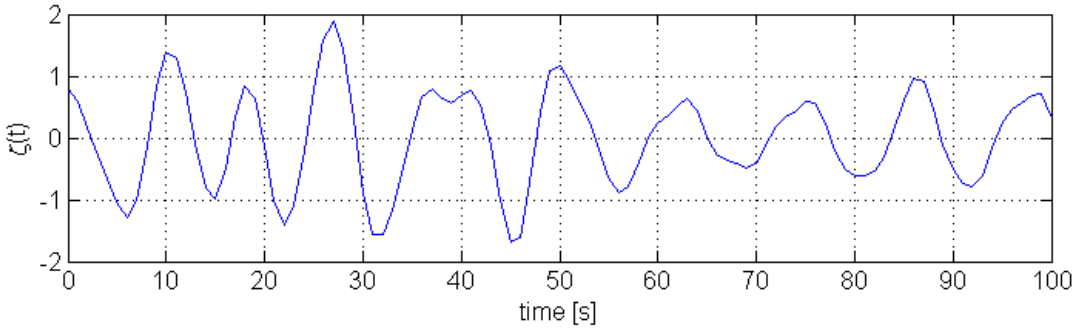

Figure 8.2: Wave elevation of sea state defined by $H_s = 2.5$ and $T_p = 9.1$.

8.3 Excitation Forces

The excitation force acting on the WEC from a regular wave of frequency $\omega = 0.85\ \frac{rad}{s}$ and wave amplitude $\zeta_A = 1$ m is shown in Figure 8.3. The blue graph indicates the excitation forces on the buoy, and red graph on the plate. The magnitude is quite large, with a amplitude of about 1 MN. The large size of the force is due to the dimensions of the WEC, see Chapter 3. The force working on the disc is smaller which is to be expected.

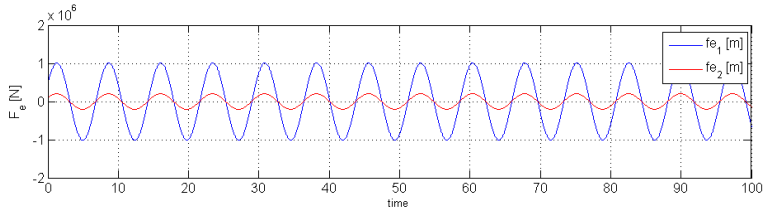

Figure 8.3: Excitation force on WEC from regular wave of frequency $\omega = 0.85\ \frac{rad}{s}$ and wave amplitude $\zeta_A = 1$ m.

The value seems reasonable by studying the amplitudes of the transfer function between the wave and excitations force given in A.1 in Appendix A. The amplitude value of the transfer function for the buoy is approximately 1 MN. The phase between the two force components is zero. From Table A.1 in Appendix A it can be seen that the phase between the force and the incoming wave is the same for the buoy and the disc for frequencies below

$\omega_w = 1.1\frac{rad}{s}$. For frequencies above this there is somewhat of a difference. Thus, there will be a phase difference between the two forces at these frequencies. Both the force components have the same frequency. The reason is that a linear relation is assumed between the wave elevation and force. This will be the case for all frequencies.

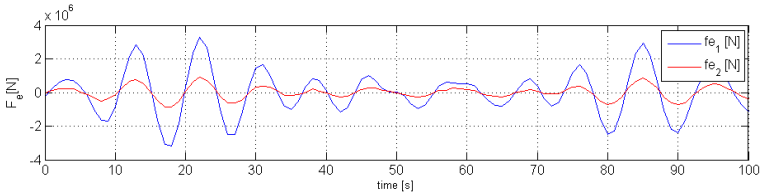

Figure 8.4: Excitation force on WEC from irregular waves of sea state defined by $H_s = 2.5$ m and $T_p = 9.1$ s.

Figure 8.4 shows the excitation force working on the WEC from irregular waves of a sea state defined by $H_s = 2.5$ m and $Tp = 9.1$ s. The blue graph indicates the buoy and red indicates the disc. The force is in the same order of magnitude as the regular wave discussed above, but varies in phase, frequency and amplitude. The forces are calculated from the theory given in Section 5.2.1. Validation of the transfer functions and phases given in Table A.1 is out of the scope of this thesis, as is validating the accuracy of linear theory. However, assuming that both of these provide a good approximation to the force combined, the calculated force seems to give a good result.

8.4 Radiation Forces

The 'Matlab Toolbox for identification of Radiation Force Models' was applied as described in Section 5.4. The approximation of the transfer function for DOF 11 is given in (8.2) and the infinite added mass is given in (8.3).

$$\hat{k}_{11}(s) = \frac{2.626 \times 10^5 s}{s^2 + 0.8879s + 0.4802} \tag{8.2}$$

$$\hat{a}_{11}(\infty) = 4.4134 \times 10^5 \tag{8.3}$$

The eigenvalues of the system were given by the roots of the transfer function (Balchen et al. 2003). In the case of (8.2) the roots were found to be

$$\lambda_1 = -0.4439 + 0.5321i \qquad \lambda_2 = -0.4439 - 0.5321i \tag{8.4}$$

The real parts of the eigenvalues were negative, thus the system is stable.

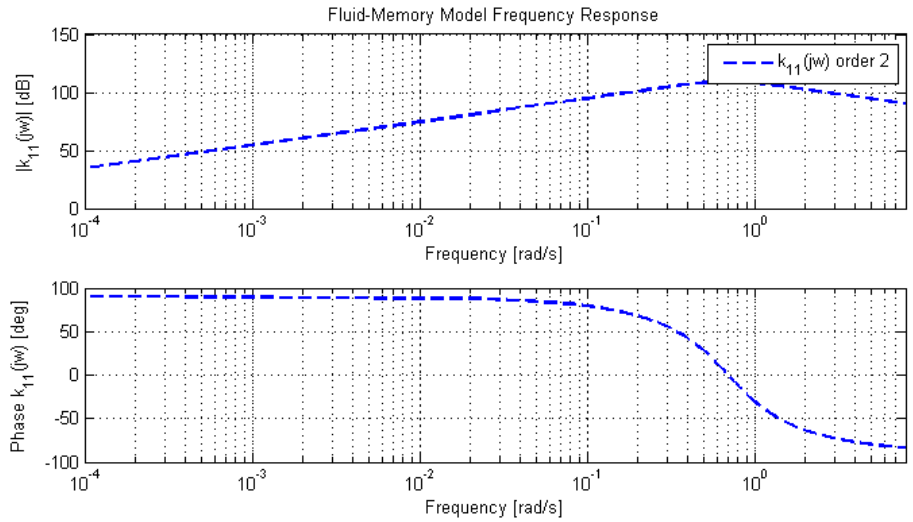

Figure 8.5: Frequency response of the identified fluid-memory model degree of freedom 11.

The linear state space equations were calculated and given by the canonical realization in (8.5)-(8.6). These matrix values were used in the additional state space equation in the Cummins equation (see Section 5.5). Figure 8.5 shows the frequency response of the identified retardation function for DOF 11, k_{11}.

$$\hat{A}_{11} = \begin{bmatrix} -0.8879 & 1.0000 \\ -0.4802 & 0 \end{bmatrix} \qquad \hat{B}_{11} = \begin{bmatrix} 2.6263 \times 10^5 \\ 0 \end{bmatrix} \tag{8.5}$$

$$\hat{C}_{11} = \begin{bmatrix} 1 & 0 \end{bmatrix} \tag{8.6}$$

Figure 8.6 shows the identification results for DOF 11. In the right-hand-side the estimated value of the added mass and damping are plotted against the original values, as explained in Section 5.4. The original values are calculated from (5.48) and (5.49). The left-hand-side shows the result of such calculations for the complex coefficient $A_{ik}(j\omega)$. The upper graph gives the amplitude and the lower graph shows the phase. The dotted lines indicate the real values of the added mass and the stippled line indicates the estimated. The graphs indicate that there is compliance between the estimated values and the real values.

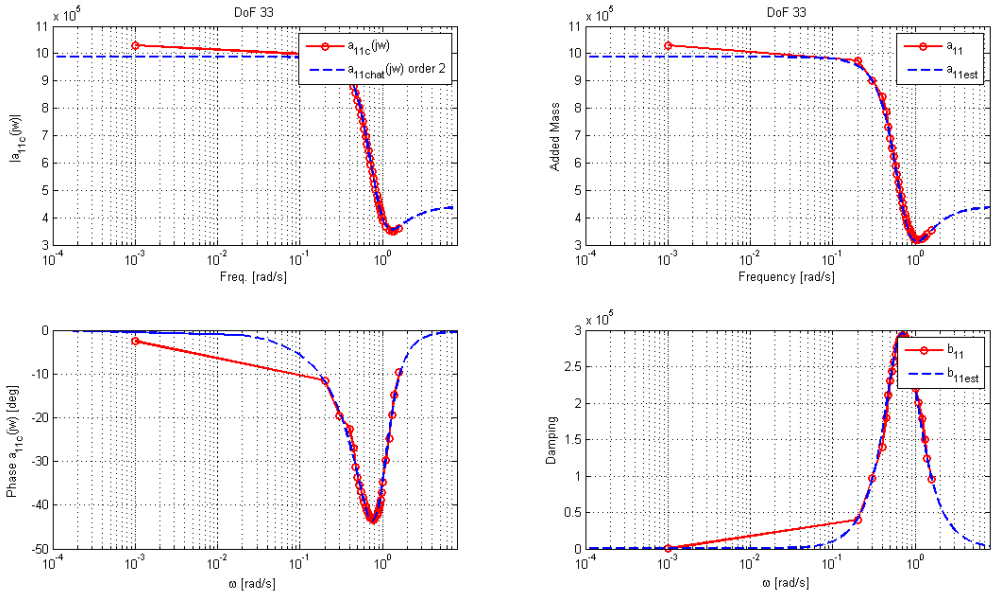

Figure 8.6: Identification results for degree of freedom 11. The complex coefficient $\tilde{\mathrm{A}}(j\omega)$ data and the response of the identified model is illustrated in the left-hand-side plots. The added mass and potential damping and their re-construction based on the estimated model is shown in the right-hand-side plots show.

Furthermore, it can be seen that the waves are generated at frequencies from ∼0.4-1.6 from the spectrum plot in Figure 8.1a, since a linear relation between the waves and response of the WEC is assumed, and the radiation forces are proportional to the velocity and acceleration. The radiation forces may also be assumed to be generated at the same frequencies. By studying the correlation between the two graphs shown in each figure for this frequency range, it is concluded that the approximation is sufficient. For frequencies lower than 0.4 there is a small difference between the two functions, but this is not important seeing as radiation forces will not be generated at these frequencies. However, for other sea states the frequency range is different from the one stated above. By studying the scatter diagram of the area given in Chapter 3 for the low energy cases, the lowest frequency of interest was found to be $\omega = 0.2\frac{rad}{s}$. The comparison values are sufficient above this value, hence the approximation gives sufficient results.

Additionally, the passivity of the system was proven to be passive by testing whether the transfer function (8.2) had a positive real part for frequencies below and above the frequencies used for parameter estimation. Thus, the parameter identification was successful and could be used for the WEC model. Similar analyses were conducted for the three remaining retardation functions. Stability and passivity were proven for all the cases and sufficient results were found by the comparison test for the frequencies of interest. In Appendix B the identification parameters for the remaining retardation functions in addition to the frequency response plots and comparison plots are given.

8.5 WEC Model

8.5.1 Regular Waves

A figure of the Simulink diagram used for calculating the motion of the WEC in regular waves is given in Figure 8.7. The left-hand-side part of the block calculates the excitation force which is input to the response calculations of the middle block. The middle block calculates the results of the state space equation, which is output of the system. The block furthest to the right shows the response output.

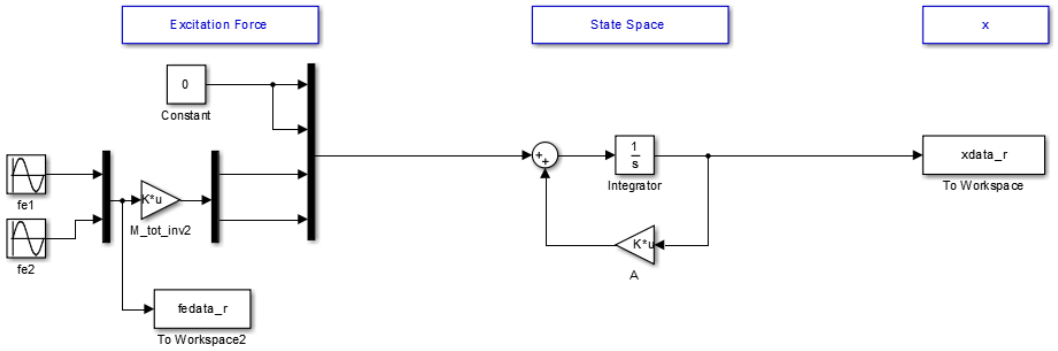

Figure 8.7: Simulink diagram for numerical calculation of WEC response in regular waves.

The calculated response of the WEC under influence of a regular wave of frequency $\omega = 0.85\ \frac{rad}{s}$ and amplitude $\zeta_A = 1$ m is given in Figure 8.8. The excitation forces are shown in Figure 8.3. The response illustrates the general motion pattern for the buoy and disc. There is less movement of the disc than the buoy, and the oscillatory motions are of different phase. The motion characteristics vary for all the frequencies, thus the power outtake varies accordingly. However, the wave of frequency $\omega = 0.85$ gives a large relative motion due to the phase shift of approximately $\frac{\pi}{2}$, which results in a substantial power outtake. Another example is given in Appendix C, for a regular incoming wave of frequency $\omega = 0.4$. Notice initialization transient of 15 s.

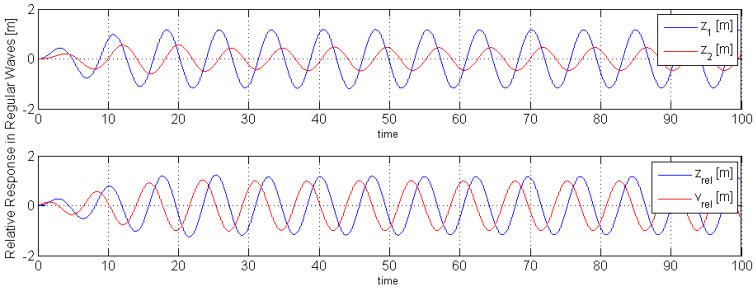

Figure 8.8: Response in regular waves of frequency $\omega = 0.85\ \frac{rad}{s}$ and amplitude $\zeta_A = 1$ m.

8.5.2 Irregular Waves

For simulations of the WEC motion in irregular waves, the Simulink diagram was extended as shown in Figure 8.9. The diagram is structured according to equations (5.53)-(5.54). The structure is similar to that of Figure 8.7, however there are two major differences. The excitation forces now consist of the pre-calculated time-series given in Section 5.2. In addition, the fluid memory effects are added as a state space arrangement (denoted fluid memory effect in the figure). From this state space the fluid memory effects $\boldsymbol{\mu}$ are calculated for each time step.

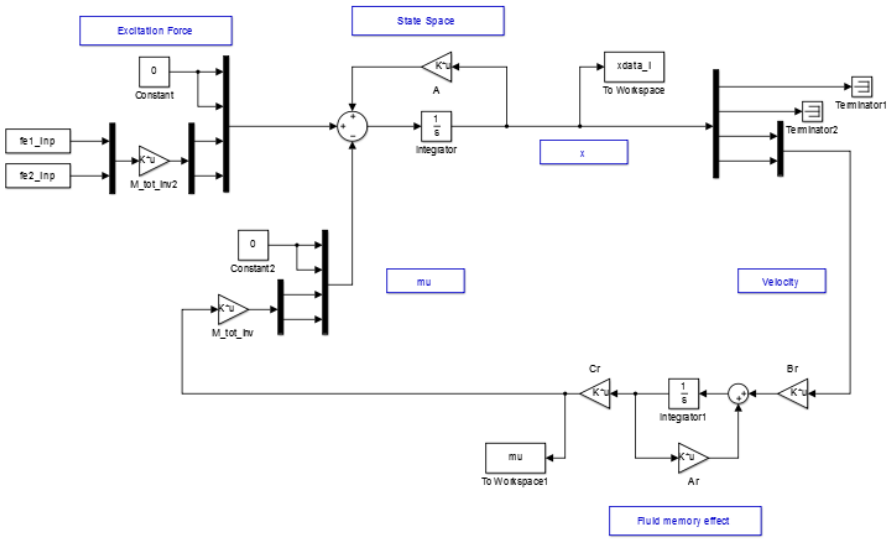

Figure 8.9: Simulink diagram for numerical calculation of WEC response in irregular waves.

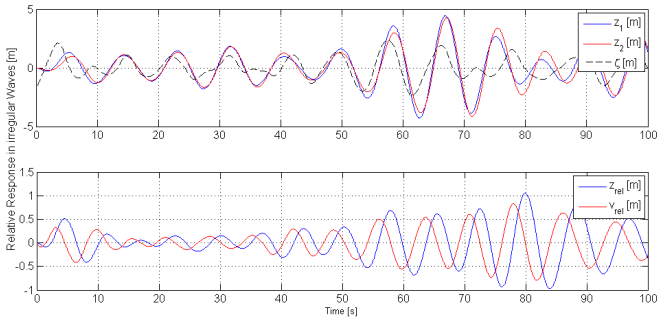

Figure 8.10: Response of WEC for sea state defined by $H_s = 2.5$ m and $T_p = 9.1$ s.

A plot of the WEC response is given in Figure 8.10 (top). From the figure it can be seen that the motion of the buoy (blue graph) and disc (red graph) are quite similar. This is to be expected because the disc is attached to the buoy. In addition, the same wave is inflicting forces on the two bodies, which results in an excitation force of equal frequency and phase

but different amplitude. However there is a small difference in the phase of the two parts. This might be caused by the different inertias and shapes of the buoy and the disc. This causes a discrepancy of the inertia and radiation forces of the two parts. Thus, the result is a relative displacement and velocity as plotted in the bottom graph.

Moreover, it can be seen that the buoy has a displacement of between 0-5 m. The wave displacement (stippled line) lies between 0-2 m, thus the WEC movement is more than twice the size. Due to the dimensions given in Chapter 3, and high inertia of the WEC, these results seem reasonable. The WEC motion follows the wave, but 'lags' behind the wave motion, which is to be expected by a floating structure. Thus, by studying the motion plots, the calculations appear to be right.

	Mean Power [kW]	STD of relative motion [m]
Thesis	209	0.802
Paper	166	0.730
Deviation %	25.9	9.86

Table 8.2: Mean power and STD of relative motion.

Table 8.5.2 shows the mean power outtake and standard deviation (STD) of the DynOcean power buoy calculated as a part of this thesis, and as a part of the paper Johannessen et al. (2011), respectively. From the table it can be seen that the power outtake calculated is 24.4 percent larger than the comparison value. Correspondingly, the standard deviation of the WEC displacement is 9.86 percent larger. The difference is significant. Small differences in results are to be expected due to different computational methods and other simplifications. In addition, a deviation of about 5-10 percent is to be expected due to the random phase of the generated wave. However, an increase of 24.4 percent might be out of the range of what is expected.

Nevertheless, some simplifications were done in this thesis, including neglecting higher order effects, for instance viscous forces and vortex shedding. These forces work as dampers on the WEC and release energy to the water. Neglecting these forces should therefore increase the power output from the WEC, which is the case for these results. This should be investigated further by comparing the calculation method and other results used in this thesis to that of the paper. Due to lack of comparison information and data, this analysis could not be done during this thesis. However, since the motion and power output were of a reasonable order, it was assumed that the simulated motion of the WEC gave satisfactory results and that the program could be utilized for further investigations.

8.6 Controller

The controller described in Section 6.4 was implemented in the Simulink diagram as shown in Figure 8.11.There is one modification to the diagram, which is the control input of $\mathbf{F_L} = u\mathbf{Lz}$ added in the 'state space loop'. The control input, denoted 'u_{inp}' in the diagram, was calculated separately in MATLAB for each iteration.

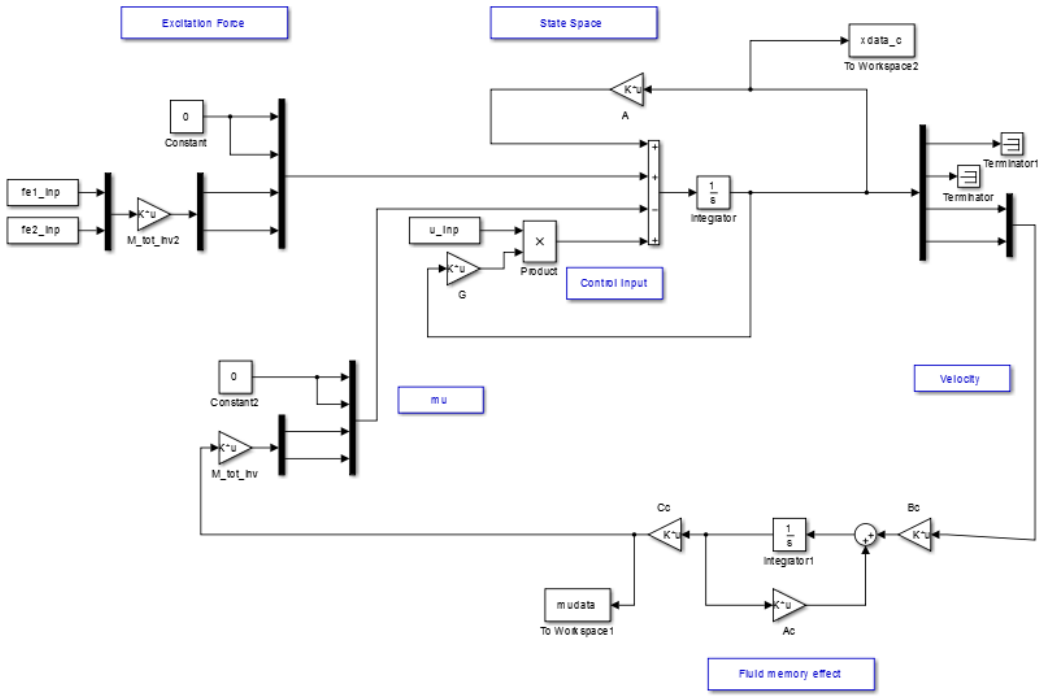

Figure 8.11: Simulink diagram for numerical calculation of WEC response in irregular waves.

8.6.1 Regular Waves

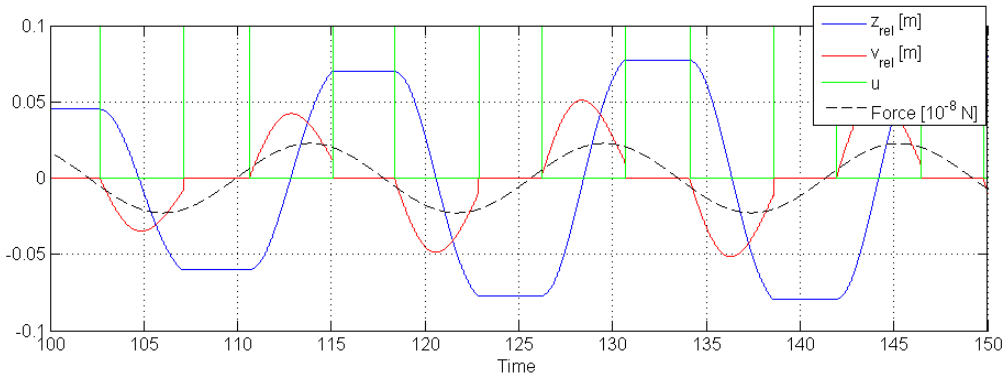

Figure 8.12: Latching control in irregular waves for $\omega = 0.4\frac{rad}{s}$, incoming wave of amplitude $\zeta_A = 1$ m.

Figure 8.12 shows the relative displacement (blue graph) and relative velocity (red graph) of the WEC. The WEC is influenced by an incoming regular wave with frequency $\omega = 0.4$ and amplitude $\zeta_A = 1$ and a latching controller. The normalized control input is the green graph in the figure. As described in Section 6.3, the optimum time instance for latching of a regular wave is when the relative velocity is zero. The optimum instance for delatcing is

such that the oscillatory motion is at its maximum at the same time as the excitation force is at its maximum (Falnes 2002). From the figure it can be seen that the WEC is latched when the relative velocity is zero. In addition, the peak of the force amplitude is almost at the same time instance as the peak of the velocity. The result is resonant motion of the WEC. To summarize, the controller appears to gives satisfactory results and increase the power output of the WEC.

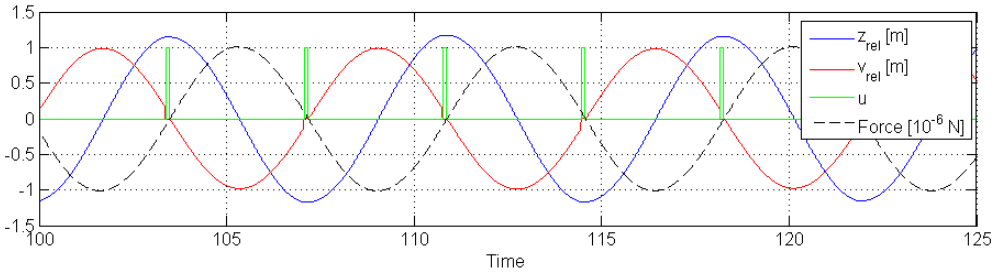

Figure 8.13: Latching control in irregular waves for $\omega = 0.85\frac{rad}{s}$, incoming wave of amplitude $\zeta_A = 1$ m.

Similarly, figure 8.13 shows the latching control phenomenon for an incoming wave of frequency $\omega = 0.85\frac{rad}{s}$ and amplitude $\zeta_A = 1$ m. The varying behavior of the controller for different incoming waves is illustrated. In this case, the controller only latches the movement for short time instances. Hence, there is not much difference in the extracted power. These results agree with the results of Schultz (2014) where it was concluded that the biggest effect of the latching controller on the Ocean Oasis in terms of increase of extracted power, was for small frequencies.

ω [rad/s]	0.40	0.85
Mean Power [kW]	21.76	287.2
Mean Power with Controller [kW]	24.36	288.7
Deviation %	10.7	0.520

Table 8.3: Mean power outtake of WEC in regular waves.

Table 8.6.1 shows the power output for the two cases mentioned above, with and without controller. The power output is larger for the second case due to the increased amount of energy in the wave. The latching control algorithm increases the power output in both cases, but more significantly for the lower frequency. Consequently, the controller performs satisfactory.

8.6.2 Irregular Waves

Figure 8.14 shows the the simulated performance of one iteration in the control algorithm given in Section 6.6. The upper graph shows the relative displacement and the lower graph shows the relative velocity. The blue and red graphs indicate controlled and uncontrolled motion respectively. A visual verification of the controller performance may be conducted.

The figure indicates the same behavior as in regular waves. The velocity is latched for $v_{rel} = 0$ and unlatched a short time after. Proper control action appears to be achieved.

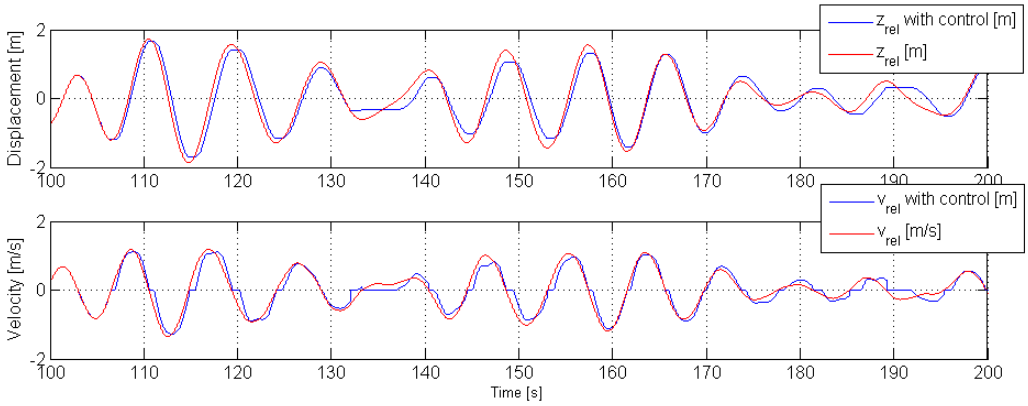

Figure 8.14: Relative response of WEC for sea state defined by $H_s = 2.5$ and $Tp = 9.1$. Upper graph shows relative displacement and lower graph shows relative velocity. Red graph shows uncontrolled motion and the blue graph shows effect on the motion by one iteration of the control algorithm.

However, by studying the power outtake, which is given in Table 8.6.2 (for the case of one iteration), it is seen that the extracted power is reduced by the controller. This is due to halt caused by the controller. The purpose of the latching is to increase the total energy. However in the case of irregular waves the power output is not increased.

	Mean Power [kW]	Mean Power with Controller [kW]	Deviation %
One iteration	169.90	159.89	-5.89
Two iterations	166.06	166.06	0

Table 8.4: Mean extracted power with and without controller for sea state defined by $H_s = 2.5$ m and $T_p = 9.1$ s.

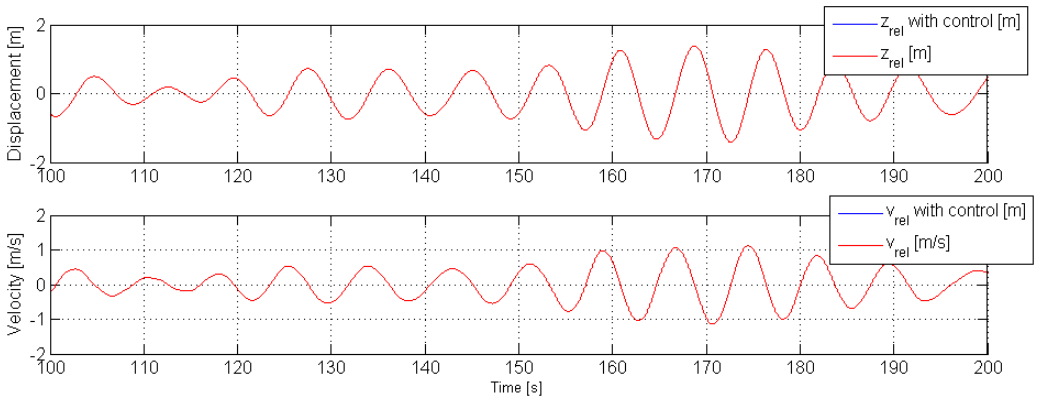

Figure 8.15: Relative response for WEC for sea state defined by $H_s = 2.5$ and $Tp = 9.1$, comparison with and without controller.

Figure 8.15 shows a plot of the controller performance for two or more iterations. The blue graph shows the response with control and the blue graph shows the response without control. The red graph is placed directly on top of the blue, which indicated that the graphs are identical. The optimum control algorithm corrects the behavior of the controller and the result is a control input vector with zeros.

$$\mathbf{u} = \mathbf{0}_{nx1} \tag{8.7}$$

From Table 8.6.2 it can be seen that the power outputs in the two cases are the same. The optimum control condition for this sea state is uncontrolled motion. Thus, there is no reason for implementing a latching controller for this sea state.

	H_s [m]	T_p [s]	P_{mean} [kW]	P_{mean} CTRL [kW]	Deviation %
One	2.5	6.5	60.074	59.352	-1.22
Two	2.5	6.5	73.144	73.144	0
One	2.5	11.5	162.32	158.29	-2.55
Two	2.5	11.5	198.76	198.76	0
One	5.5	14.5	204.63	187.90	-8.90
Two	5.5	14.5	330.34	330.34	0

Table 8.5: Mean extracted power with and without controller.

Table 8.6.2 shows the extracted power for the remaining case sea states. The converging value of the control input is zero for all the cases. The reason might be that the controller only increases the extracted energy for waves with a small value of the frequency. For irregular waves, being a sum of regular waves, the high frequency components will give the local peaks and thus be determinative for the controller.

To summarize, correct performance of the controller may be assumed, that is optimal control is achieved. However the optimum control input for a latching controller is a vector of zeros. Thus, the controller does not increase power output and by that it is not really useful. A more thorough discussion of the latching control algorithm is out of the scope of this thesis.

8.7 Estimation

Even though the control algorithm developed for DynOcean at this stage was unnecessary, an improved method might be developed in the future. Testing the performance of the estimator was therefore completed.

Due to the unknown amount of noise, it was assumed that the mathematical model of the ocean wave could be 'trusted' more than the measurement. The R error covariance matrix was therefore given a larger value than Q. After testing the system the following values of the matrices were selected.

$$Q = \begin{bmatrix} 0.2 & 0 & 0 & 0 \\ 0 & 0.1 & 0 & 0 \\ 0 & 0 & 0.01 & 0 \\ 0 & 0 & 0 & 0.01 \end{bmatrix} \qquad R = 6 \tag{8.8}$$

However, the hight value of R introduced a delay of the estimated wave signal. This could degrade the performance of the system and should be considered in the case of realization of the consent.

8.7.1 Regular Waves

The estimator was tested with a simulated incoming wave of frequency $\omega_w = 0.4\frac{rad}{s}$ and corresponding wave data (see Section 8.1). For the first case the noise power was given a value of $p_n = 0.001$. Figure 8.16 (top) shows the result of the estimation. In the top graph the real wave elevation (blue graph) is plotted with the measurement noise (cyan graph). The performance of the filter is quite satisfactory for this noise level.

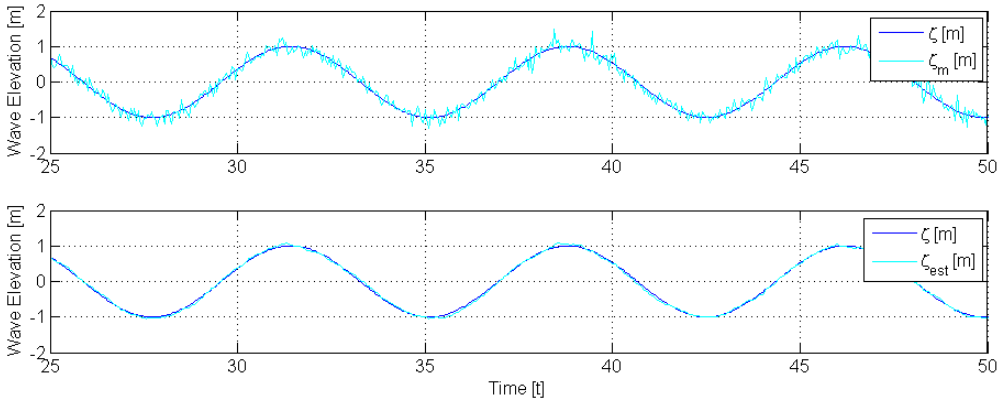

Figure 8.16: Performance of EKF with noise power $p_n = 0.001$.

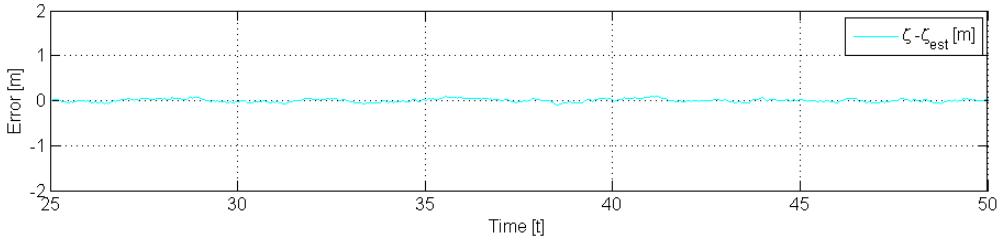

Figure 8.17: Error plot for noise power $p_n = 0.001$.

The standard deviation of the error was found to be $\sigma_{p_n=0.001} = 0.0018$ m, which is a low value. This level of error is not likely to affect the performance of the system. The mean

offset, that is, the middle value of the error was $e_{mean} = 0.0032$ m, which is also low. Figure 8.17 gives a plot of the deviation between the estimated and real value. The figure illustrates the low error. From this noise level the filter gives quite satisfactory results.

p_n	STD deviation [m]	Mean offset [m]
0.001	0.0018	0.0032
0.01	0.0125	0.0041
0.1	0.1215	0.0034

Table 8.6: Standard deviation and mean offset.

Similar analysis was done for noise power values of $p_n = \{0.01, 0.1\}$. Table 8.7.1 gives the values of the standard deviation and mean offset for all the three cases. For a power noise of $p_n = 0.01$ the STD was found to be $\sigma_{p_n=0.01} = 0.0125$ m (plots are given in Appendix C). This is still low for a wave of amplitude $\zeta_A = 1$, and will unlikely affect the performance of the system. However, the simulation for noise power $p_n = 0.01$ gave a STD of $\sigma_{p_n=0.1} = 0.125$ m. This high value of the error may cause problems when the estimated wave elevation is utilized for control purposes. Figure 8.18 and 8.19 show the estimator performance and the error respectively. The high level of measurement noise and estimation error is illustrated. It can be concluded that the EKF model derived has satisfactory performance for estimation of a regular wave for low-medium levels of noise. If there are high noise levels it may be beneficial to reconsider the filter algorithm.

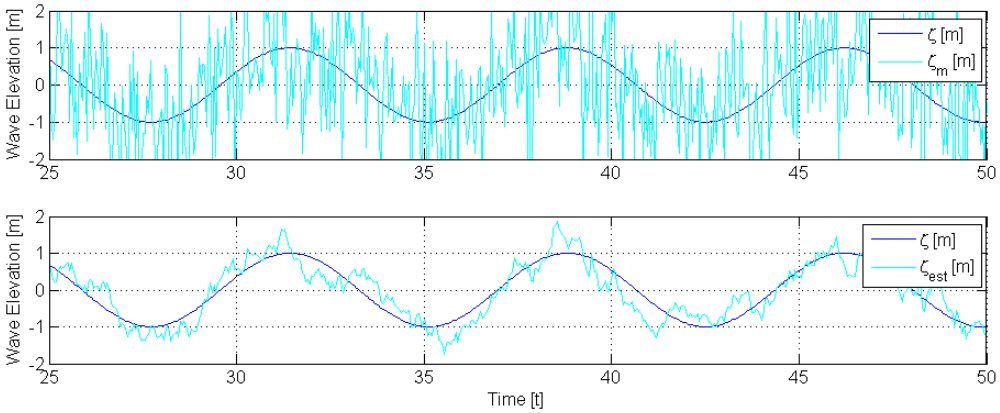

Figure 8.18: Performance of EKF with noise power $p_n = 0.1$.

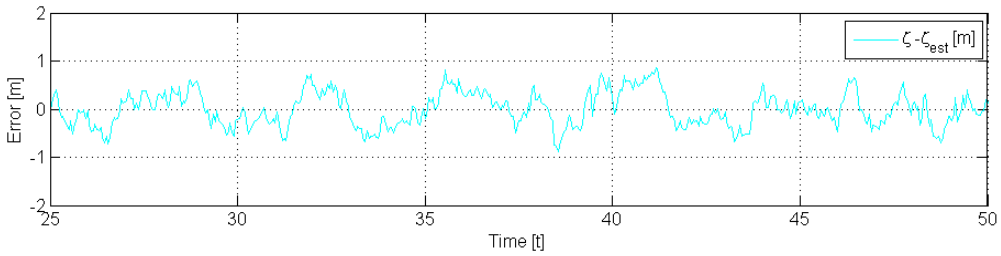

Figure 8.19: Error for noise power $p_n = 0.1$.

8.7.2 Irregular Waves

The performance of the estimator in irregular waves defined by $H_s = 2.5$ m and $T_p = 9.1$ s. Table 8.8.1 gives the values of the STD and mean offset for the three cases. The values of the standard deviation are somewhat larger than for regular waves. As for regular waves, the low-medium noise levels results in sufficiently low estimation error. The mean offset increases for increasing levels of noise. The main difference from regular to irregular waves it that there is a time varying phase shift, which is caused by the simplification of the mathematical model which is approximated as a regular wave. However, as can be seen form Figure 8.21 and 8.21 the performance is satisfactory for sufficiently low frequencies. Figures from the other cases are given in Appendix C.

p_n	STD deviation [m]	Mean offset [m]
0.001	0.0169	0.00382
0.01	0.0279	0.0082
0.1	0.1591	0.0194

Table 8.7: Standard deviation and mean offset.

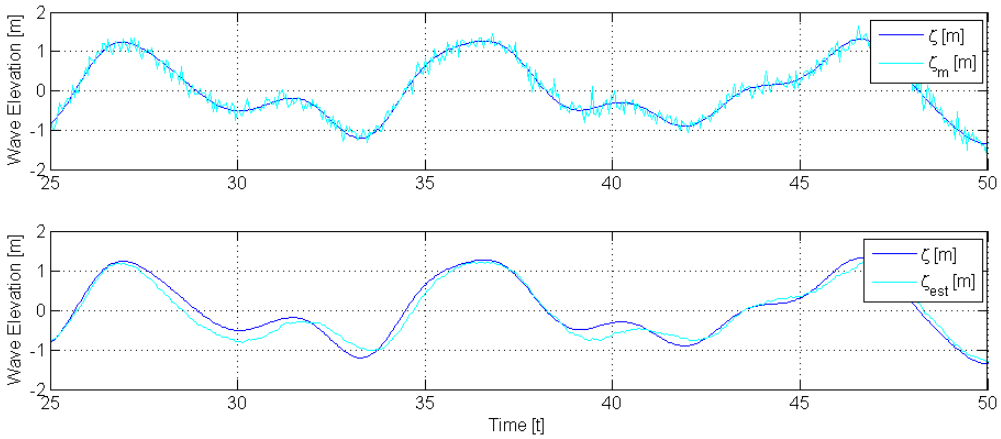

Figure 8.20: Performance of Kalman filter with noise power $p_n = 0.001$.

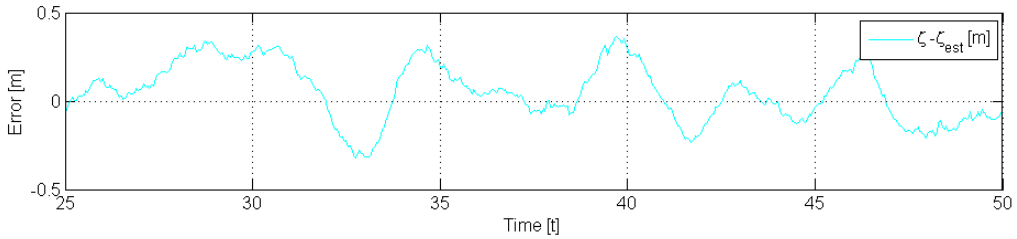

Figure 8.21: Error for noise power $p_n = 0.001$.

8.8 Complete System Simulations

All the components discussed above were gathered to a complete system in MATLAB. The estimated wave elevation was utilized for excitation force calculations, which were input to the controller. In the following discussions of the results of the system performance tests are given.

8.8.1 Regular Waves

A regular wave of frequency $\omega = 0.4\frac{rad}{s}$ and corresponding phase and amplitude was studied for the purpose of testing the complete system dynamics. The first step of the analysis was evaluation the estimated excitation force, F_{em}, calculated from the estimated wave elevation ζ_{est}.

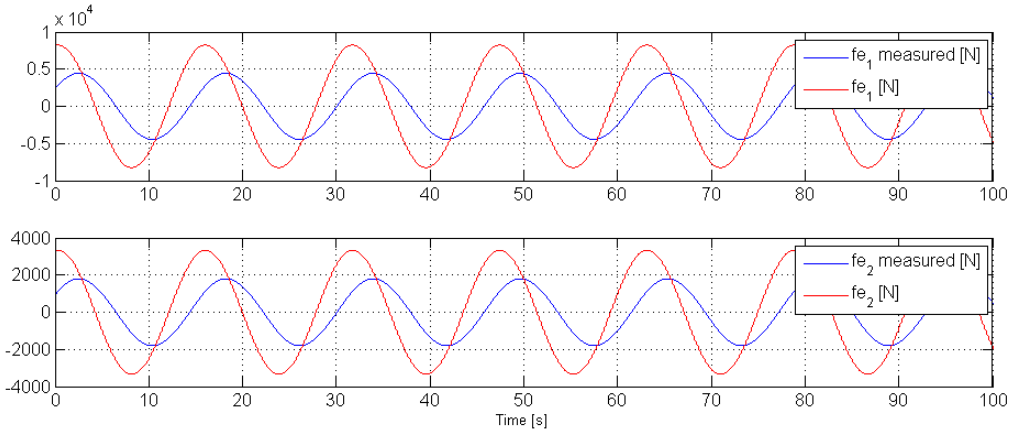

Figure 8.22: Error in the excitation force calculated from the measured wave elevation due to computational method. Upper graph shows forces on the buoy and the lower graph shows forces working on the disc.

Excitation Force

The method of computing the excitation force is given in Section 5.2.2. The wave measurement is Fourier transformed into frequency domain and the amplitude and phase information of the frequency domain wave elevation is used for calculation the excitation force. The function 'fft' in MATLAB was utilized for these calculations. However, some computational errors were introduced by using this method. In Figure 8.22 the excitation calculated from the method is plotted (blue graph) against the real value of the excitation force (red graph). From the figure it can be seen that there is a large error between the two graphs. There is a significant difference in both amplitude and phase. The delay of the graph was found to be $\delta s = 2.23$ s and the difference in amplitude was $\delta fe_1 = 692$ N.

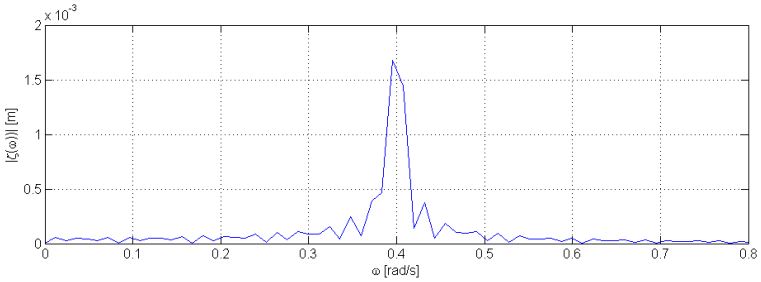

Figure 8.23: Frequency domain wave elevation amplitude plotted for numerical computations of step length $\Delta T = 0.001$ s.

The errors in the excitation force may be due to the inaccuracies in the frequency domain amplitude on the wave elevation, which is plotted in Figure 8.23. From the figure it can be seen that the graph is 'toothed', which indicates that the step length of the calculation is to small, which may cause errors in the results. By increasing the step size from $\Delta T = 0.001$s to $\Delta T = 0.0001$s the graph is smoother as shown in Figure 8.24.

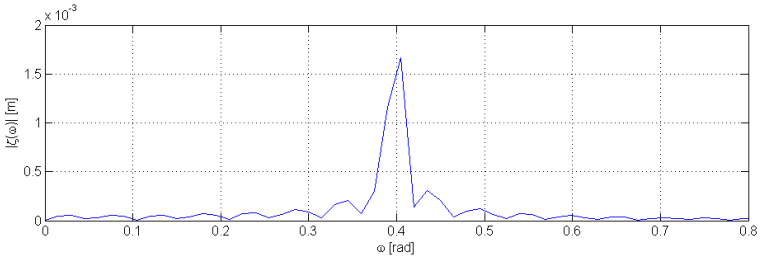

Figure 8.24: Frequency domain wave elevation amplitude plotted for numerical computations of step length $\Delta T = 0.0001$ s.

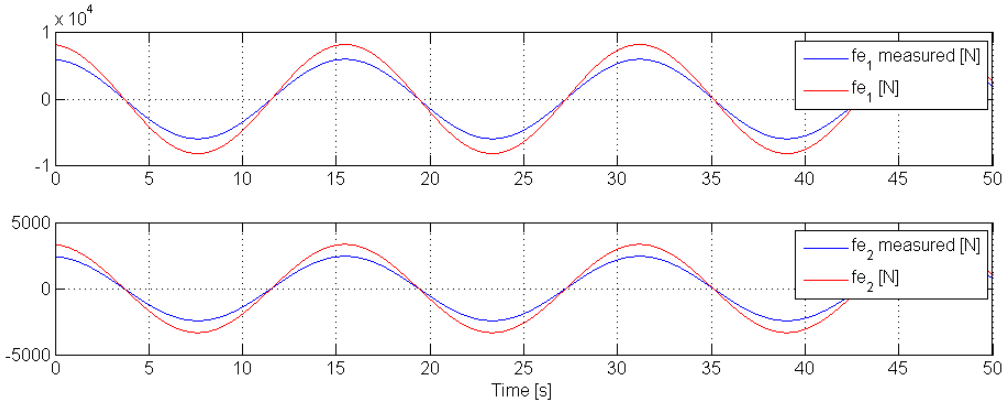

Figure 8.25: Error in the excitation force calculated from the measured wave elevation due to computational method. Numerical computations of step length $\Delta T = 0.0001$ s. Upper graph shows forces on the buoy and the lower graph shows forces working on the disc.

Figure 8.25 shows how the excitation force calculations are improved by increasing the step size. It can be assumed that the error will be reduced even more by reducing the step size. However this would decrease computational efficiency of the real-time control system. Large delays might be introduced, which degrades the performance even more. The figures above only give one example of a frequency. For the other frequencies in the system similar results occur. Some with a larger error and some with a smaller error. The same argumentation can be done for the phase. This error could be reduced by increasing the step size or developing a method for finding the correct value. However, this would also increase the computation time and cause a unwanted delay.

This fault in the excitation force calculations might cause problems for the performance of the control algorithm. It might be possible to develop an 'fft' algorithm for real-time applications, not long term statistics, which is the case for the recent method. However, this is a complex research area which is unknown to the author. Thus, it may be concluded that another method for calculating the excitation force should be explored. These studies are left to further work and the described method is used throughout this thesis.

Including measurement noise

The effect of including measurement noise was studied by using the simulated measured wave signal as input to the system, and excluding the EKF. A noise power of $p_n = 0.01$ was introduced. This gave a variance of 0.01 m, which was a high value compared to the wave amplitude of $\zeta_a = 0.0036$ m for this case. The delay of the graph was found to be $\delta s = 2.22$ s and the difference in amplitude was $\delta fe_1 = 689$ N. Only a small change was found between the graph including measurement noise and the graph without the noise. Thus, the result of commuting the excitation force from the Fourier transform is that the noise is neglected.

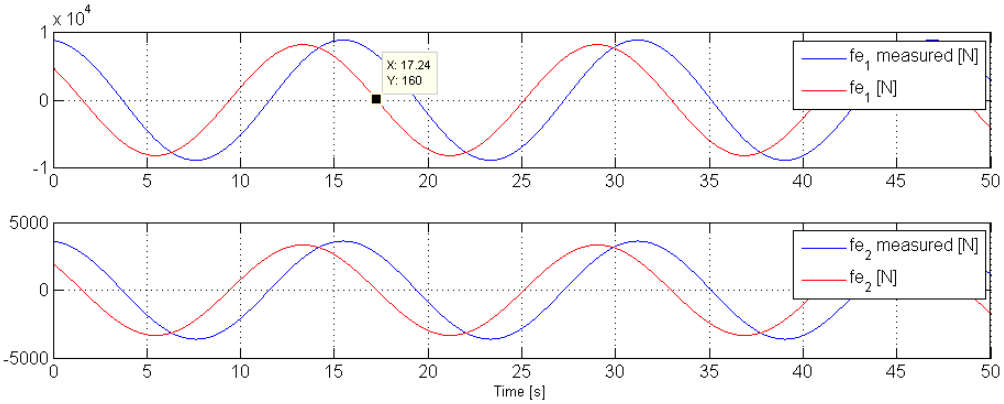

Figure 8.26: Error in the excitation force calculated from the measured wave elevation due to computational method and measurements noise of $p_n = 0.01$. Upper graph shows forces on the buoy and the lower graph shows forces working on the disc.

Delay caused by EKF

By weighing the EKF with a large R matrix, a delay may introduced into the system, see Figure 8.27. For the case of regular waves, this delay may influence the calculated excitation force and give it a phase shift. This may affect the performance of the controller. Figure 8.28 shows the excitation force calculated from the delayed estimate of the wave elevation. The estimated excitation force it improved for this case, with delay of $\delta s = 0.522$ s and difference in amplitude was $\delta fe_1 = 238$ N. In this case the phase shift is partially corrected. However if the phase between the estimated excitation force and the real value is shifted in the opposite, the effect of a filter time delay will be an increased phase difference between the two forces.

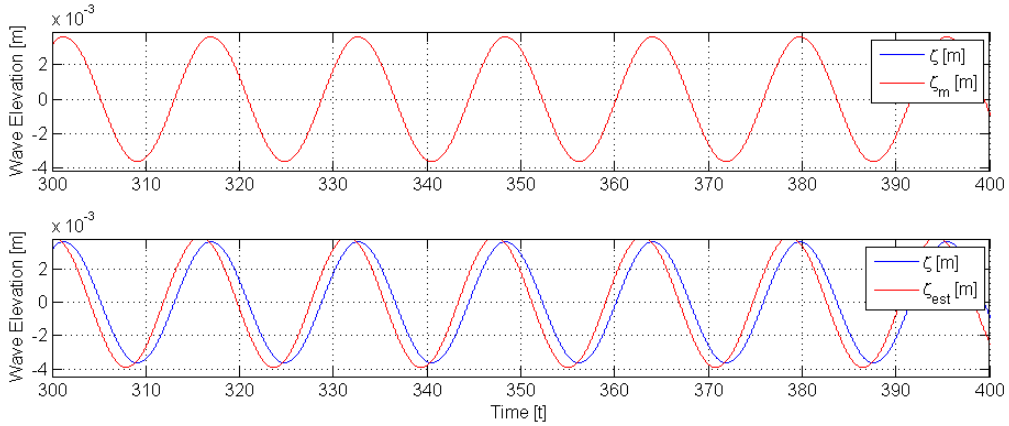

Figure 8.27: Delay caused by EKF. Computed without measurement noise.

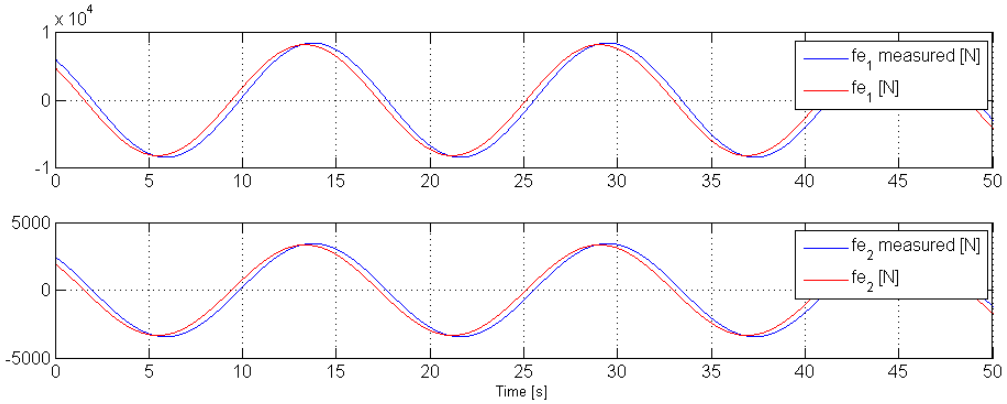

Figure 8.28: Excitation force calculated from estimate with delay caused by EKF.

Total System

The total system was tested, including the noise, phase delay and computational error. The resulting motion response is given in Figure 8.29. The control algorithm has satisfactory performance. Table 8.8.1 shows the extracted power for the uncontrolled WEC and WEC under influence of controller with estimated wave. From the table it can be seen that the control output is increased regardless of the errors caused by the estimator. The low value of the power outtput is due to the small amplitude studied in this case.

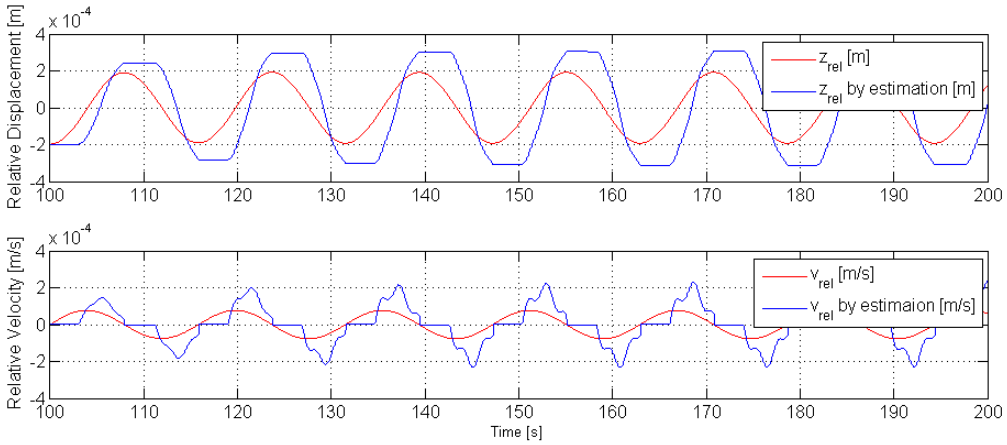

Figure 8.29: Performance of the total system for irregular waves. The upper graph shows the relative displacement and the lower graph shows the relative velocity. Red and blue graph indicates uncontrolled motion and motion under influence of controller and estimator.

	Power [W]
WEC	0.0465
Controller with estimator	0.0490

Table 8.8: Mean power outtake of complete system.

8.8.2 Irregular Waves

The full system was tested for irregular waves. The optimal control was found to be no control. Hence, there was no need for the controller or an estimator. The estimator could only degrade the performance and decrease the power output. Nevertheless, testing the effect of the estimator on the control system may enlighten some interesting aspects for further development of control and estimation algorithm. Hence, the full system was tested for the sea state defined by $H_s = 2.5$ and $T_p = 9.1$.

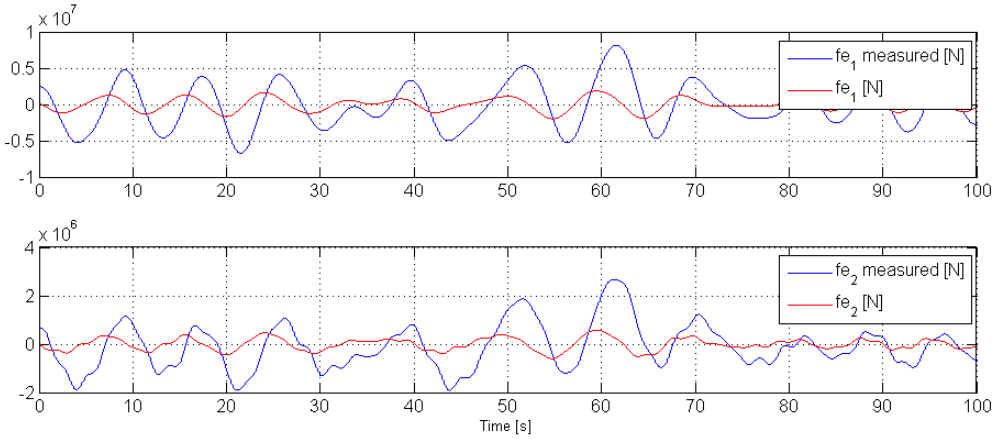

Figure 8.30: Error in excitation force calculations due to faulty computational method. The upper graph shows the excitation force working on the buoy and the lower graph shows the force working on the disc.

The calculated excitation force is given in Figure 8.30. From the figure it can be seen that the estimated force is quite different from the real force. The force is calculated as a sum of many regular waves. All the error from the regular waves were summed up, resulting in a poor estimate of the excitation force. By increasing the step size, in addition to total estimation time, the calculated force was improved. However, as described previously this would increase the computational time and introduce a time delay. The frequency domain wave elevation amplitude is given in Figure 8.31.

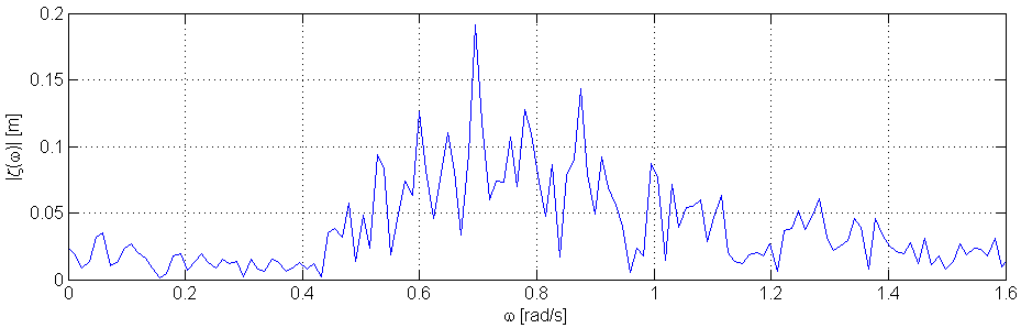

Figure 8.31: Frequency domain wave elevation amplitude for irregular waves.

As described for the regular waves the system is not affected by the noise, due to the computational method. However, for a full system test a noise of $p_n = 0.01$ was added for verification. Figure 8.32 show the deviation between the simulated real value and the value estimated by the EKF.

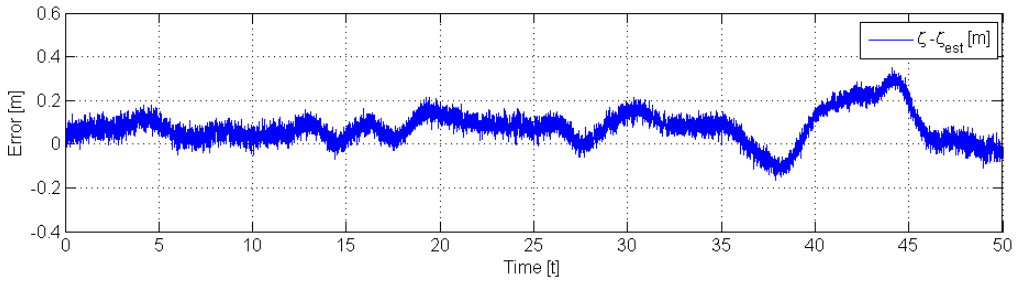

Figure 8.32: Deviation between real and estimated wave. Added noise power of $p_n = 0.01$

The result of the simulation is given in Figure 8.33. For the case of irregular waves the optimal control input converged towards a vector of zeros. Hence, the introduced error had no effect on the controller. There was no need for more analysis of full system performance with regard to the EKF because the filter did not have an effect when there was zero control input.

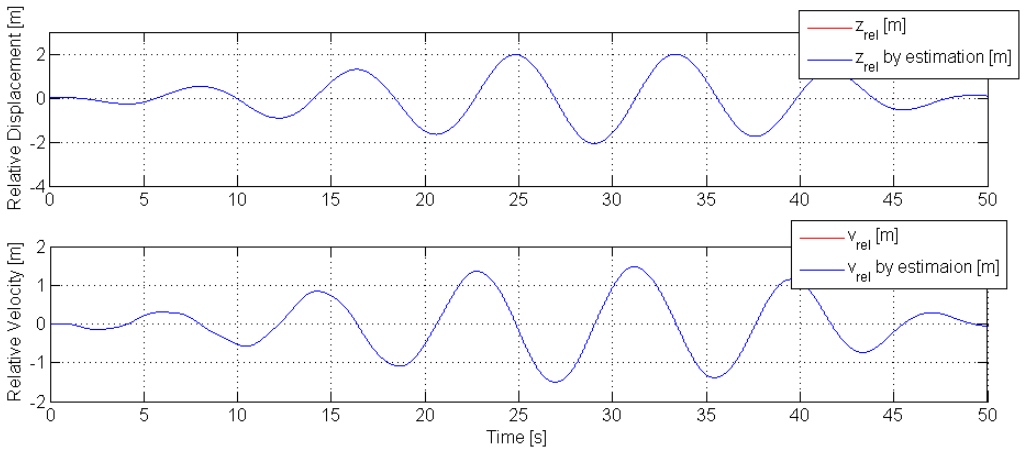

Figure 8.33: Response of WEC in irregular waves for the sea state defined by $H_s = 2.5$ and $T_p = 9.1$ under influence of controller with estimated excitation force as input.

Chapter 9

Concluding Remarks

9.1 Conclusion

The aim of this thesis has been to explore methods for control and estimation of the Ocean Oasis wave energy converter in irregular waves. The focus has lied on solving the challenges of real-time implementation of control algorithms for a wave energy converter (WEC). As a result of a literature survey the challenges of time-domain modeling of marine structures were recognized and Latching control was found to be one of the most common control methods for this type of wave energy converter. In addition, a common approach to estimation was found to be the Kalman filter. These findings were the basis for further development of control and estimation schemes.

Theory of ocean waves and wave energy extraction was studied to get a better understanding of the control objective. In addition, background knowledge of modeling of marine structures was established. The model of the WEC utilized in the thesis was based on the model developed in Schultz (2014) for regular waves. However, the system dynamics model was extended to time-domain model of a WEC influenced by irregular waves. The fluid-memory effects were approximated as linear time-domain models and the excitation force was calculated from pre-calculated time series.

Furthermore, a study of Latching control was conducted. The control algorithm utilized in this thesis was inspired by the work done in Schultz (2014), and was extended to include the effect of irregular waves. However, the main focus of the thesis was developing an estimation strategy for the purpose of controlling the vessel. A simulation setup was established and measurement methods decided. An approach to the Extended Kalman filter was developed for sea wave estimation. The wave elevation was modeled as a regular wave.

To test the model performance, simulations were conducted in MATLAB & Simulink. The simulation data developed for the DynOcean, which is similar to the Ocean Oasis, was utilized for the simulations due to lack of simulation data for the Ocean Oasis. In order to ensure correct performance of the model, each part was simulated and evaluated separately. The mathematical model of the WEC under influence of irregular waves was compared to

a previous study of DynOcean. The performance was as expected, thus the performance of the controller was validated.

Moreover, the control algorithm was tested by simulations and found to give correct behavior according to Latching theory. However, the control method resulted in neither an increase in efficiency nor a reduction in intermittency. The optimal control algorithm converged to zero control. Thus, it was concluded that Latching control was not a suitable control algorithm for the Ocean Oasis. The estimation algorithm gave satisfactory performance for low-medium noise levels (noise power of 0.01 - 0.1 m), with standard deviations in the range $\sigma = 0.01 - 0.03$ m for a sea state defined by $H_s = 2.5$ and $T_p = 9.1$. However, if the measurement noise was expected to contain higher levels of noise, the filter should be reconsidered or further developed.

Full system tests, including modeled WEC, controller and estimator were conducted. The method for calculating the excitation force based on the wave measurement did not work as expected and resulted in wrong excitation force estimates. However, by testing the full system with prediction errors and a faulty excitation force calculation method the controller still converged to zero control. Thus, the system was not affected by excitation force errors, neither by the prediction errors.

9.2 Recommendations for Future Work

From the conclusion it is clear that Latching as a control method for the Ocean Oasis should not be explored further. Other control methods may be investigated. However, most control algorithms developed for the heaving buoy type of WEC are based on optimizing the phase between the structure and the excitation force, as is the case for Latching. Seeing as there was no effect of the Latching controller, other control methods of the same type may not be beneficial.

It might be interesting to consider changing the structure of the WEC so that the power extraction could be closer to optimum. The shape could be evaluated by considering the theory developed for optimum power extraction for WECs. The purpose of the controller is to ensure optimal power extraction for all sea states. A change in the structure is most likely needed for functioning control functions as well. A change in the structure is most likely needed for functioning control as well.

If a more efficient control method were to be developed, an interesting topic would be to develop the estimator further. If the measurement devices were to be installed on the WECs, an approach would be to extend the mathematical model to include the WEC dynamics. This might increase the accuracy of the estimated wave due to a more accurate mathematical model. An important step in further development is improving the excitation force calculations. One interesting method is the causal approach to calculating the non-causal excitation force given in Falnes (2002). Furthermore, it may be beneficial to estimate the excitation force directly by measuring the pressure and modeling the estimated force based on these

measurements.

Bibliography

Babarit, A. & Clément, A. H. (2006), 'Optimal latching control of wave energy device in regular and irregular waves', *Applied Ocean Research* **28**, 77–91.

Baker, N. J. & Mueller, M. A. (2001), 'Direct drive wave energy converters (in french).', *Revue des Energies Renouvelables,* .

Balchen, J. G., Andresen, T. & Foss, B. A. (2003), *Reguleringsteknikk*, Institutt for teknisk kybernetikk, NTNU.

Barstow, S., Mørk, G., Mollison, D. & Cruz, J. (2008), *Ocean Wave Energy*, number pp 93-132 *in* 'Green Energy and Technology (Virtual Series)', Springer Link. Chapter 4.

Belmont, M. R., Horwood, J. M. K., Thurley, R. W. F. & Baker, J. (2006), 'Filters for linear sea-wave prediciton', *Ocean Engineering* **33**, 2332–2351.

Bjerregård, M. (2014), Methods for sea state estimation, Master's thesis, Technical University of Denmark.

Bjørnstad, E. (2011), Control of wave energy converter with constrained electric power take off, Master's thesis, Norwegian University of Science and Technology.

Brown, R. & Hwang, P. (2012), *Introduction to Random Signals and Applied Kalman Filtering,*, 3rd edn, John Wiley & Sons, Inc.

Budal, K., Falnes, J. & Onshus, T. (1979), Optimal phase control of a power-buoy, Technical Report 480934.00, Sintef.

Chabaud, V., Steen, S. & Skjetne, R. (2013), Real-time hybrid testing for marine structures: Challenges and strategies, *in* 'ASME 2013 32nd International Conference on Ocean, Offshore and Arctic Engineering', Vol. 5. cited By 0.

Counsil, W. E. (2013), World energy perspective; cost of energy technologies, Technical report, London: World Energy Council.

Cruz, J. (2008), *Ocean Wave Energy - Current Status and Future Perspectives Bristol*, Springer.

DNV GL (2014), Ocean oasis: Wave powered seawater desalination, Technical report, DNV GL, Oslo.

Drew, B., Plummer, A. R. & Sahinkaya, M.-N. (2009), A review of wave energy converter technology, *in* 'Proceedings of the Institution of Mechanical Engineers, Part A: Journal of Power and Energy'.

EMEC (2015), 'Wave developers', [Online: accessed 08.03.2015].
URL: *http://www.emec.org.uk/marine-energy/wave-developers/*

EMEC (n.d.), 'Pelamis wave power', [Online: Accessed 24.04.2015].
URL: *http://www.emec.org.uk/about-us/wave-clients/pelamis-wave-power/*

Falnes, J. (2002), *Ocean Waves and Oscillating Systems*, 1 edn, Cambridge University Press.

Falnes, J. (2007), 'A review of wave-energy extraction', *Marine Structures* **20**, 185–201.

Falnes, J. (2015), 'Om primært opptak av bølgjeenergi og om kjell budals arbeid ved nth med utvikling av bølgjekraftverk.', PowerPoint presentation. NTNU, Trondheim.

Falnes, J. & Hals, J. (2012), 'Heaving buoys, point absorbers and arrays', *Philiosophical Transactions of the Royal Society A: Mathematical, Physical and Engineering Sciences.* .

Faltinsen, O. M. (1998), *Sea Loads on Ships and Offshore Structures*, Cambridge University Press.

Faltinsen, O. M. (2005), *Hydrodynamics of High-Speed Marine Vehicles*, Cambridge University Press.

Fernandes, C. (n.d.), 'Current technologies', [Online: Accessed 24.04.2015].
URL: *http://owc-wec.weebly.com/current-technologies.html*

Fusco, F. (2009), 'Forecasting requirements in the optimal control of wave energy converters.'. National University of Ireland Maynooth, electronic Engineering Department.

Giron-Sierra, J. M. & Jimenez, J. F. (2010), 'State-of-the-art of wave measurement for ship motion prediction', *Control Applications in Marine Systems* .

Hals, J. (2010), Modelling and phase control of wave-energy converters, PhD thesis, Norwegian University of Science and Technology.

Henderson, R. (2006), 'Design, simulation, and testing of a novel hydraulic power take-off system for the pelamis wave energy converter.', *Renewable Energy* .

Hespanha, J. P. (2009), *Linear Systems Theory*, Princeton University Press.

Hua, J. & Palmquist, M. (1994), *Wave estimation through ship motion measurement*, Trita-FKT, Naval Architecture, Department of Vehicle Engineering, Royal Inst. of Technology.
URL: *https://books.google.no/books?id=N9djMQAACAAJ*

Johannessen, T. B., Brandsvoll, R. A. & Palmstrøm, A. (2011), A system for wave driven desalination, *in* 'Proceedings of the ASME 2011 30th International Conference on Ocean, Offshore and Arctic Engineering OMAE2011'.

Karimirad, M. (2014), *Offshore Energy Structures*, Springer International Publishing Switzerland.

Kazantzis, N. & Kravaris, C. (1999), 'Time-discretization of nonlinear control systems via taylor methods', *Computers & Chemical Engineering* **23**(6), 763 – 784.
URL: *http://www.sciencedirect.com/science/article/pii/S0098135499000071*

Madhi, F., Sinclair, M. E. & Yeung, R. W. (2014), 'The "berkeley wedge": an asymmetrical energy-capturing floation breakwater of high performance.', *Marine Systems & Ocean Technology* **9**(1), 05–16.

MathWorks (2015), 'Band-limited white noise', [Online: Accessed 14.06.2015].
URL: *http://se.mathworks.com/help/simulink/slref/bandlimitedwhitenoise.html*

MATLAB & Simulink (2014a), 'R2014a'. MathWorks.

Muetze, A. & Vining, J. R. G. (2006), 'Ocean wave energy convertion - a survey', *IEEE* .

Myrhaug, D. (2007), *TMR4180 Marin Dynamikk - Uregelmessig sjø*, Fakultetet for ingeniørvitenskap og teknologi - NTNU Trondheim. Compendium.

NASA/JPL (n.d.), 'Jason 3', [Online; accessed 11.05.2015].
URL: *http://www.jpl.nasa.gov/missions/details.php?id=5997*

Newman, J. N. (1977), *Marine Hydrodynamics*, 6 edn, The Massachusetts Institute of Technology.

Nielsen, U. D. (2005), Estimation of Directional Wave Spectra from Measured Ship Reponses, PhD thesis, Technical University of Denmark.

Nielsen, U. D. (2008), 'The wave buoy analogy — estimating high-frequency wave excitations', *Applied Ocean Research* **30**(2), 100 – 106.
URL: *http://www.sciencedirect.com/science/article/pii/S014111870800031X*

NNMREC (2015), 'Pelamis attenuator'.
URL: *http://nnmrec.oregonstate.edu/pelamis-attenuator*

Ogilvie, T. (1964), 'Recent progress towards understanding and prediction of ship motions', *Sixth Symposium on Naval Hydrodynamics* .

Palmstrøm, A. & Brandsvoll, R. A. (2011), Wave energy driven desalination of seawater - experimental investigation of the hydrodynamic performance, Master's thesis, Norwegian University of Science and Technology.

Perez, T. & Fossen, T. I. (2008a), 'Joint identification of infinite-frequency added mass and fluid-memory models of marine structures', *Modeling, Identification and Control* .

Perez, T. & Fossen, T. I. (2009), 'A matlab toolbox for parametric identification of radiation-force models of ships and offshore structures', *Modeling, Identification and Control* **30**(1), 1–15.

Pettersen, B. (2007), *TMR4247 Marin Teknikk 3 - Hydrodynamikk*, Fakultetet for ingeniørvitenskap og teknologi - NTNU Trondheim. Compendium.

Recommended Practice DNV-Rp-C205 - Environmental Conditions and Environmental Loads (2010).

Ren21 (2014), Renewables 2014 global status report, Technical report, Renewable Energy Policy Network for the 21st Century.

Ringwood, J. V., Bacelli, G. & Fusco, F. (2014), 'Energy-maximizing control of wave-energy converters', *IEEE Control Systems Magazine* .

Ross, D. (1995), *Power From the Waves*, Oxford University Press.

Salter, S. (1974), 'Wave power', *Nature* **249**, 720–724.

Schultz, E. (2014), 'Latching study of wave energy converters'. Project Thesis, Norwegian University of Science and Technology.

Simon, D. (2006), *Optimal State Estimation*, John Wiley & Sons, Inc.

Steffen, W., Richardson, K., Rockström, J., Cornell, S. E., Fetzer, I., Bennett, E. M. & Biggs, R. (2015), 'Panetary boundaries: Guiding human development on a changing planet', *Science* **347**.

Taghipour, R., Perez, T. & Moan, T. (2008), 'Hybrid frequency-time domain models for dynamic response analysis of marine structures.', *Ocean Engineering* **35**, 685–705.

Tedeschi, E. & Molinas, M. (2010), 'Control strategy of wave energy converters optimized under power electronics rating constraints', *3rd international conference on Ocean Energy (ICOE10)* .

The United Nations World Water Development Report 4: Managing Water under Uncertainty and Risk. (2012). 4.

Thorpe, T. W. (1999), A brief review of wave energy, Technical Report R120, EnergyTechnologySupportUnit (ETSU). A report production for the UK Department fo Trade and Industry.

Voronovich, V., Holmes, B. & Thomas, G. (2005), 'A preliminary numerical and experimental study of wave prediction', *6th European Wave and Tidal Energy Conference* .

Appendix A

Concept Information

Table A.1: Excitation force coefficient and phase data.

$\omega_w[rad/s]$	$h_{1,\zeta f}(\omega_w)[N]$	$\angle h_{1,\zeta f}(\omega_w)[rad]$	$h_{2,\zeta f}(\omega_w)[N]$	$\angle h_{2,\zeta f}(\omega_w)[rad]$
0,001	2991000	0	1499000	0
0,2	2796015	0,003	1328007	0,003
0,3	2565315	0,016	1139140	0,016
0,4	2277191	0,044	921086	0,044
0,45	2122576	0,066	811348	0,066
0,475	2044334	0,079	757747	0,079
0,5	1965556	0,093	705669	0,093
0,525	1887298	0,109	655120	0,109
0,55	1810629	0,127	606501	0,127
0,575	1733605	0,147	560009	0,147
0,6	1658282	0,168	515738	0,168
0,625	1584675	0,191	473777	0,191
0,65	1511884	0,215	434213	0,215
0,675	1441859	0,242	397128	0,242
0,7	1373683	0,27	362500	0,27
0,725	1307316	0,3	330219	0,3
0,75	1243720	0,332	300355	0,332
0,775	1181977	0,365	272789	0,365
0,8	1122982	0,401	247404	0,401
0,825	1066102	0,438	224176	0,438
0,85	1011469	0,477	202996	0,477
0,875	959285	0,518	183740	0,518
0,9	909280	0,561	166208	0,561
0,925	861677	0,606	150393	0,606
0,95	816217	0,653	136088	0,653
0,975	772899	0,701	123237	0,701
1	731699	0,752	111729	0,752
1,1	586407	0,972	76928	0,972
1,2	468795	1,222	55849	1,221
1,3	374513	1,501	44086	1,498
1,4	299667	-1,331	38719	-1,338
1,6	196994	-0,632	41320	-0,645
1,8	132526	0,118	62281	0,152
2	88679	0,961	131212	1,048
2,2	91581	-1,214	689590	-1,141
2,4	4271	1,399	512504	0,059
2,8	40783	-0,651	950813	-0,705
3	8393	-1,209	147716	-0,55

Table A.2: Frequency dependent added mass

ω_w	$a_{11}(\omega_w)$	$a_{22}(\omega_w)$	$a_{12}(\omega_w)$	$a_{21}(\omega_w)$
0.001	1029000	4035000	484400	485800
0.2	965100	4021000	442800	444200
0.3	928800	4018000	415200	416600
0.4	824700	4009000	358900	360400
0.45	758900	4007000	327800	329400
0.475	724500	4007000	312700	314300
0.5	689800	4008000	298200	299900
0.525	655400	4011000	284600	286400
0.55	621700	4014000	272100	273900
0.575	589100	4019000	260800	262600
0.6	557900	4024000	250800	252700
0.625	528400	4031000	242000	244000
0.65	500800	4039000	234600	236600
0.675	475200	4048000	228600	230600
0.7	451700	4059000	223700	225800
0.725	430400	4070000	220100	222200
0.75	411200	4082000	217500	219700
0.775	394200	4094000	215900	218100
0.8	379100	4108000	215200	217500
0.825	366000	4122000	215300	217600
0.85	354700	4138000	216000	218400
0.875	345100	4154000	217400	219800
0.9	337100	4170000	219200	221600
0.925	330400	4188000	221400	223900
0.95	325100	4206000	224000	226500
0.975	320900	4225000	226800	229400
1	317700	4245000	229900	232500
1.1	312900	4332000	243400	246200
1.2	316700	4435000	257700	260700
1.3	324700	4559000	272200	275600
1.4	334600	4709000	287200	291100
1.6	355100	5131000	321500	327400
1.8	374400	5861000	371800	382200
2	394100	7484000	473700	497300
2.2	438200	15930000	970500	1086000
2.4	372800	-3083000	-86270	-245700
2.8	455000	12340000	986800	788600
3	351800	607800	-721900	34830

Table A.3: Frequency dependent radiation damping

ω_w	$b_{11}(\omega_w)$	$b_{22}(\omega)$	$b_{12}(\omega_w)$	$b_{21}(\omega_w)$
0.001	45.39	11.4	22.75	22.75
0.2	30100	6875	14390	14390
0.3	89060	18020	40070	40050
0.4	163200	27870	67460	67420
0.45	199500	30700	78280	78240
0.475	216200	31450	82490	82450
0.5	231700	31750	85800	85750
0.525	245700	31620	88160	88110
0.55	258000	31090	89580	89540
0.575	268600	30200	90080	90040
0.6	277300	29020	89720	89690
0.625	284200	27590	88560	88530
0.65	289300	25970	86680	86680
0.675	292600	24230	84200	84210
0.7	294200	22410	81200	81230
0.725	294400	20570	77800	77850
0.75	293100	18750	74080	74160
0.775	290500	16960	70150	70260
0.8	286900	15260	66090	66230
0.825	282200	13650	61990	62160
0.85	276800	12150	57900	58100
0.875	270700	10770	53880	54120
0.9	264000	9515	49990	50260
0.925	256900	8379	646250	46560
0.95	249500	7365	42700	43040
0.975	241900	6461	39350	39730
1	234100	5662	36230	36640
1.1	203300	3381	25980	26500
1.2	174600	2153	19090	19680
1.3	149500	1544	14920	15510
1.4	128200	1325	12810	13330
1.6	95680	1753	13130	13140
1.8	73680	4917	19780	18360
2	60160	26400	42790	37070
2.2	68560	689900	231700	203300
2.4	17820	1068000	-101800	-92150
2.8	376.3	3466000	-48470	-32610
3	71340	1164000	528900	67200

Appendix B

Radiation Forces

(re-write chapter: new understanding of comparison plot and complex coefficient). Section 8.4 discusses the results of the radiation model obtained by applying the Matlab Toolbox for Identification of Radiation Force Models (Perez & Fossen 2009). In this chapter the estimated parameters of the radiation force model described in Section 5.4 are given. In addition, plots of frequency response of the retardation functions are given.

As described in Section 5.4.2, the values of the fluid memory effect obtained should be checked by comparing the identified added mass with values calculated from (B.1) . Results of the comparison are plotted and given in following chapters.

$$A_{ik}(j\omega) \triangleq \frac{B_{ik}}{j\omega} + A_{ik}(\omega) \tag{B.1}$$

B.1 Degree of Freedom 12

The approximation of the transfer function for DOF 11 is given in (B.2) and the infinite added mass is given in (B.3). The linear state space equation can then be given by the canonical realization in (B.4)-(B.5).

$$\hat{k}_{12}(s) = \frac{5.8352 \times 10^4 s}{s^2 + 0.6524s + 0.3322} \tag{B.2}$$

$$\hat{a}_{12}(\infty) = 2.9031 \times 10^5 \tag{B.3}$$

$$\hat{A}_{12} = \begin{bmatrix} -0.6524 & 1.0000 \\ -0.3322 & 0 \end{bmatrix} \qquad \hat{B}_{12} = \begin{bmatrix} 5.8352 \times 10^4 \\ 0 \end{bmatrix} \tag{B.4}$$

$$\hat{C}_{12} = \begin{bmatrix} 1 & 0 \end{bmatrix} \tag{B.5}$$

Figure B.1 shows the frequency response of the identified retardation function for DOF 11, k_{12}, and Figure B.2 shows the identification results for DOF 11. In the left-hand-side plot the comparison of the identified added mass and the calculation done from (B.1) are

shown. In the right-hand-side the estimated value of the added mass and damping are plotted against the original values.

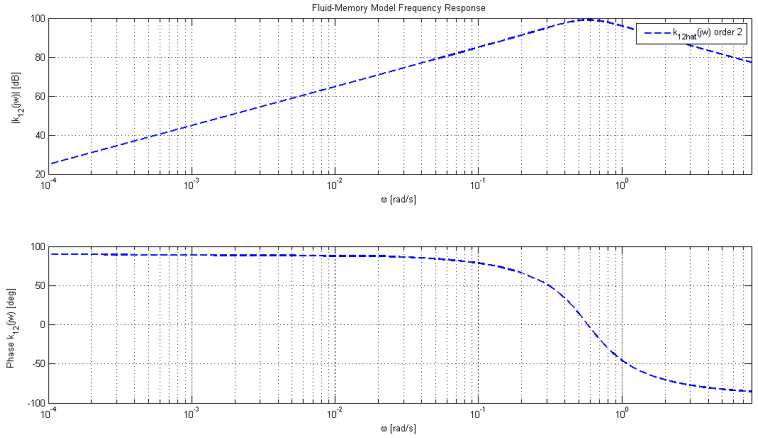

Figure B.1: Frequency response of the identified fluid-memory model degree of freedom 12.

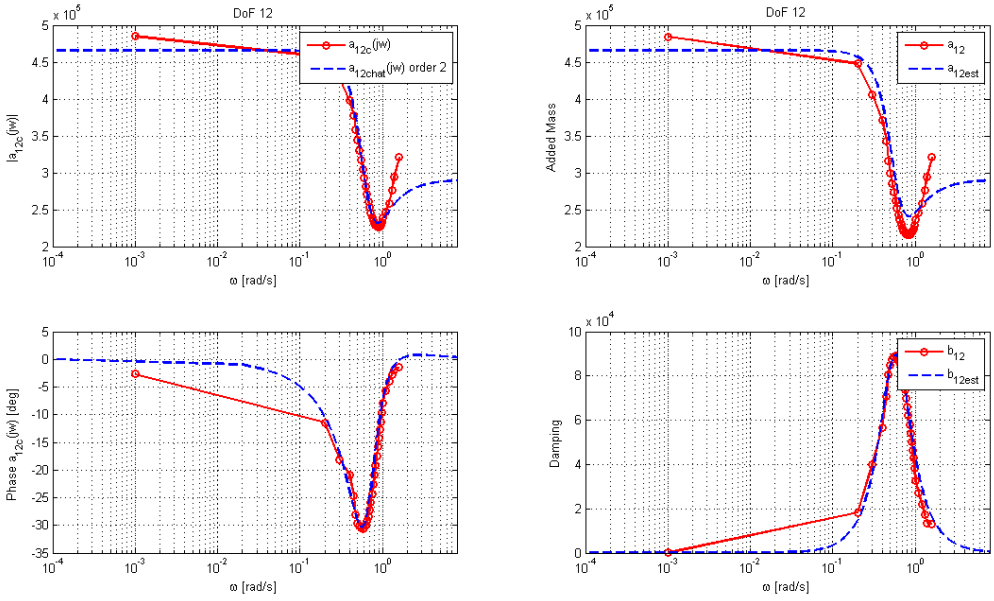

Figure B.2: Identification results for degree of freedom 12. The complex coefficient data and the response of the identified model is illustrated in the left-hand-side plots. The added mass and potential damping and their re-construction based on the estimated model is shown in the right-hand-side plots show.

B.2 Degree of Freedom 21

The approximation of the transfer function for DOF 11 is given in (B.6) and the infinite added mass is given in (B.7). The linear state space equation can then be given by the canonical realization in (B.8)-(B.9).

$$\hat{k}_{21}(s) = \frac{5.782 \times 10^4 s}{s^2 + 0.6464s + 0.3296} \tag{B.6}$$

$$\hat{a}_{21}(\infty) = 2.9225 \times 10^5 \tag{B.7}$$

$$\hat{A}_{21} = \begin{bmatrix} -0.6464 & 1.0000 \\ -0.3296 & 0 \end{bmatrix} \qquad \hat{B}_{21} = \begin{bmatrix} 5.7816 \times 10^4 \\ 0 \end{bmatrix} \tag{B.8}$$

$$\hat{C}_{21} = \begin{bmatrix} 1 & 0 \end{bmatrix} \tag{B.9}$$

Figure B.3 shows the frequency response of the identified retardation function for DOF 11, k_{21}, and Figure B.4 shows the identification results for DOF 11. In the left-hand-side plot the comparison of the identified added mass and the calculation done from (B.1) are shown. In the right-hand-side the estimated value of the added mass and damping are plotted against the original values.

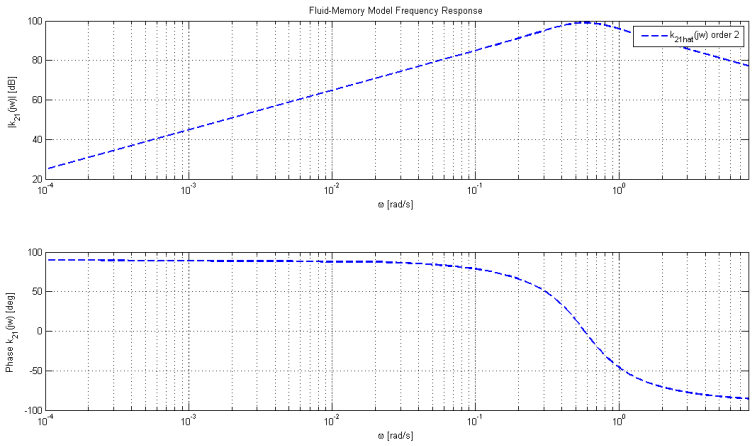

Figure B.3: Frequency response of the identified fluid-memory model degree of freedom 21.

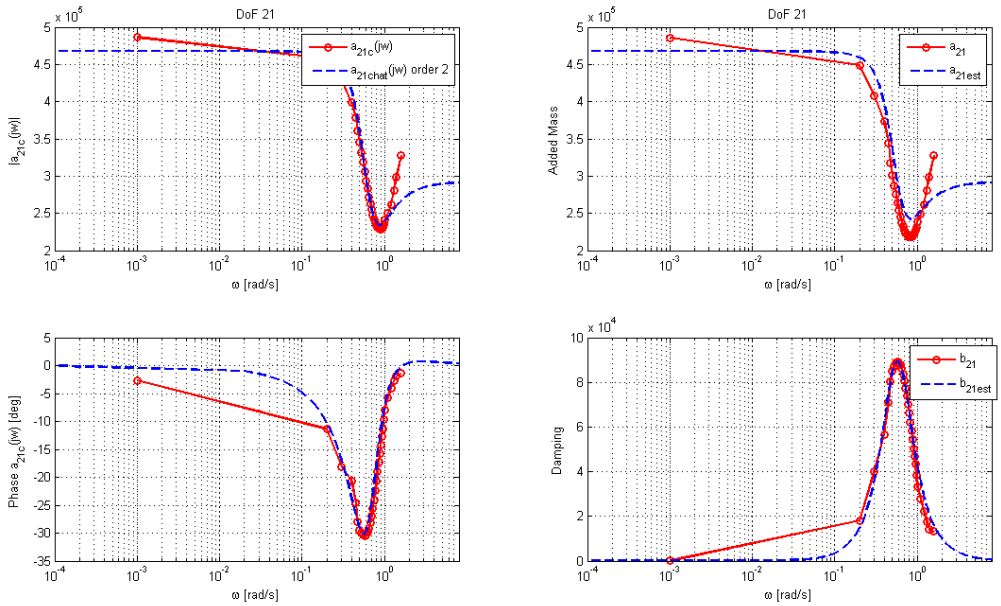

Figure B.4: Identification results for degree of freedom 21. The complex coefficient data and the response of the identified model is illustrated in the left-hand-side plots. The added mass and potential damping and their re-construction based on the estimated model is shown in the right-hand-side plots show.

B.3 Degree of Freedom 22

The approximation of the transfer function for DOF 11 is given in (B.10) and the infinite added mass is given in (B.11). The linear state space equation can then be given by the canonical realization in (B.12)-(B.13).

$$\hat{k}_{22}(s) = \frac{1.023e07s^2 + 3.338e06s}{s^3 + 0.4352s^2 + 5.965s + 1.795} \tag{B.10}$$

$$\hat{a}_{22}(\infty) = 2.1889 \times 10^6 \tag{B.11}$$

$$\hat{A}_{22} = \begin{bmatrix} -0.4352 & 1.0000 & 0 \\ -5.9651 & 0 & 1.0000 \\ -1.7945 & 0 & 0 \end{bmatrix} \qquad \hat{B}_{22} = \begin{bmatrix} 1.0232 \times 10^7 \\ 0.3338 \times 10^7 \\ 0 \end{bmatrix} \tag{B.12}$$

$$\hat{C}_{22} = \begin{bmatrix} 1 & 0 \end{bmatrix} \tag{B.13}$$

Figure B.5 shows the frequency response of the identified retardation function for DOF 11, k_{22}, and Figure B.6 shows the identification results for DOF 11. In the left-hand-side plot the comparison of the identified added mass and the calculation done from (B.1) are

shown. In the right-hand-side the estimated value of the added mass and damping are plotted against the original values.

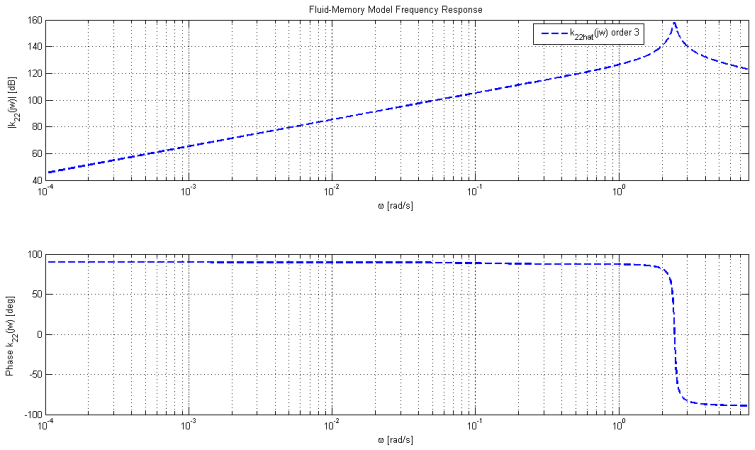

Figure B.5: Frequency response of the identified fluid-memory model degree of freedom 22.

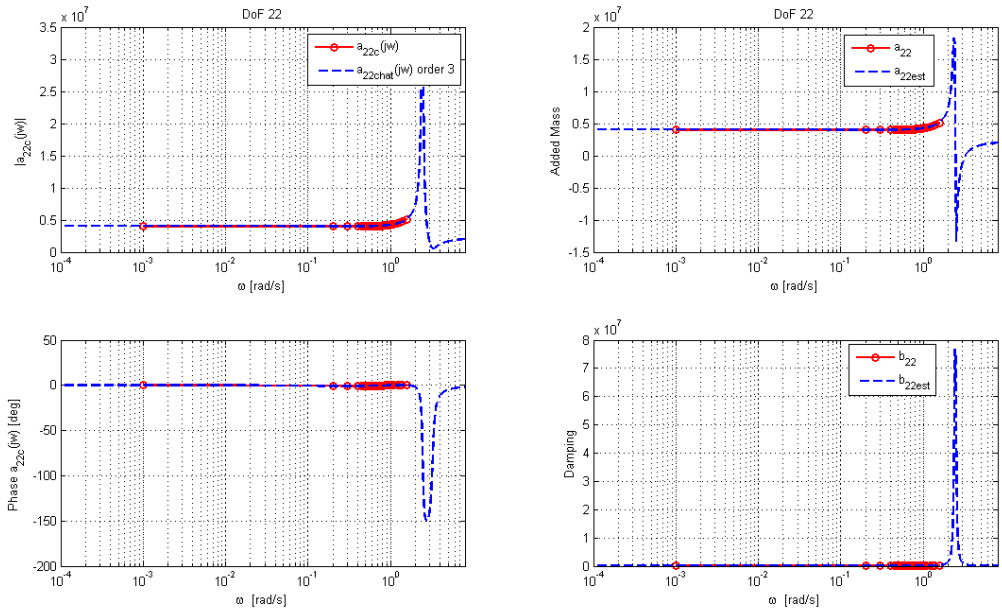

Figure B.6: Identification results for degree of freedom 22. The complex coefficient data and the response of the identified model is illustrated in the left-hand-side plots. The added mass and potential damping and their re-construction based on the estimated model is shown in the right-hand-side plots show.

Appendix C

Additional Results

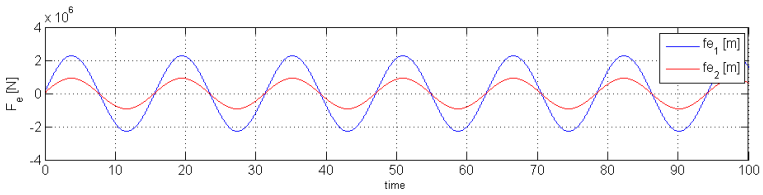

Figure C.1: Excitation force from regular waves for frequency $\omega = 0.4\ \frac{rad}{s}$ and wave amplitude $\zeta_A = 1$ m.

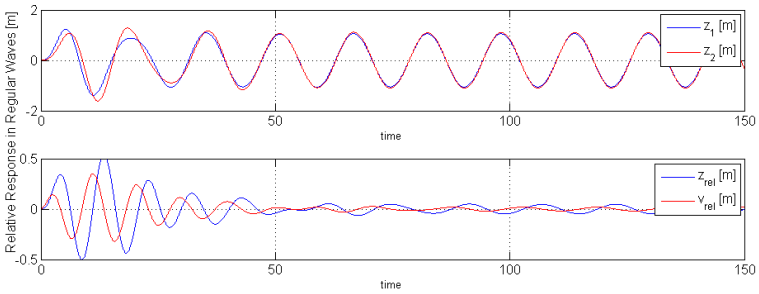

Figure C.2: Response in regular waves of frequency $\omega = 0.4\ \frac{rad}{s}$ and amplitude $\zeta_A = 1$ m.

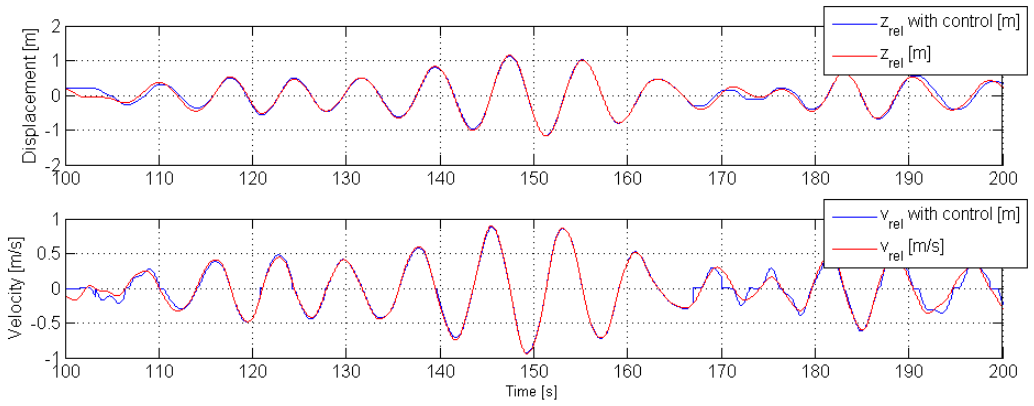

Figure C.3: Relative responce for WEC for sea state defined by $H_s = 2.5$ and $Tp = 6.5$, comparison with and without controller. One iteration.

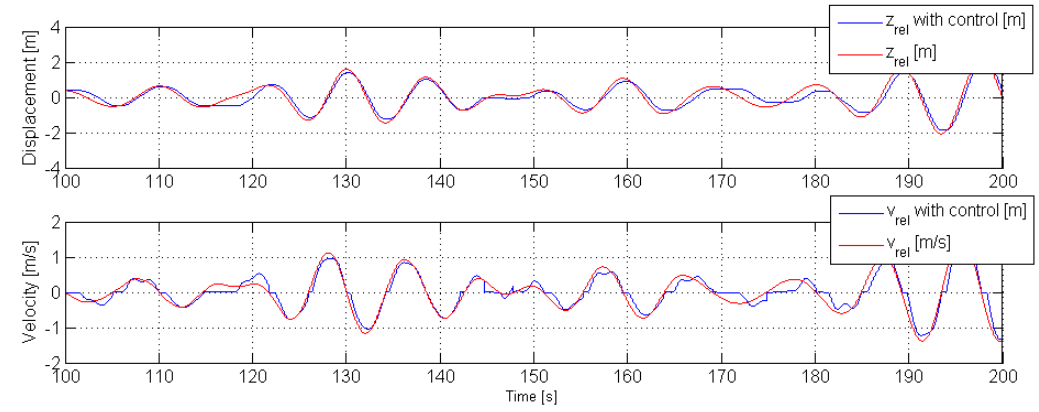

Figure C.4: Relative responce for WEC for sea state of $H_s = 2.5$ and $Tp = 11.5$, comparison with and without controller. One iteration.

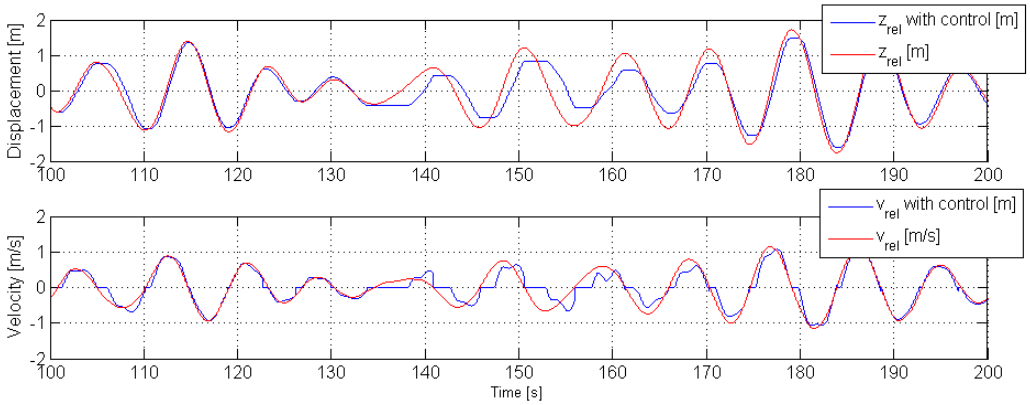

Figure C.5: Relative responce for WEC for sea state of $H_s = 5.5$ and $Tp = 14.5$, comparison with and without controller. One iteration.

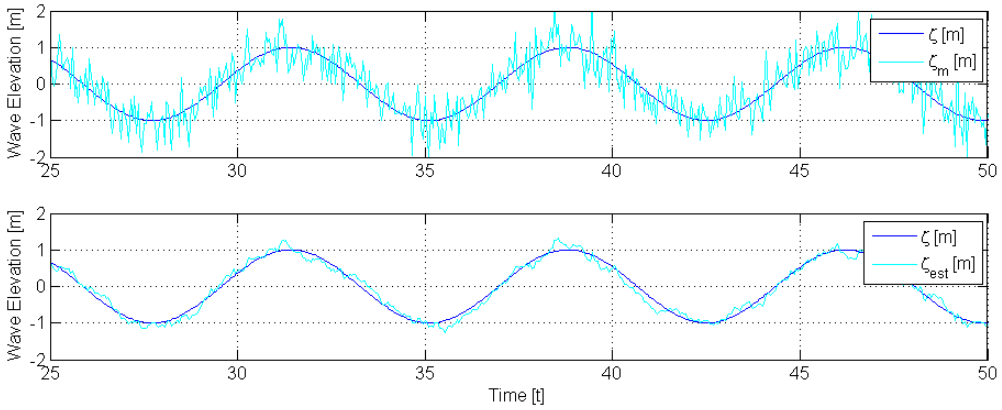

Figure C.6: Performance of Kalman filter with noise power $p_n = 0.01$, in regular waves.

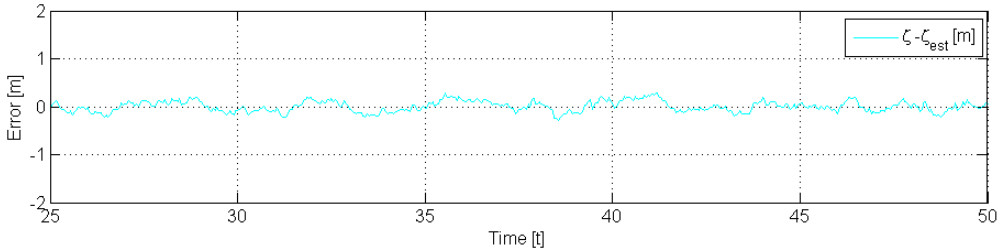

Figure C.7: Error for noise power $p_n = 0.01$, in regular waves.

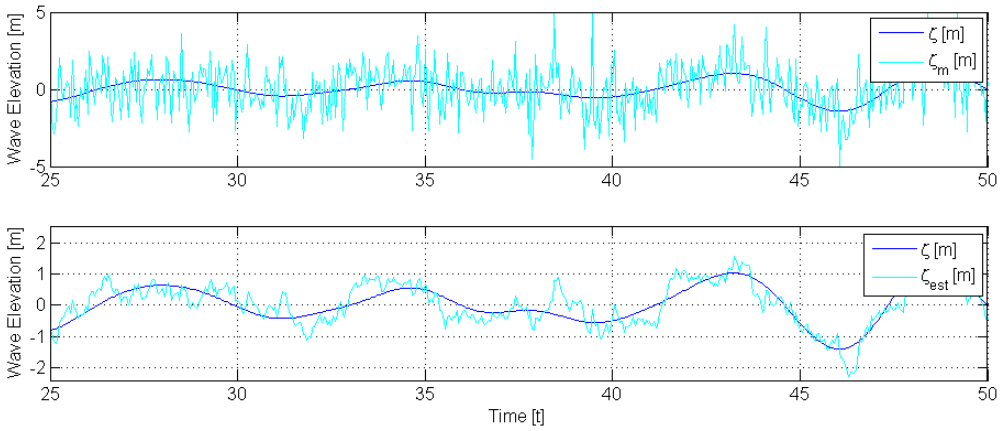

Figure C.8: Performance of EKF with noise power $p_n = 0.1$, in irregular waves.

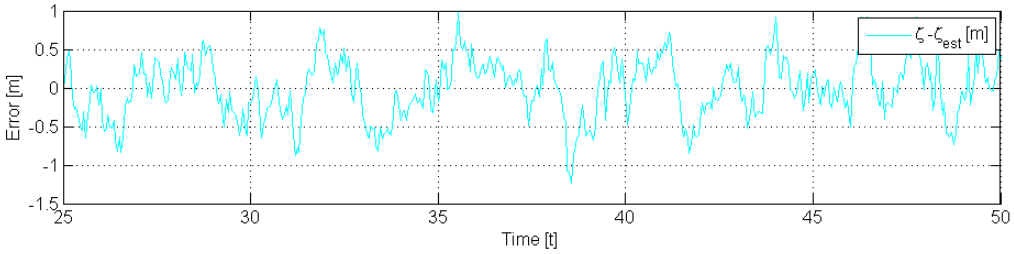

Figure C.9: Error for noise power $p_n = 0.1$, in irregular waves.